

Compact Deployable Antenna for CubeSat Units

A Senior Project Sponsored by NASA's Jet Propulsion Laboratory

by

Sarah Bolton

Dominic Doty

Peter Rivera

Mechanical Engineering Department

California Polytechnic State University

San Luis Obispo

2014-2015

Statement of Disclaimer

Since this project is a result of a class assignment, it has been graded and accepted as fulfillment of the course requirements. Acceptance does not imply technical accuracy or reliability. Any use of information in this repo is done at the risk of the user. These risks may include catastrophic failure of the device or infringement of patent or copyright laws. California Polytechnic State University at San Luis Obispo and its staff cannot be held liable for any use or misuse of the project.

Contents

List of Tables	iv
List of Figures	v
Executive Summary	vii
Chapter 1: Introduction	1
Problem Definition	1
Objectives	1
Quality Function Deployment	3
Formal Engineering Requirements	5
Management Plan	6
Project Management	7
Chapter 2: Background Research	8
Types of Antennas	8
Materials	11
Alternate Structures	12
Hoberman Spheres	12
Inflatable Structures	12
Current Products	13
AENEAS	13
AstroMesh Deployable Mesh Reflector	14
LightSail-1	15
Manufacturing and Testing	16
Investment Casting	16
Electronic Discharge Machining (EDM)	16
Coordinate Measuring Machines	16
Chapter 3: Design Development	16
Ideation	16
Top Concepts	18
Concept Selection	24
Feasibility	26
Chapter 4: Final Design	27
Developing the Nonagon	27

The Nonagon.....	30
Paraboloid: Mesh and Net Design	32
Telescopic Mast	33
Materials and Cost.....	34
Truss Structure	34
Parabolic Dish: Mesh and Netting	34
Cost Breakdown.....	35
Analysis and Further Testing.....	35
Truss Analysis.....	36
Paraboloid Systematic Error	37
Telescopic Tubes.....	39
Design Verification Plan.....	40
Manufacturing, Assembly, and Maintenance	41
Truss Manufacturing	41
Truss Assembly.....	42
Paraboloid Mesh and Net Assembly	42
Maintenance	43
Failure Modes and Safety	43
Chapter 5: Product Realization.....	46
Manufacturing.....	46
Sliders	46
Vertices	49
Struts:.....	53
Spacers:.....	55
Eye Hooks:.....	55
Cap Plugs:	56
Assembly	57
Truss Assembly.....	57
Net Assembly.....	60
Realized Design	62
Chapter 6: Design Verification.....	64
Physical Inspections	65

Thermal Testing:	65
Structural Testing:	67
Cable Tie Testing:	68
Vibrational Testing:	68
Chapter 7: Conclusions	69
References	70
Appendix A: Quality Function Deployment	72
Appendix B: Final Drawings	73
Revision A Drawings – From Detailed Design	73
Revision B Drawings: From Realized Product	80
Appendix C: Vendor List	85
Appendix D: Component Specifications and Data Sheets	86
Appendix E: Detailed Supporting Analysis	93
Appendix F: Gantt Chart	109
Appendix G: Operators Manual with Safety Guidelines	111
Appendix H: Detailed Budgets	112
Appendix I: Concept Design Hazard Identification Checklist	114
Appendix J: Future Work and Recommendations	116

List of Tables

Table 1: List of required and the corresponding optional goals for the deployable satellite system (DAS).....	2
Table 2: Requirements based on customer voice.....	3
Table 3: Weighted importance of engineering measures, extracted from updated QFD and customer requirements	4
Table 4: Formal Engineering Requirements for the CubeSat Antenna Deployment System.	5
Table 5: Timetable of relevant milestones and their associated due dates.....	7
Table 6: Material properties comparison (MatWeb, 2014).....	11
Table 7: Results of initial brainstorming session.....	17
Table 8: Pugh matrix used to narrow down concepts.....	18
Table 9: Decision matrix identifying top concept.....	24
Table 10: Complete cost breakdown of the project by part.....	35
Table 11: Characteristics of the Telescopic Tubular Mast compared with predicted CubeSat values.....	39
Table 12: Design Verification Plan of required design specifications.....	40
Table 13: Potential failure modes with critical numbers at or over a threshold of 60.....	44
Table 14: Tools used to CNC Mill sliders.....	46
Table 15: Tooling used to CNC facing fixture	48
Table 16: List of CNC tools used to make fixture for vertices.....	50
Table 17: List of tools used to make test struts	54
Table 18: Testing results for realized Nonagon.....	64

List of Figures

Figure 1: Yagi-Uda antenna radiation pattern (Poole, Yagi Antenna/Yagi-Uda Antenna, 2014)...	9
Figure 2: Parabolic antenna gain (Poole, Parabolic Reflector Antenna Gain, 2014).	10
Figure 3: Focal, Cassegrain, Gregorian reflectors (Poole, Parabolic Reflector Antenna Feed Systems, 2014).....	10
Figure 4: Off axis reflector (Poole, Parabolic Reflector Antenna Feed Systems, 2014).	11
Figure 5: Hoberman Sphere expanded and collapsed (Hoberman Associates, Inc., 2014).	12
Figure 6: Depiction of the USC/SERC Aeneas satellite when deployed (Kramer, 2012).....	13
Figure 7: Depiction of the USC/SERC Aeneas satellite while stowed inside the CubeSat housing (Kramer, 2012).....	13
Figure 8: Rendering of the AstroMesh when deployed	14
Figure 9: Rendering of the AstroMesh reflector.....	15
Figure 10: LightSail-1 with deployed solar sail (Davis, 2014).	15
Figure 11: Ideation based on inflatables and biomimicry.	17
<i>Figure 12: AstroMesh in the process of deploying</i> (Marks, Keay, Kuehn, Fedyk, & Laraway, 2012).....	19
Figure 13: Hat rack concept design sketch.....	20
Figure 14: Flower petal concept sketch.....	21
Figure 15: Depiction of a TEMBO® deployable structure (TEMBO Deployable Structures, 2014).....	21
Figure 16: Deck of cards demonstrating the idea of using revolved set of plates to form a circular disc	22
Figure 17: Schematic of the Hoberman Sphere expansion and contraction (Computers in Theory and Practice, 2013).....	22
Figure 18: Hoberman Sphere design concept sketch.....	22
Figure 19: Umbrella concept design.	23
Figure 20: Image of open USC/SERC Aeneas Satellite (Kramer, 2012).....	24
Figure 21: Sectional view of the deployed antenna with respect to a 6U CubeSat.	25
Figure 22: A single side of the drum truss structure showing its expansion and collapse.....	25
Figure 23: Drum concept wireframe generated in MATLAB.....	26
Figure 24: Collapsible square frame based truss structure.....	27
Figure 25: An early prototype of the drum support using a collapsible scissor frame.	28
Figure 26: Drum prototype in the deployed configuration, scaled up with 1cm = 1in.	28
Figure 27: Drum prototype in the stowed configuration, scaled up with 1cm = 1in.	29
Figure 28: Close up view of the slider and spring mechanism.....	29
Figure 29: Nonagon when fully deployed.....	30
Figure 30: Models of Nonagon components (Top: cap, slider, spacer, strut. Bottom: vertex).	30
Figure 31: Singular side of the Nonagon.....	31
Figure 32: Stowed Nonagon truss model.	31
Figure 33: Geodesic net pattern of multiple surfaces.....	32
Figure 34: Complete graph of the nonagon net design.	33
Figure 35: SolidWorks concept model of telescopic mast.....	33
Figure 36: Boundary conditions for gravitational loading.....	36

Figure 37: Graphical results of the paraboloid systematic error in centimeters derived from the nonagon net shape.....	38
Figure 38: Binding pattern for the Kevlar thread and carbon tow.....	43
Figure 39: CAM image of the slider during CNC code generation.....	46
Figure 40: Pattern of sliders after CNC machining.....	47
Figure 41: Soft jaw fixture used to face sliders to correct height.....	47
Figure 42: Fixture used to drill holes in winglets of sliders.....	48
Figure 43: Sliders mounted in vise of CNC machine.....	48
Figure 44: Sliders with holes after completion of CNC drilling operation.....	49
Figure 45: Tube stock cut to design length of vertices.....	49
Figure 46: Fixture used to mill slots of vertices.....	50
Figure 47: Stock milled down and used as support cores for vertices.....	51
Figure 48: Vertices mounted in vise of CNC machine.....	51
Figure 49: Fixture designed with deep bores for support cores. Two locating slots assist in aligning stock.....	52
Figure 50: Vertices with slots after completion of CNC milling operation.....	52
Figure 51: Fit check of sliders and vertices.....	53
Figure 52: Struts used for the final antenna prototype.....	53
Figure 53: Stock used to mill testing struts in CNC machine. Here, struts have already been cut off from stock.....	54
Figure 54: Fixture used to face down testing struts to the correct thickness.....	54
Figure 55: Jig used to drill holes in spacers.....	55
Figure 56: Stages of manufacturing (left to right) for the threaded eye hooks.....	56
Figure 57: Cap plugs inserted in vertices.....	56
Figure 58: Outline of vertex assembly steps (not to scale).	58
Figure 59: Left: Internal look at a vertex when truss is deployed (not to scale) Right: SolidWorks assembly of vertex and components.....	58
Figure 60: Scissor truss side assembly.....	59
Figure 61: SolidWorks side strut assembly.....	59
Figure 62: Carbon tied with Kevlar, initial test. Quarter provided for scale.....	60
Figure 63: Kevlar tied with Kevlar. Quarter background for scale.....	60
Figure 64: Test of single net line with tension ties.....	61
Figure 65: Net manufacturing jig.....	61
Figure 66: Render of the Nonagon with telescoping mast.....	62
Figure 67: The final assembled design with placebo mast and Kevlar tension ties connecting the truss to the mast.....	63

Executive Summary

CubeSats are an appealing platform for space exploration due to their low build and launch costs. Due to their small size, communication rates are often severely limited, preventing missions beyond low earth orbit. A low cost, high gain, high frequency antenna is needed to extend the capabilities of CubeSats.

The goal of the project was to design and build an axisymmetric parabolic antenna that could be deployed from a 10cm x 10cm x 15cm (1.5U) volume and operate at Ka band frequencies. The design selected consisted of an expanding perimeter truss supporting a tensioned mesh reflector. The perimeter truss was a nine sided polygon, or nonagon, with spring loaded scissor expanding sides.

The original scope of the project spanned the entirety of a functioning antenna. This included a feed horn, mast, reflector, full stowage and deployment hardware. Through the length of the project it became clear that it was too large an undertaking for such a short length of time, and the project was focused on the deployable perimeter truss.

The finished design met size and weight requirements and deployed successfully. Significant work is still left to produce a functioning reflector, and verify performance across all environmental conditions. Overall however, the drum tensioned reflector is a promising design for high gain CubeSat antennas and should be developed further.

Chapter 1: Introduction

Problem Definition

A CubeSat is a miniaturized, simplified satellite where one unit is equivalent to a 10cm x 10cm x 10cm volume. While CubeSat units provide a less expensive alternative for space research and other forms of academia, they have limited communication rates, which causes difficulty in sending these satellites beyond lower Earth orbit (LEO) where reliable high speed communication is crucial. Additionally, the instrumentation of CubeSat units is restricted by their relatively small internal volume. The combination of small volume and simplified designs makes optimizing signal communication challenging for CubeSats, especially when attempting to keep the units at a relatively low cost point.

Seeking a solution, NASA's Jet Propulsion Laboratory (JPL), the leading U.S. center for robotic exploration of the solar system, has requested the design of a compact, parabolic, deployable antenna that can be integrated with a CubeSat to provide the high gain required for long distance space communication. For this project, the objective was narrowed in scope from designing and prototyping the collapsible satellite dish, as well as the mechanism used to deploy the satellite system from a stowed position in the CubeSat unit to solely designing and prototyping the collapsible satellite dish and generating ideas for deployment mechanisms. The deployable antenna system (DAS) will be designed and manufactured with specifications that will allow for a feed antenna and other electrical or mechanical components to be installed after the completion of this stage of the project.

There are key requirements that JPL has proposed for the DAS, including optional stretch goals that can be adopted into the design of the DAS if the time and resources are available. Main prerequisites for the design include: an antenna dish diameter of 0.5m, a 0.05m feed hole at the dish vertex, a mass less than 1kg, and a stow size that will fit within a 1.5U CubeSat unit. Of the optional stretch goals provided by JPL, it was decided that a larger diameter of 0.75m would take priority since a larger dish diameter provides higher gain, enabling longer distance transmissions. However, it was quickly determined by the team that reaching the minimum requirements would be a challenge, and the stretch goals were eliminated.

Manufacturing, assembly, and testing of the DAS and its sub-components was completed by the team members assigned to this project using machines and instrumentation available at California Polytechnic State University (Cal Poly). However, for the design specifications that include extreme deployment or operation temperatures and precise surface tolerances, testing was optional or may be completed with the assistance of JPL at a later date as these testing environments are more difficult to replicate in Cal Poly laboratories.

Objectives

The overarching objective of this project is to design, prototype, and test a compact deployable antenna that can be stowed within a 1.5U CubeSat while providing the high gain necessary for deep space network (DSN) communication. The main area of focus for the project is the development of a collapsible satellite dish, with a secondary focus on the mechanism that will deploy the satellite dish from a stowed position. Due to the small volume available for DAS, the prototype will require a design that occupies minimal space within the CubeSat unit, while still preserving the ability to deploy into an effective high-gain antenna.

The key requirements established by JPL for the design of DAS will serve as a guide for the development of the prototype function and testing requirements. Stretch goals for this project have also been provided by JPL and will be implemented into the design if all key requirements have been met in the early stages of the project. Testing will be done to ensure that the final design satisfies the key requirements laid out by the sponsor. A list of required and stretch goals for the DAS can be found below in Table 1.

After further evaluation of the project proposal for the deployable antenna system (DAS), JPL has concluded that the required goals stated in the proposal are to be carried out as planned with only a few minor changes to nominal values. Stretch goals for DAS will only be pursued if the required goals have been met, and it is still early in the detailed design phase.

As requested by JPL, the nominal surface tolerance of DAS was changed from the original value stated in the project proposal. The proposal noted a required surface tolerance of 0.4mm RMS, with no stretch goal options. However, the required surface tolerance has been changed to 0.56mm RMS, with an optional stretch goal of 0.4mm RMS. Antenna signal transmission and data rates depend on the surface accuracy of the reflector, and so small tolerances would be ideal for this application. However, achieving increasingly tight tolerances will prove to be difficult, may require more time to achieve, and can increase the overall cost of the project.

Table 1: List of required and the corresponding optional goals for the deployable satellite system (DAS).

Required Goals	Stretch Goals
Deployable axisymmetric parabolic antenna ¹	-
Antenna Diameter of 0.5m	Increase antenna diameter to 0.75m
f/D = 0.5 (Ratio of focal length to dish diameter)	-
0.05m feed hole at vertex of dish	-
RF Ka Band, ~34 GHz	Increase frequency to 37.5 GHz
Design Temperature Deploy, -15 C to 20 C (AFT)	-
Operation Temperature, -70 C to 110 C (AFT)	-
Functional Torque/Force Margin > 100%	-
Mass < 1kg	Keep mass of upgraded unit below 1.75 kg
Spacecraft based on 6U CubeSat	-

¹ One concept features an off axis design, which deviates from the axisymmetric and f/D requirements listed in Table 1.

Stow within a 1.5U CubeSat	Stow upgraded unit within a 2.5U CubeSat
Surface Tolerance of 0.56mm RMS (Manufacturing, thermal, and systematic errors)	0.4mm

Quality Function Deployment

In order to rank the key requirements for this project, Quality Function Deployment (QFD), also known as “House of Quality,” was used to identify the project needs that are stressed by the voice of the customer. In our case, we had a singular customer – JPL. QFD takes the engineering design requirements, and matches them with the quality needs of the customer in order to establish levels of importance that best reflect what the customer is looking for in a design. QFD helps transform the voice of the customer (VOC) into criteria that define the engineering specifications of a product.

Using suggestions from the customer, other alterations were made to the QFD to improve legibility of the matrix. A “Goal” row was added at the top of the “Measures” section to show the desired improvement direction for a given engineering measure. The target values under “Measures” were also separated from the technical specification in order to improve clarity of this information.

From the QFD, it was determined that light weight, high data rate, and space required were the most critical design parameters voiced by JPL for the deployable satellite project. The three design parameters mentioned above will have priority during the design phase of the project, with all other parameters following in order of importance. From the project proposal, JPL suggested minor changes to the levels of importance for the design parameters of DAS which have now been implemented. The updated rankings are depicted in Table 2.

Table 2: Requirements based on customer voice.

Customer Voice	Level of Importance 1 (low) to 5 (high)
Light Weight	4
Low-Cost	3
Durability	4
Surface Finish	1
High Data Rate	5
Size/Space Required	5
Compactness	5

While the levels of importance for durability, high data rate, and space required remained unchanged from the original project proposal, the other design needs were changed to reflect the suggestions of the customer.

Weight is an important factor for the payload limit of the spacecraft transporting the CubeSat to the outer orbits of Earth. While important, it was suggested to not be as crucial as, for example, high data rate. For this reason, the importance of lightweight was demoted from Level 5 to Level 4. Because CubeSat units are intended to be a low cost avenue into space exploration, the customer suggested increasing the level of importance of low-cost from Level 2 to Level 3. The surface finish of the final assembly, not including the reflective radio frequency (RF) surface, plays no major role in the strength of the RF signal being transmitted by the antenna. The importance of “high data rate” accounts for the improved surface finish of the reflective surface (e.g. antenna dish), making all other surfaces of the assembly inconsequential. In order to remove this ambiguity, the customer voice for “surface finish” represents all non-reflective surfaces. For this reason, it was suggested to reduce this need from Level of 4 to Level 1. Compactness corresponds with the stow space required for storage within the CubeSat unit, and it is beneficial to improve the compactness of a design that has a limited work space. The work space for this project is a 1.5U CubeSat, and increasing the compactness of DAS allows for more space that can potentially house other instruments for various experiments. JPL suggested an increase in the level of importance for compactness from a Level 3 to a Level 5.

The engineering specifications were also weighed against the voice of the customer using the QFD chart, where the antenna diameter and surface tolerance resulted as the two most important design specifications for the deployable antenna. The weighted importance results presented in Table 3 are extracted from the QFD. These weights are calculated by determining strong, medium, and weak correlations between the design parameters voiced and the engineering measures, and then multiplying the importance of the design parameter (1-5) by each correlation in the parameter’s row. Next, in each column of engineering measures, the results of this correlation multiplication are summed. Finally, those column totals are added together to determine the overall weight, and each column total is divided by the overall weight and multiplied by 100. This calculation generates the weights seen below in Table 3.

With the updated customer needs now ranked appropriately, a new QFD matrix was generated to reflect the weighted importance of these needs with their new levels of importance for the DAS design. The levels of weighted importance were again calculated by matching the engineering specifications of the DAS to the needs of JPL, and determining whether a strong, medium, or weak correlation exists between the two subsets of design requirements. The updated results of the QFD analysis are depicted in Table 3 and the new QFD chart used to generate these results can be found in Appendix A.

Table 3: Weighted importance of engineering measures, extracted from updated QFD and customer requirements

Engineering Measures	Weighted Importance (%)
Antenna Diameter of 0.5m	26.03
f/D = 0.5 (Ratio of focal length to dish diameter)	12.17

0.05m feed hole at vertex of dish	9.36
RF Ka Band, ~34 GHz	8.61
Design Temperature Deploy, -15 C to 20 C (AFT)	0.75
Operation Temperature, -70 C to 110 C (AFT)	2.25
Mass < 1kg	8.05
Stow within a 1.5U CubeSat	16.85
Functional Torque/Force Margin > 100%	0.75
Surface Tolerance of 0.56mm RMS (Manufacturing, thermal, and systematic errors)	15.17

As noted in Table 3, the antenna diameter, 1.5U stow space, and surface tolerance resulted as the three most important design requirements for the DAS. The new weighted design specifications will be prioritized accordingly as the design phase progresses for the DAS.

Formal Engineering Requirements

Additionally, in accordance with the QFD, we created a formal engineering requirements table, Table 4, which relates our engineering specifications with a corresponding requirement, tolerance, risk and compliance. The risk of each specification is determined as either high, medium, or low (H, M, L) and indicates the difficulty of meeting each requirement. The compliance column outlines how we will verify that each requirement is met. These compliance requirements may be verified by Testing (T), Inspection (I), Analysis (A), or Similarity (S) to existing designs.

Table 4: Formal Engineering Requirements for the CubeSat Antenna Deployment System.

Spec	Description	Target	Tolerance	Risk	Compliance
1	Dish Diameter	0.5 m	+0.25 m	H	I
2	Focal Length to Diameter Ratio	0.5	None	L	A, I
3	Feed Hole Size	0.05 m	None	L	I
4	RF Ka Band	34 GHz	+3.5 GHz	H	A, T, S
5	Deploy Temperature	-15°C to 20°C	Within range	L	T
6	Operation Temperature	-70°C to 110°C	Within range	H	A, S
7	Surface Tolerance (RMS)	0.56 mm	-0.16 mm	H	A, T, I
8	Mass	<1 kg	None	M	T
9	CubeSat Stow Size	1.5U	None	H	I
10	Functional Torque/Force Margin	>100%	None	L	A, T
11	Cost	<\$7000	None	L	I

Our highest-risk engineering targets were determined as dish diameter, Ka band, operation temperature, surface tolerance, and stow size. These were identified as high risk requirements through research of similar systems. The diameter is high risk because it determines the overall size of the reflector, and the CubeSat stow size is high risk for the same reason, with the inclusion of any other support or deployment structures. Ka band operation, operation temperature range, and surface tolerance are all high risk because of their interrelated nature and the fact that achieving high data rates is the principal purpose of the DAS.

Management Plan

A management plan is necessary for continuous progress through the design, build, and test process. In order to allow team members to feel confident in the project and management, their roles were chosen based on individual strengths and competency, as such our team broke up the management roles into overarching or general roles and section specific leads. Our team was broken into four general roles: budgeter, communicator, data manager, and manager.

General Project Roles

Budgeter: Juan Togual

- Tracks team budget and expenditures
- Approves all purchases

Communicator: Peter Rivera

- Communicates with our sponsor via email, phone, etc.
- Schedules team meetings and sends out task assignments

Data Manager: Dominic Doty

- Organizes and tracks all digital and physical information

Manager: Sarah Bolton

- Assigns general tasks to team members and follows up on task progress
- Enforces team contract

Aside from their major roles, each member functioned as either a section lead or section support. Section leads acted as managers for various subsets of the project such as Analysis, Modeling, Manufacturing, and Testing. The rest of the team then supported the section lead by completing smaller, necessary tasks that lay within the member's skill level and the scope of that subset. These roles became incredibly important over the project's timeline and, as strengths became more apparent, transitioned leads around halfway through the project.

Section Leads

Analysis: Juan Togual, Dominic Doty

- Structural Analysis
- Thermal Analysis
- Dynamic Analysis

Modeling: Sarah Bolton, Dominic Doty

- Produce solid models (SolidWorks)
- Determine driving tolerance locations
- Create detailed component and assembly drawings
- Compile B.O.M.

Manufacturing: Peter Rivera, Sarah Bolton

- Ensure manufacturability throughout entire design process
- Assist in developing fabrication process for the design
- Handle machining, welding, casting, and overall assembly of the final product
- Determine the best manufacturing process for each component

Testing: Juan Togual, Peter Rivera

- Select which testing methods most accurately demonstrate the fulfillment of the requirements
- Compile test data in a meaningful way
- Determine any improvements that should be made based on test results.

Project Management

The design process followed a typical industry model of design, build, and test with periodic design review checkpoints to ensure timely delivery of a product that fulfills the sponsor's needs. The major sections of the process are defining the problem and establishing requirements, concept generation, concept selection and approval, detailed design, manufacturing, testing, and a final report of results. Table 5 displays a timetable of the project's milestones and major deadlines.

Table 5: Timetable of relevant milestones and their associated due dates.

Item	Date
Preliminary Design Report and Review	December 5, 2014
Critical Design Report and Review	February 12, 2015
Manufacturing and Test	March 2015 – May 2015
Senior Design Expo	May 29, 2015
Final Project Report	June 5, 2015

This report is the last of these milestones: the Final Project Report. The team has researched the issue presented by the sponsor to understand the underlying mechanics of the system, previous solutions to the problem, and gather more information about spaceflight in general. Using this information we were able to fully understand the problem and condense the project to a few core goals. We then used the Quality Function Deployment method, discussed in the Objectives section and found in Appendix A, to determine key design requirements. Then, we used our research and understanding to generate a Gantt Chart with its associated Task Breakdown table, found in Appendix F, and plethora of potential solutions to the problem. These potential solutions were then narrowed down into a single concept with associated initial

calculations. This concept was prototyped extensively and iterated to become a functioning initial design. The functional prototype assisted the team in making design decisions, choosing materials, and generally reducing complications that arose. The initial design was then further altered until a consensus was reached that our design fixed any known complications. A second, scaled prototype was then fabricated based off the initial design to ensure that all the known complications had been fixed. Finally, the team manufactured and tested our final product. Manufacturing, assembly, and test plans were generated. All components were ordered, created, or outsourced. Throughout the manufacturing and assembly process, small components or segments were tested to ensure suitability. The net and truss were assembled and tested as a completed product.

This Final Project Report covers the full extent of the design, build, and test process. It covers all background research, concept generation and selection, detailed design and analysis, manufacturing, assembly, and testing results. The success of the project compared to the problem statement and requirements is evaluated and any improvements or future plans are noted. This document allows the complete design history to be passed off to the sponsor with the prototype.

Chapter 2: Background Research

To better understand the problem at hand, a variety of areas pertaining to the design of a space communications system were researched. The main areas of inquiry were types of antennas, properties of common aerospace materials, and similar products in the design space. The types of antennas researched included Yagi-Uda, horn, and parabolic. Some brief background information on directivity and gain of antennas was included to support general knowledge of radiofrequency communications. The materials section covers information about aerospace materials frequently used for their low coefficients of thermal expansion, high specific strength, and low out-gassing. Finally, other existing antenna solutions, including Aeneas and AstroMesh Deployable Reflector, were researched to see what has already been done in the field.

In addition to the above research, sections have been added to address areas of interest that arose during idea generation and the final design stage. These include research on inflatable structures, thin plastic films, LightSail-1, Hoberman spheres, greater depth of research on the AstroMesh Deployable Mesh Reflector, and manufacturing methods. Similarly, during the manufacturing and testing phase, research into coordinate measuring machines occurred in order to assist in parabolic shape and component measurements.

Types of Antennas

A wide variety of antennas are used for various radiofrequency (RF) applications. The purpose of an antenna is to convert RF waves to electrical signals. Gain, in decibels isotropic (dBi), is a measurement of the efficiency of this conversion. Decibels isotropic compare the gain of an antenna to that of an ideal isotropic radiator, which radiates evenly in all directions. Since real RF waves have both magnitude and direction, dBi is affected by both the electrical efficiency of the antenna as well as its directivity, or how focused the radiation is in one direction.

For almost all applications of antennas, high electrical efficiency gain is desirable; however, in terms of directivity demands vary. Due to the radiated RF being focused in a smaller area, a directive antenna has a higher gain than a non-directive antenna of the same electrical

efficiency. Directivity can be desirable in some applications but not in others because of the smaller RF area. A FM radio station with a transmission antenna on top of a mountain would not consider a directive antenna as ideal, since a radio station wants to transmit over a large area, and not one particular area. On the other hand, a satellite would be better suited by a highly directive antenna because its transmissions need only be received in one small area of earth, and radiation directed into space would serve no purpose. For this reason, we tailored our research to highly directive antennas (Poole, Parabolic Reflector Antenna Gain, 2014).

Several common types of directive antennas are Yagi-Uda, horn, and parabolic. The Yagi-Uda and parabolic antennas are probably the most common types of directional antennas used in consumer applications. The Yagi-Uda antenna produces a radiation pattern with one main lobe, or area of high intensity. This is main lobe is typical of a directive antenna, with smaller lobes in other directions.

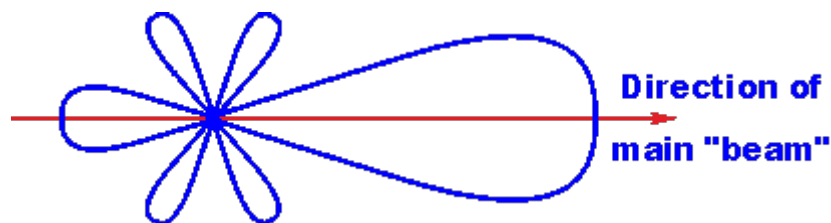


Figure 1: Yagi-Uda antenna radiation pattern (Poole, Yagi Antenna/Yagi-Uda Antenna, 2014).

Yagi antennas are limited to a gain maximum of about 20 dB (Poole, Yagi Antenna/Yagi-Uda Antenna, 2014), making them impractical for our application. Another issue with Yagi antennas is that they are typically based on a half wave dipole antenna. For the very high frequencies we are operating at, this makes the antenna impossibly short.

Horn antennas utilize a horn shaped waveguide to channel radiation into the driven element. These antennas are very directive and produce reasonable amounts of gain, on the order of 20 dBi. Horn antennas are classified by their shape: rectangular, cylindrical, and profile or spline. Rectangular horns are the most common form of horn antennas because of their ease of manufacture and are often used as reference standards for measuring gain. However, rectangular horns suffer from more spillover, or larger radiation intensity in an undesired direction. Cylindrical horns are typically smaller and more directive than rectangular, but also suffer from more cross polarization. Profile horn antennas are specially designed horns with a non-basic geometric shape that produce maximum gain with minimum cross polarization at the desired frequency. Often profile designs can suffer from low bandwidth or highly specific frequency requirements, but some designs can produce reasonable bandwidth at the cost of gain or polarization losses (del Rio Bocio, 2009).

Parabolic antennas are the most common antennas, with the most recognizable form being the satellite television receiver. Parabolic antennas utilize a paraboloid reflector that focuses RF energy into a single point. Typically, a horn type antenna is placed here to further guide the radiation into the driven element. Parabolic antennas are highly directive and provide exceptional gain, on the order of 30 to 40 dB (Poole, Parabolic Reflector Antenna Gain, 2014). Gain for the parabolic antenna is dependent on the size of the reflector with respect to the wavelength of the RF being transmitted, the efficiency of the driven element, and the accuracy of the reflective surface.

$$\text{Gain } G = 10 \log_{10} k \left(\frac{\pi D}{\lambda} \right)^2$$

Figure 2: Parabolic antenna gain (Poole, Parabolic Reflector Antenna Gain, 2014).

The gain of an ideal parabolic antenna is shown in Figure 2, where k is the efficiency of the feed antenna, D is the diameter of the reflector, and λ is the wavelength. The main reason why parabolic reflectors work so well is because all possible rays incident on the surface of the reflector travel the exact same distance to the focal point. This is desirable because if the waves travel different distances, they can be out of phase when they reach the feed antenna and cause destructive interference. For this reason, the reflector must adhere to the ideal paraboloid shape to within 1/20th of a wavelength.

Parabolic antennas can take several forms. The two main types are axisymmetric and off axis. Axisymmetric antennas are perfectly symmetrical around an axis drawn through the focal point and vertex of the paraboloid. Feed location can vary for axisymmetric designs, with the principal versions being focal feed, Cassegrain, or Gregorian as seen in Figure 3. Focal feed is the simplest, as the feed antenna is located directly at the focal point of the paraboloid. Cassegrain and Gregorian style reflectors both operate under the same principle, but add a second reflector just in front of or behind the focal point. In the case of Cassegrain reflectors, the second reflector is convex, while for the Gregorian it is concave. Both reflectors create a new focus point just behind the vertex of the larger reflector, and the feed is located there. One advantage of these reflectors is that a large feed and wiring for the feed do not need to be mounted in front of the reflector where they can block radiation from reaching the reflector. Another advantage of a dual reflector system is more uniform reflector illumination. Reflector illumination is dependent on the focal ratio F/D , with values closer to one being more favorable. Dual reflector designs have a much longer effective focal length than their focal feed counterparts, which in turn yields focal ratios much closer to one for a similarly sized main reflector (Love, Rudge, & Olver, 1982).

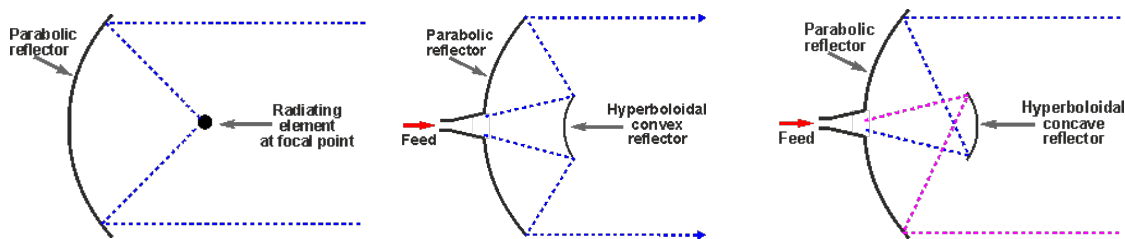


Figure 3: Focal, Cassegrain, Gregorian reflectors (Poole, Parabolic Reflector Antenna Feed Systems, 2014).

Off axis reflectors, such as the one shown in Figure 4, utilize a different portion of the paraboloid shape, namely an outer area that does not include the vertex. Placing the feed antenna off axis allows the feed to remain at the focal point while not casting a shadow on the reflector. This is advantageous as any area of the reflector that is blocked by the feed antenna is rendered useless. Satellite television receivers commonly utilize this type of system.

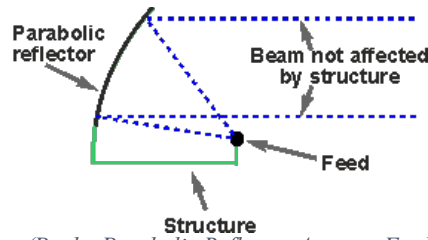


Figure 4: Off axis reflector (Poole, *Parabolic Reflector Antenna Feed Systems*, 2014).

Materials

Materials selection for satellite RF reflectors pose an interesting challenge because of the combination of broad thermal ranges, high accuracy requirements, and RF reflectivity. A deployed satellite antenna must withstand temperatures from over 110 °C down to -70 °C. An appropriate material must maintain high strength and stiffness over this range, with minimal thermal distortion. Zero gravity in orbit means that loads after deployment are relatively small, but the system must also withstand the rigors of launch. To prevent destructive interference, parabolic reflectors must also be very accurate to the ideal shape; therefore, they must not change shape over the operating temperature range, which necessitates a material with a low coefficient of thermal expansion (CTE). The accuracy requirements also create challenges in manufacturing, as the material must also be machinable. In addition, for a material to be reflective to RF signals, it must be highly electrically conductive. Conductivity can be added via post process plating to a material, but differing CTEs can cause fractures and delamination between the coating and the substrate.

Commonly used for a variety of purposes, metallized films are well known for their use as radiative insulation in the form of space blankets. Plastic films, commonly Mylar or Kapton, are vacuum metalized, typically with aluminum. This leaves a thin layer of aluminum on the surface giving the film extremely reflective characteristics and a lower surface resistance. Kapton also has the benefit of an extremely wide temperature operating range, quoted by DuPont to span from -269°C to +400°C (DuPont, 2011). The light weight, RF performance, and extreme flexibility of metallized films make them an excellent candidate for use in space antennas. Several common metallic and thin film materials are listed below in Table 6.

Table 6: Material properties comparison (MatWeb, 2014)

Material	Linear CTE [um/m°C]	Resistivity [Ohm-cm]	Density [g/cc]	Yield Tensile Strength [MPa]	Modulus of Elasticity [GPa]
Aluminum 7076-T61	21.6	4.30E-06	2.84	470	67
Beryllium	14.5	4.30E-06	1.844	240	303
BeNi M220C	14	2.87E-05	8.03	1100	180
Nitinol (Low Temp)	NA	7.60E-05	6.45	100	28
Nitinol (High Temp)	NA	8.20E-05	6.45	560	75
HexPly M47 Carbon Prepreg	NA	NA	NA	920	40
285 Kevlar Prepreg	NA	NA	NA	558	26.9
7791 E-Glass Prepreg	NA	NA	NA	372	20.7
48 Gauge Mylar	17.0	NA	1.39	179	NA
Kapton HN	20.0	NA	1.42	70	NA

Alternate Structures

Hoberman Spheres

Charles Hoberman invented several methods of construction of expanding truss structures, the most common of which is the Hoberman sphere, a common children's toy as seen in Figure 5. The toy has diameter ratio of 1.8 between the smaller and larger forms. This makes it an attractive scaffolding to build an expandable antenna upon. The great number of joints causes a general lack of rigidity; unfortunately, reducing the number of joints increases the collapsed diameter. Hoberman Associates has made several installations of metal spheres, which are significantly stronger than the toy version, but it remains to be seen if these spheres would hold the tolerances required. The sphere also proves attractive because of the integrated structure for mounting a secondary reflector or a feed horn. Hoberman structures are patented; however, the patent was granted in 1990 and has since expired. The Hoberman expanding structures as a whole are a possible support system for a deployable reflector (U.S. Patent No. 5024031A, 1990).

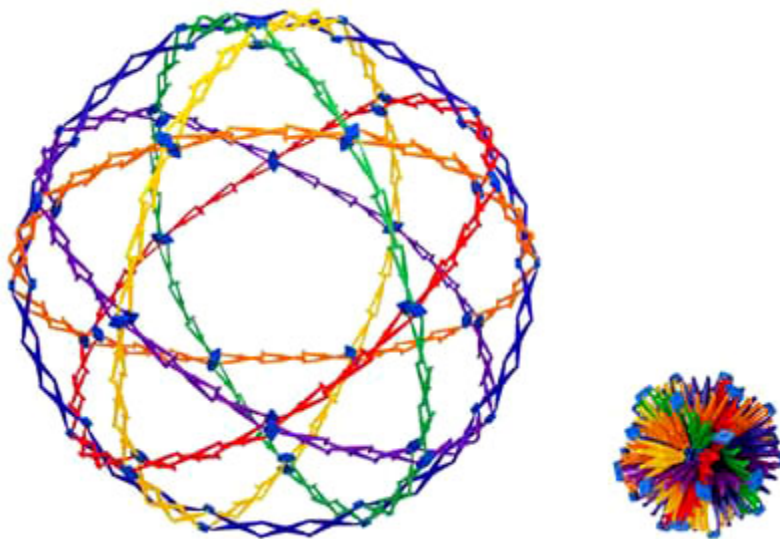


Figure 5: Hoberman Sphere expanded and collapsed (Hoberman Associates, Inc., 2014).

Inflatable Structures

Inflatable antennas have been investigated in the past, most notably the “Inflatable Antenna Experiment” launched on STS 77 in 1996. This mission used a 14 meter reflector constituted of an inflatable torus and three inflatable mounting struts. These were made of neoprene coated Kevlar fabric. The main reflector utilized a combination of Mylar and aluminized Mylar. Though not often utilized, “Inflatable structures allow low storage volumes, low cost, are lightweight and are easy to deploy” (Veldman & Vermeeren, 2001). Another proposed direction was to utilize inflatable structures that are filled with a two part expanding foam rather than gas. This eliminates any issue of the structure losing pressure over time, and also makes it immune to puncture. This design is seriously limited by the strict absence of pressure vessels in CubeSat units for safety of the primary launch load.

Current Products

AENEAS

Developed as a partnership project between students from the University of Southern California (USC) and Space Engineering Research Center (SERC), Aeneas is a 3U CubeSat that launched on September 13, 2012. The project's overarching goal was to design an antenna that could track the location of cargo containers at a global scale.

The design specifications of the Aeneas satellite called for a collapsible antenna that could be deployed from the 3U CubeSat housing. It was manufactured with a dish diameter of 0.5m and a reflective mesh that was supported by 30 ribs, which can be seen in Figure 6.

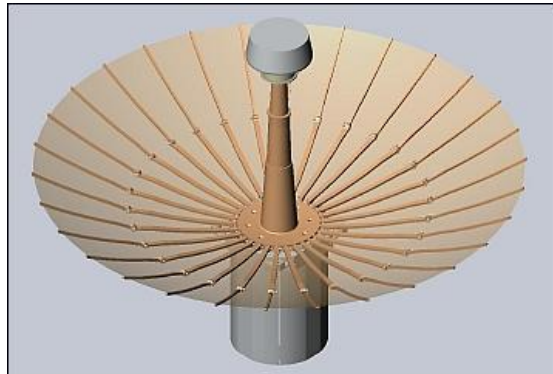


Figure 6: Depiction of the USC/SERC Aeneas satellite when deployed (Kramer, 2012).

Each rib is connected to a central hub. This central hub is contained within the CubeSat housing until the dish and antenna are ready to be deployed as shown in Figure 7. A spring attached to the base of the central hub is used to propel the hub out of the CubeSat housing, while a series of torsional springs in the rib joints extend the arms to form the full parabolic dish.

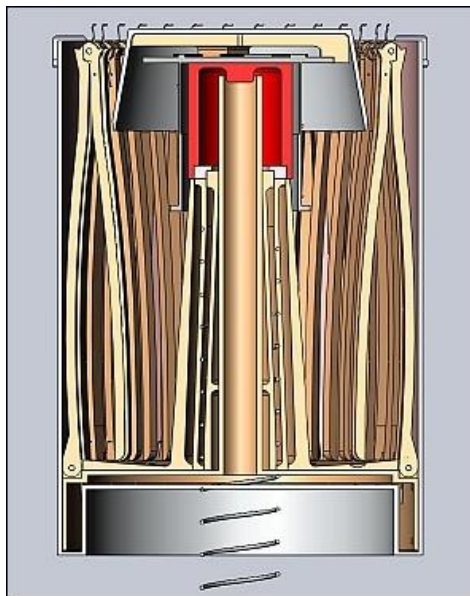


Figure 7: Depiction of the USC/SERC Aeneas satellite while stowed inside the CubeSat housing (Kramer, 2012).

Unfortunately, there are problems and risks that arise from using this type of design for a deployable antenna. Due to the complexity of the deployment mechanism and small internal

volume available within the CubeSat unit, the ribs must be retracted in unison. By retracting the ribs in unison, the formation of undesired torsional moments can be prevented, which keeps the deploying mechanism aligned and functioning. Since the base of the ribs are connected to the central hub of the satellite dish, any sudden upward force on the outermost link of the rib will induce stresses at both the midspan and base joints of the rib, which can cause misalignment. Therefore, the deployment scheme must be stowed and deployed in a slow and controlled manner to prevent mechanical failure or entanglement of the satellite dish mesh.

AstroMesh Deployable Mesh Reflector

AstroMesh is a family of deployable parabolic RF reflectors for use in spacecraft. The reflectors utilize a foldable graphite and aluminum truss as a rigid circular frame, which can be seen in Figure 8. The truss system is extremely lightweight and yields a net-zero coefficient of thermal expansion due to its design, providing an exceptionally accurate reflector surface at all temperatures.

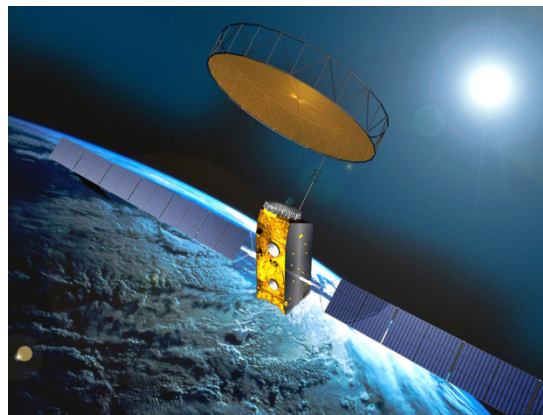


Figure 8: Rendering of the AstroMesh when deployed

The reflector surface itself is made of woven gold plated molybdenum wire, which is extremely stable in changing thermal conditions and conductive, making it a good candidate for an RF reflector. The molybdenum is woven into a mesh that gives it an elastic quality. Additionally, since the openings in the mesh are fine relative to the transmission wavelength, the mesh appears as an opaque surface to RF energy. As seen in Figure 9, the molybdenum mesh is stretched over the graphite truss similar to a drum, and then covered with a geodesic pattern of graphite tape. The same graphite tape pattern is stretched over the bottom of the truss. A connection is made between the two tape patterns at every vertex; by tightening these connections the molybdenum mesh is stretched into an approximation of the required reflector shape (Marks, Keay, Kuehn, Fedyk, & Laraway, 2012).

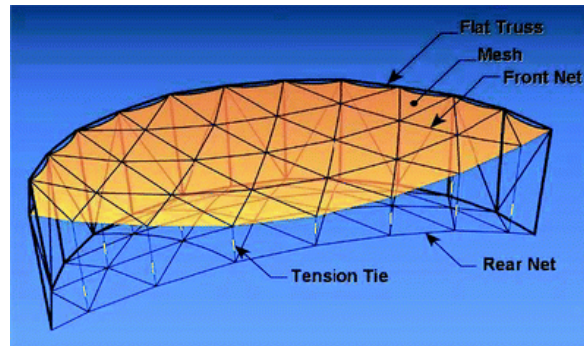


Figure 9: Rendering of the AstroMesh reflector

The AstroMesh deployable reflector utilizes an off axis design, which offers several advantages, including the ability to mount the feed directly inside the body of the satellite. This is beneficial because the need for more structures attached to the reflector is eliminated and the electrical routing is shortened.

Upon further research, we noted that the AstroMesh deployable truss utilizes parallelogram based collapse function. A circle is approximated by a series of parallelograms with variable length struts. Fixed diagonals and longerons, which makeup the perimeter of the rings, hold the large load of the tensioned reflector net. A single cable driven by a motor actuates the entire system, which can be driven slowly over a long period of time to expand the reflector to its full size. One feature of the structure is that the trusses latch into a shape at full deployment. This allows the motor to be deactivated after deployment is complete.

LightSail-1

LightSail-1 is a CubeSat based proof of concept for solar sailing. The spacecraft is a 3U CubeSat with the addition of a 350m² solar sail made of aluminized Mylar film 0.2 thousandths of an inch thick. The design uses four booms that deploy from the corners of the craft, which pulling the corners of the Mylar film with them. The booms are made of a coiled shape similar to a tape measure that extends in a rigid beam when uncoiled. All four booms are deployed by a single electric motor. The LightSail-1 concept shows the resiliency of aluminized Mylar, as well as its ability to compact. While the LightSail-1 structure is not useful for antenna design because it is flat, as seen in Figure 10, it does provide an interesting basis for large inflatable concepts (Overbye, 2009).

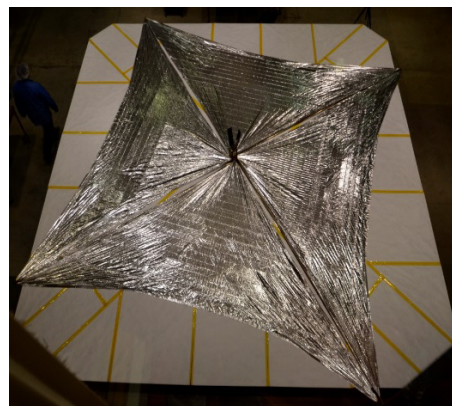


Figure 10: LightSail-1 with deployed solar sail (Davis, 2014).

Manufacturing and Testing

Investment Casting

Investment casting is a method based on lost wax casting allowing accurate reproduction of complex geometry parts. The parts are first replicated in wax, either by directly machining the wax or making a master die and casting wax replicas. The wax replicas are then assembled onto a tree sprue and dipped in a ceramic slurry or plaster. After the slurry hardens into a shell around the wax, the wax is melted out of the shell, which can now be used for casting. The process is longer and more involved than traditional sand casting or lost wax casting, but typically produces surface finishes on the order of 1.6 micrometers. This is a similar level of surface finish to milling or extruding. The major advantage of the process however is in its ability to create many identical parts very quickly (The Library of Manufacturing, 2015).

Electronic Discharge Machining (EDM)

Electronic Discharge Machining is a non-traditional machining method used to make complex geometries in hard to machine parts. A variety of different forms of EDM are used, commonly for tool and die making, as well as machining alloys that are too difficult to machine with traditional cutters. The main feature of interest for this project however is the wire based branch of EDM. This process uses a continuously moving thin wire electrode allowing the tool to cut small irregular holes or profile cuts in a variety of thicknesses of materials with extremely high accuracy. Typical wire EDM machining processes can achieve 0.004 mm accuracy with a 0.335 mm kerf. The ability to machine small features very accurately makes it a promising process for the manufacture of extremely small parts required for deployable reflectors (Xact Wire EDM Corporation, 2015).

Coordinate Measuring Machines

Coordinate Measuring Machines, CMMs, are used to precisely identify part features and characteristics, particularly with respect to other features. They utilize a CAD based part model and trace a probe tip along the surface or profile of a part as many times as prescribed by the machine operator. CMMs provide rapid feedback on part tolerances. Due to this rapid feedback and ability to measure complex geometries, our team considered using one to measure the parabolic shape of the net and mesh to determine if we achieved the correct shape. Unfortunately, the footprint of CMMs at Cal Poly are too small to fit our antenna without adapting the footprint through the use of a rotary table or other such equipment that would allow us to measure one section of the parabolic shape at a time.

Chapter 3: Design Development

Ideation

The initial brainstorming sessions split the CubeSat antenna deployment system into five major topics: mechanism, force, material, shape, and dish. The mechanism dealt with the process of creating the dish shape, force, the component causing the deployment motion. We then proceeded to write down as many different items in each topic as possible. Through the course of the session, we noticed that the dish ideas overlapped with other sections, namely the materials, mechanism, and shape sections. Therefore, we reassigned those ideas into the particular sections

they overlapped. This initial brainstorming session generated multiple ideas; however, no larger concepts resulted. From these lists, the impractical, ridiculous, dangerous, and unfeasible ideas were eliminated, leaving the ideas found in

Table 7.

Table 7: Results of initial brainstorming session.

Mechanism	Force	Material	Shape
Umbrella	Springs	Composites	Parabolic
Accordion	Pulley	Graphite	Off axis
Drum	Gas	Aluminum film	Multi-reflector
Inflatable	Magnets	Titanium	Array
Origami (Fold out)	Kinetic	Nitinol	
Flower	Solar/Thermal	Molybdenum	
Helical (Spin out)	Electrical	Gold	
Flaps/Fan blades	Motors	Beryllium	
Slides/Extending ribs	Foam/Chemical reaction	Thermosets/plastics	

Another brainstorming session focused on the unusual, but not unfeasible ideas such as inflation as a method of creating the dish shape or using solar power that were introduced during the initial session, these ideas expanded how we thought about our design. Figure 11, seen below, is an example of this session. After this session, we started thinking about protective materials, biomimicry and natural parabolas, and current products such as parachutes, telescopes, and grandfather clocks that had a particular trait which could be useful in our design.

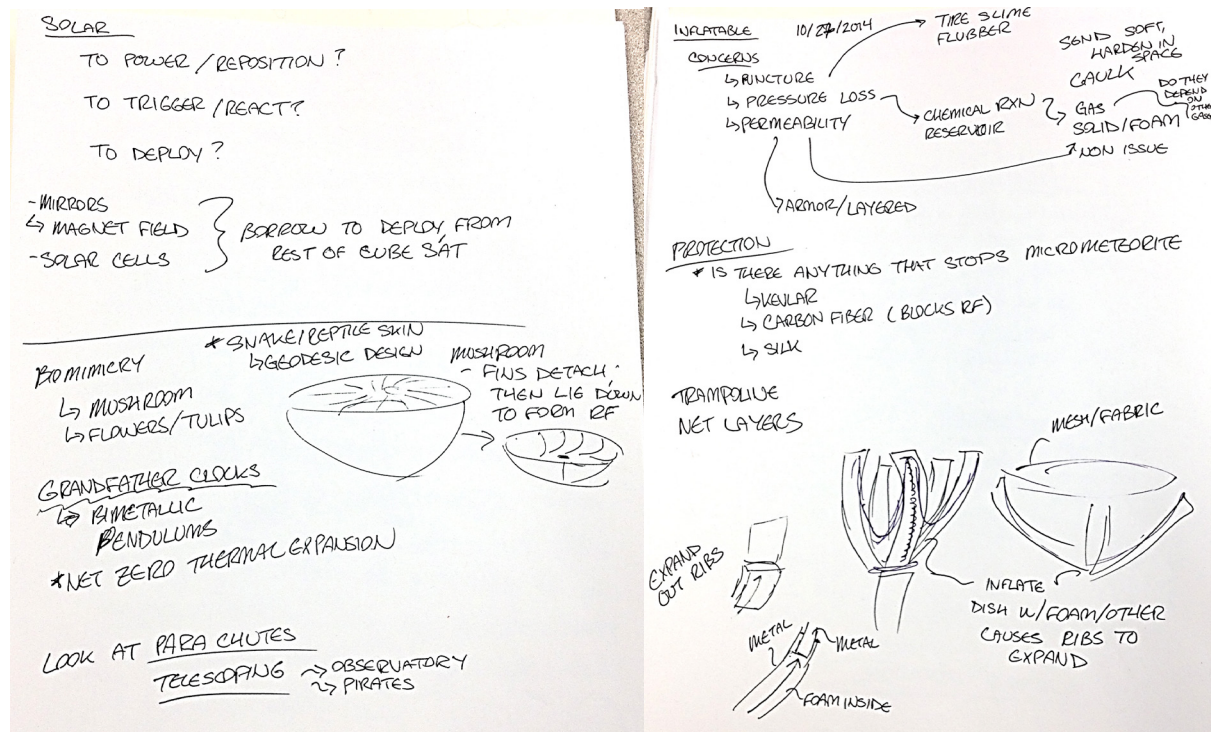


Figure 11: Ideation based on inflatables and biomimicry.

As a team, we utilized brainwriting, which is a silent, five minute process where each team member writes as many ideas as possible, then the papers are switched and the process repeats with the team members commenting and improving upon the other’s ideas until the paper returns to its original owner. At this point, we recognized that we had brainstormed many ideas, but few complete concepts. Therefore, each team member was asked to create three detailed concepts based off our previous discussions, idea generation sessions, and the three general dish design categories (rigid, mesh, and inflatable). Using a Pugh Matrix, seen in Table 8, we narrowed these twelve ideas down into five top concepts to further explore, augment, and develop before determining a final design.

Table 8: Pugh matrix used to narrow down concepts.

Type	Mesh				Rigid			Inflatable		
Concept	Umbrella (datum)	Drum Concept	Hat Rack	Hoberman's Sphere	The Fan Blade	Flower Petals	The Spreader	The Bloator	Inflatable Bag	The Accordion
Manufacturability	D	-	+	-	-	-	-	S	-	-
Rigidity	A	S	-	-	-	+	S	+	-	+
Mesh Surface Accuracy	T	+	+	+	S	-	-	S	-	-
Compactness	U	+	S	S	+	-	+	+	+	-
Feed Horn	M	+	S	+	-	S	-	-	+	S
Weight	D	S	S	-	S	-	-	-	-	S
Cost	A	S	S	-	S	S	S	-	S	-
$\Sigma+$	T	3	2	2	1	1	1	2	2	1
$\Sigma-$	U	1	1	4	3	4	4	3	4	4
ΣS	M	3	4	1	3	2	2	2	1	2

Top Concepts

Drum

The drum style reflector offers several distinct advantages over other styles of reflectors because of its extremely compact design and off axis feed. The major advantage of the off axis design is the ease of mounting the feed horn. All other design types require either a secondary reflector or a front mounted feed horn. This can block a significant portion of the reflector surface, reducing its efficiency. A front mounted structure also poses a significant kinematic challenge, as most axisymmetric designs house a significant portion of their linkages in the center of the reflector, directly where the secondary reflector or feed horn must be mounted. While this design is very similar to the AstroMesh reflector, seen in

Figure 12, research indicates that the patent (Thomson, 1997) on the AstroMesh reflector has recently expired.

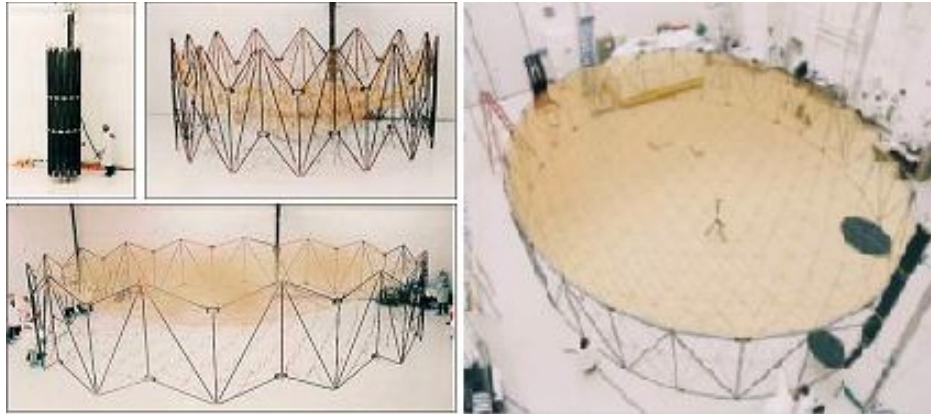


Figure 12: *AstroMesh* in the process of deploying (Marks, Keay, Kuehn, Fedyk, & Laraway, 2012).

Hat Rack

The hat rack idea involves a set of vertical ribs that are arranged in a circular pattern during the stowed position of the antenna mechanism. Preliminary conceptual design and drawing can be seen in Figure 13. Once deployment has been triggered, a compressed spring forces these ribs thru angled slots and allows the emerging ribs to form a conical frame like that of a funnel. An elastic mesh tied to the ribs would stretch along with the ribs to form the final conic surface that would be used to transmit RF signals. This concept design uses relatively simple parts while still providing the surface accuracy necessary for strong signal transmission. However, a drawback to this design is the lack of an ideal parabolic dish shape that is used to optimize data rates for satellites.

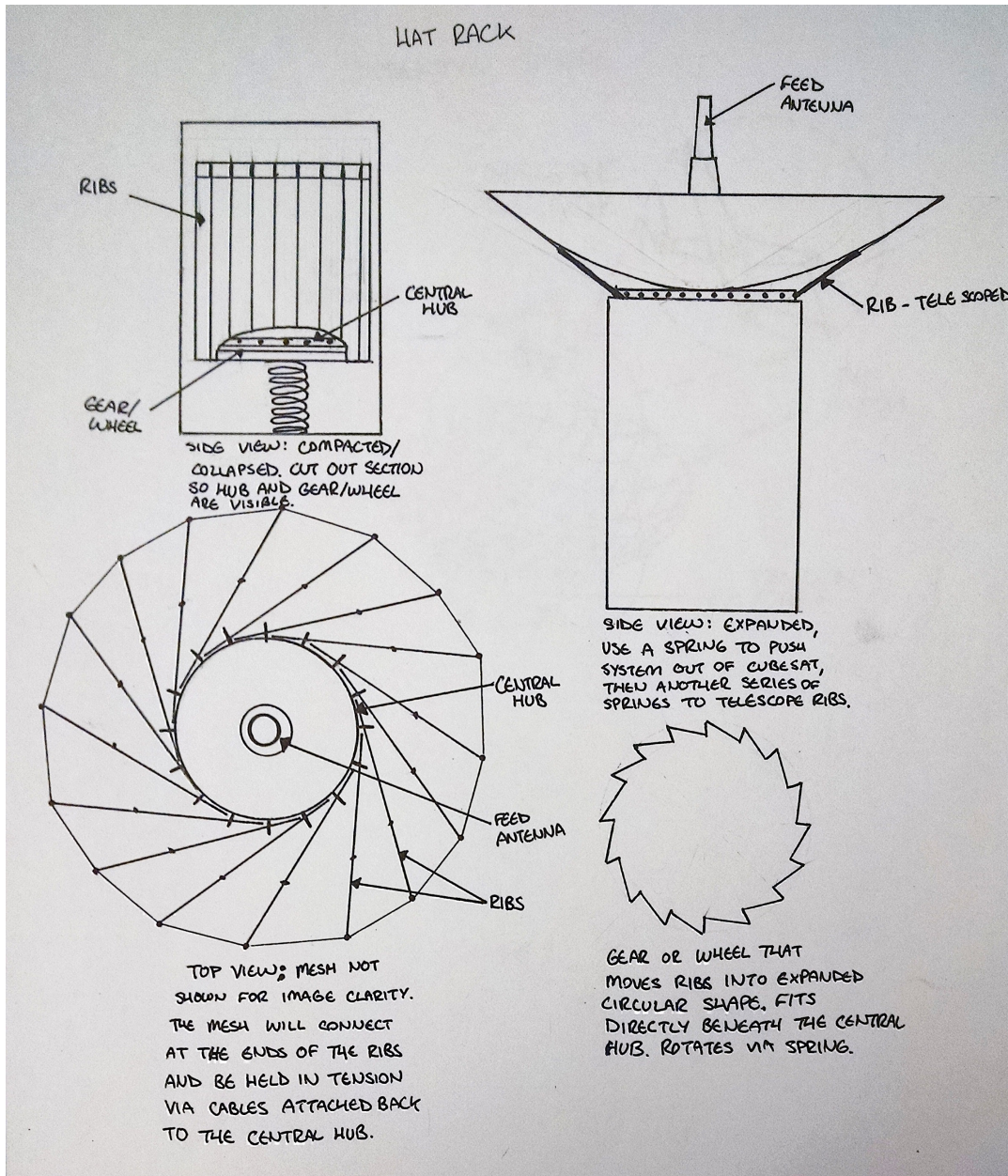


Figure 13: Hat rack concept design sketch.

Flower Pod or Petals

The flower pod was another concept design that is being considered for the DAS. This design would be stowed in the CubeSat in its “pod” form during transport to outer space, and deployed into the expanded form once the CubeSat is released into orbit. The concept sketch for this design is shown in Figure 14.

Flower Petal Design

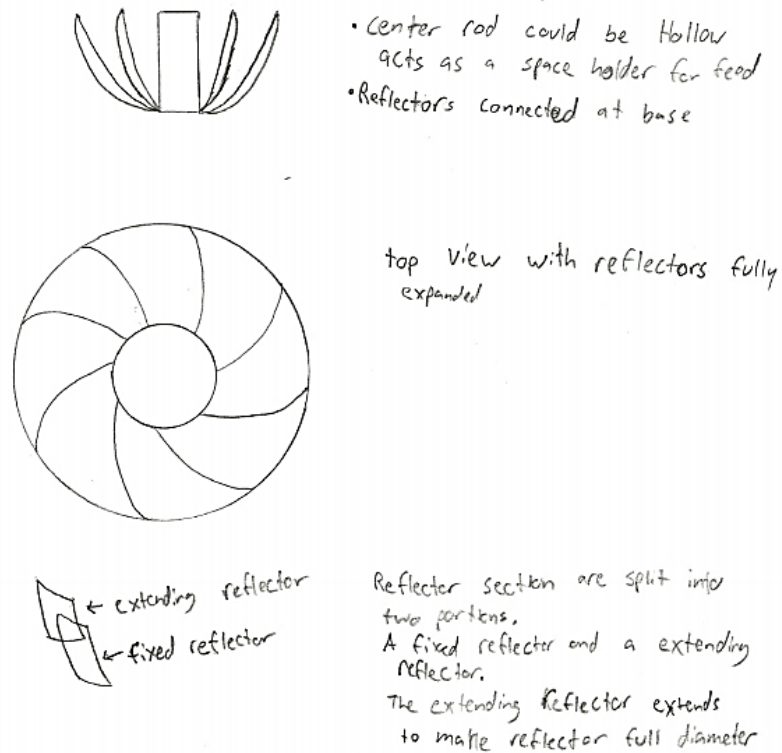


Figure 14: Flower petal concept sketch.

In Figure 15, the deployment of the flower pod can be seen. While this design can potentially provide a reasonable dish surface area, a careful stowage and deployment scheme would be necessary in order to minimize entanglement and failure of full deployment.

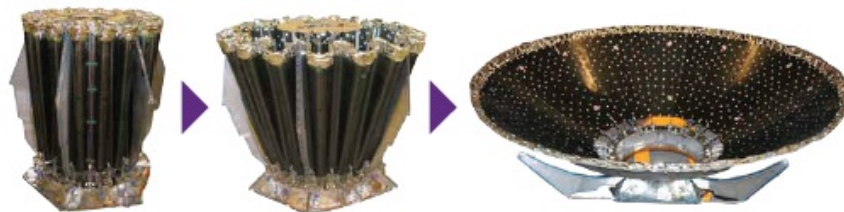


Figure 15: Depiction of a TEMBO® deployable structure (TEMBO Deployable Structures, 2014).

A stacked set of plates could also be revolved around an axis to form the circular surface of the antenna dish, as shown with a deck of cards in Figure 16. Since the plates would not be long enough to reach the required diameter of 0.5m, we would have to extend the plates to reach the required diameter. Meeting the diameter requirement with this design necessitated a process of stacking and connecting plates by extending ribs. While relatively simple in design, this type of arrangement could negatively affect signal transmission since the reflective surface would contain many “steps” from the overlay, and would not form the smooth surface that is ideal for

signal transmission. Another negative outcome is that the plate's surface would have to be machined to precise measurement and this will result in longer manufacturing times with added costs.



Figure 16: Deck of cards demonstrating the idea of using a revolved set of plates to form a circular disc

Hoberman Sphere

The Hoberman Sphere was also a favored concept design due to its compactness, which is displayed in Figure 17. Like the AstroMesh, the Hoberman Sphere is a relatively lightweight design with small and thin subcomponents, and has a large expansion ratio. However, this design also requires a complex assembly of components in order to form the expanded arrangement of circular support rings. One approach to design the deployable satellite dish is to use a hemispherical arrangement that will form the parabolic dish of the antenna as seen in Figure 18.

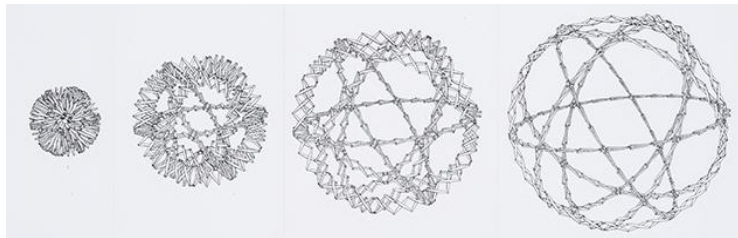


Figure 17: Schematic of the Hoberman Sphere expansion and contraction (Computers in Theory and Practice, 2013).

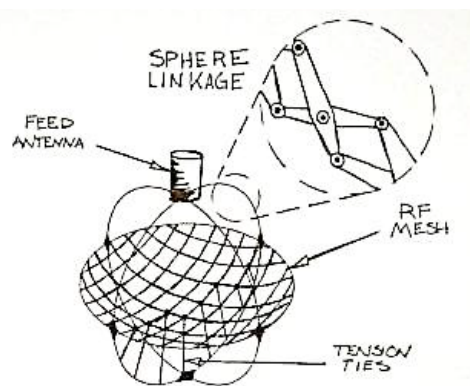


Figure 18: Hoberman Sphere design concept sketch.

Umbrella

An umbrella style design, seen in Figure 19, is not dissimilar from the Aeneas and other current products in the microsatellite high gain antenna segment. Using a series of articulating rigid ribs, the reflector unfolds from its compressed state like an umbrella, stretching an RF mesh

into an approximation of the ideal reflector. This design suffers from poor systematic error due to the flat surfaces between ribs.

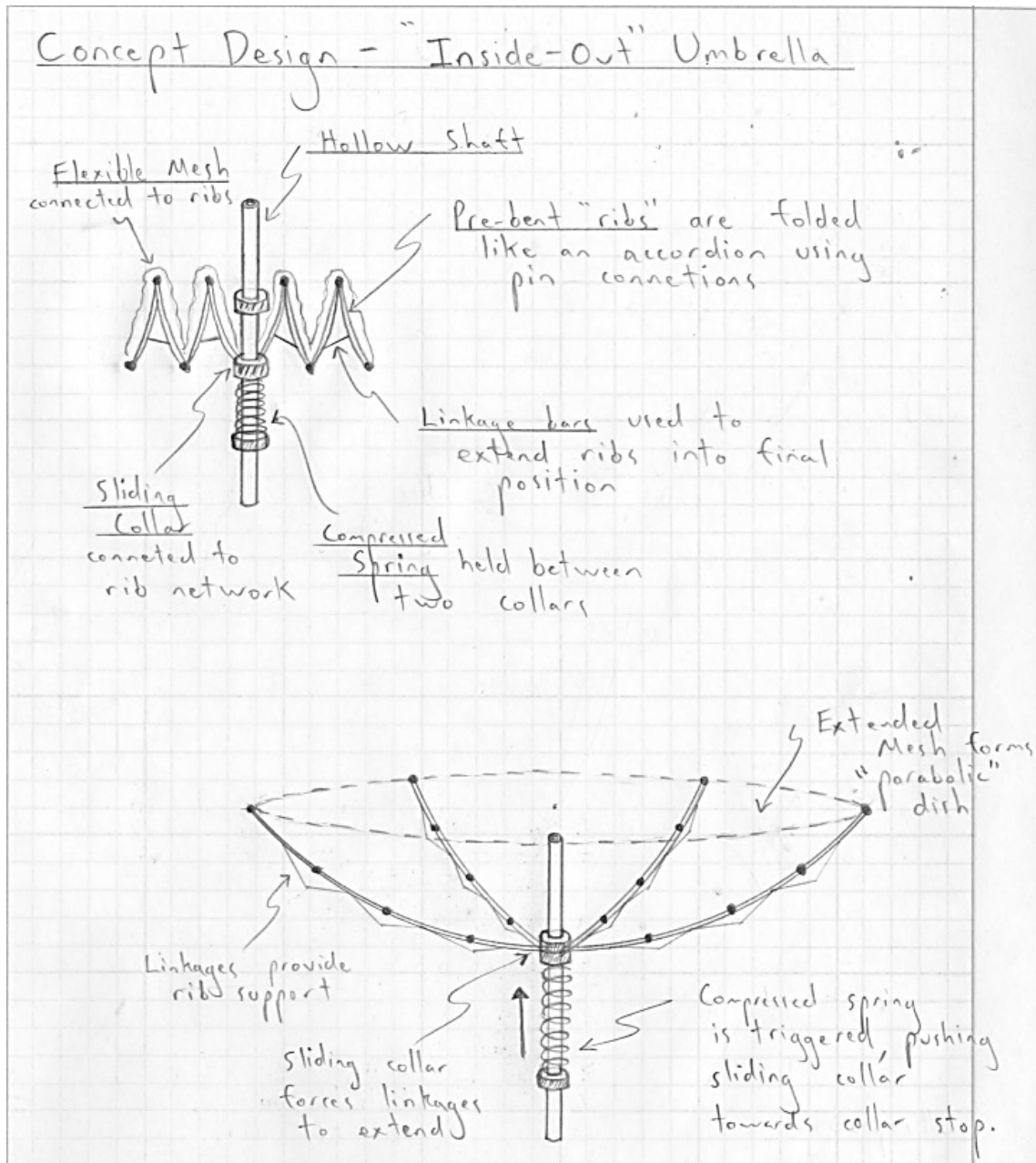


Figure 19: Umbrella concept design.

The number of ribs necessary to approximate a reflector is greatly increased by the much higher surface accuracy required by Ka band operation, as seen with Aeneas, Figure 20. This makes the umbrella style design less appealing.

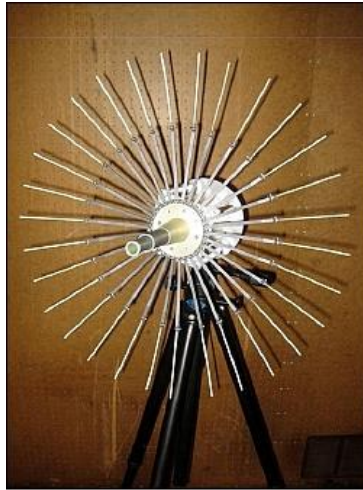


Figure 20: Image of open USC/SERC Aeneas Satellite (Kramer, 2012).

Concept Selection

Through the various ideation processes, a plethora of ideas were examined; however, only the five ideas previously discussed, with the umbrella concept functioning as a control evaluation, were deemed developed enough to continue as top ideas. To select the number one concept from these top concepts, a decision matrix was used. The decision matrix evaluates all the concepts on seven different criteria, where each criterion is given a weight to signify its importance. To compute the total score for each design, the design's score in each category is multiplied by the weight of that category, and then summed with all other categories. The decision matrix is shown below in Table 9.

Table 9: Decision matrix identifying top concept.

Category	Weights	Umbrella (datum)	Drum Concept	Flower Petals	Hat Rack	Hoberman's Sphere
Manufacturability	3.0	0.0	-1.0	-1.0	1.0	-1.0
Rigidity	2.0	0.0	0.0	1.0	-1.0	-1.0
Mesh Surface Accuracy	7.0	0.0	1.0	-1.0	1.0	1.0
Compactness	6.0	0.0	1.0	-1.0	0.0	0.0
Feed Horn	1.0	0.0	1.0	0.0	0.0	1.0
Weight	5.0	0.0	0.0	-1.0	0.0	-1.0
Cost	4.0	0.0	0.0	0.0	0.0	-1.0
Weighted Score		0	11	-19	8	-6

The categories directly correlate with customer requirements, while the weights and individual design scores were assigned via team discussion with respect to associated risk. The scores indicate the highest ranking concepts: drum concept, hat rack, and umbrella. There is a

large division between the top two concepts, the middle concept, and the lowest two concepts. This is advantageous because it provides a clear winner, the drum, and a backup design, the hat rack, should it be necessary. Figure 21 provides an overall look at the drum concept, while Figure 22 displays how the drum would collapse and expand to meet our engineering requirements.

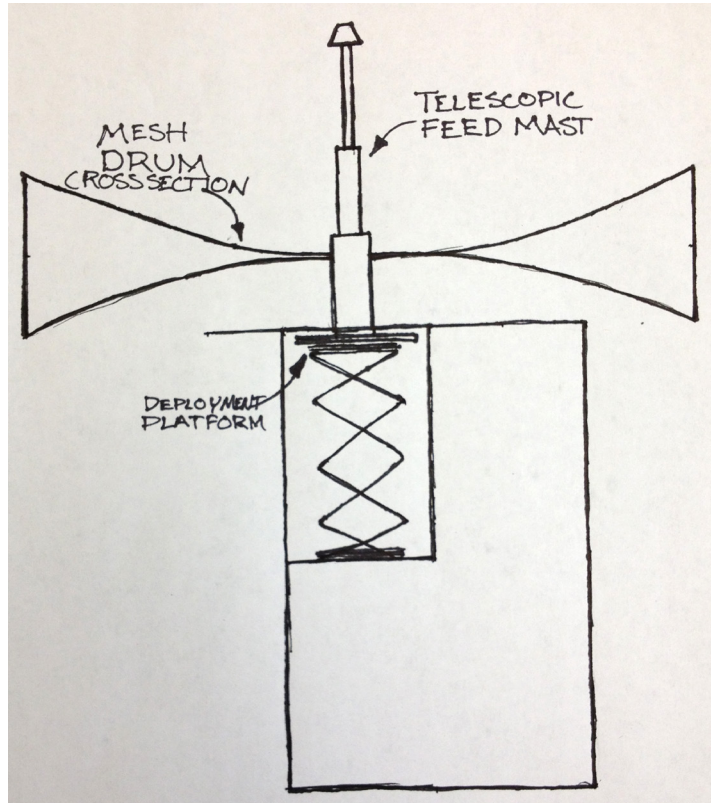


Figure 21: Sectional view of the deployed antenna with respect to a 6U CubeSat.

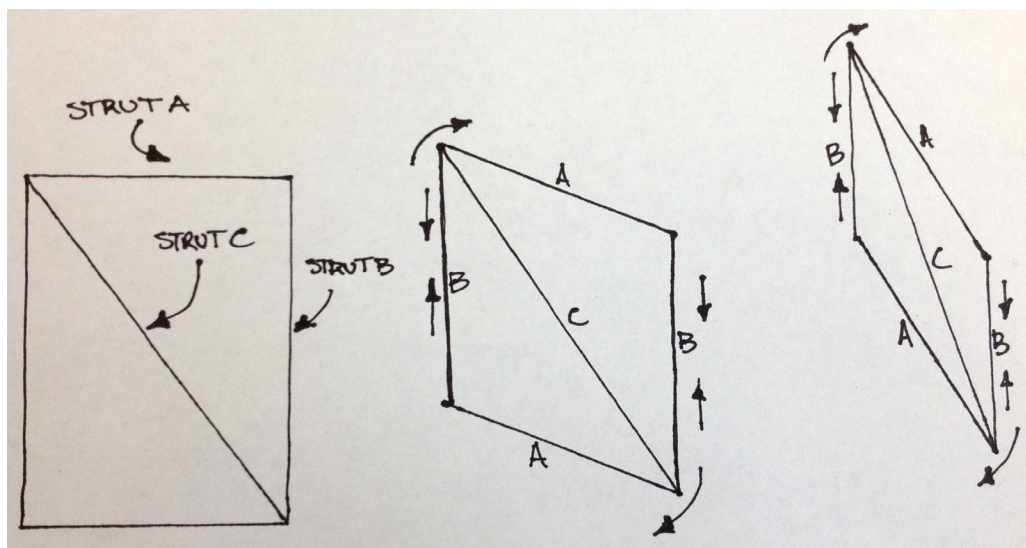


Figure 22: A single side of the drum truss structure showing its expansion and collapse.

Feasibility

We believe our drum design is feasible due to the fact that there have been antennas similar to our current design. Thermal testing done on the AstroMesh from Northrop Grumman has proven that the reflector's maximum temperature does not reach 100 °C. The AstroMesh antenna's efficiency was greater than 60% at a frequency of 30 GHz, which is near the intended operating frequency of 34 GHz (Mark, Kuehn, Fedyk, & Laraway, 2012). Since the AstroMesh was functional and operational in space, we firmly believe that our design can withstand launch and operate in space.

To further understand the mechanics of the system, a MATLAB script file was developed that generates a wireframe of the truss for any amount of expansion. This program also allows the exploration of the effects of different system dimensions, including the number of sides of the approximating polygon and the diameter and depth of the reflector. All future truss models will be made using SolidWorks. Figure 23 shows a wireframe generated by the MATLAB script file.

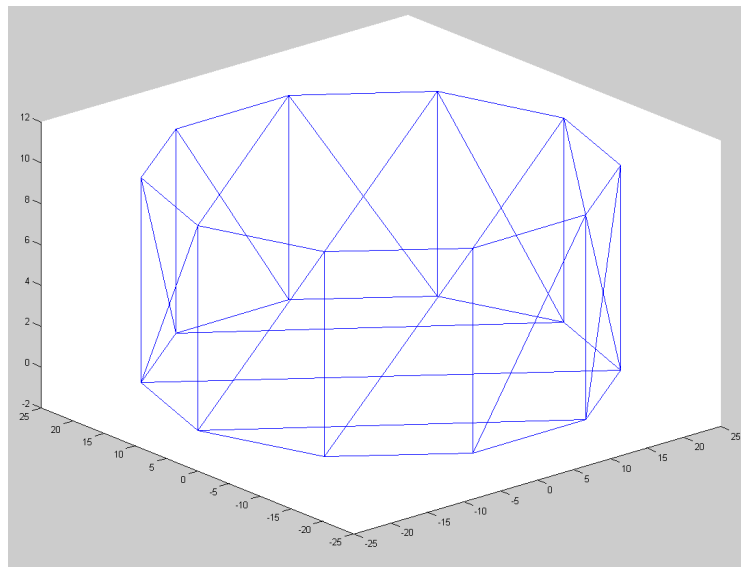


Figure 23: Drum concept wireframe generated in MATLAB

A few of the concerns that we have on the top design are the manufacturability, rigidity, and mesh surface accuracy. The drum design contains a large number of components and members, which can cause the accuracy of the mesh surface to be distorted. Thermal gradients, failure to fully deploy, and launching mechanism failure, for example, can cause the mesh surface's accuracy to exceed the tolerance required by JPL. Deployable support struts should be thin; this can reduce the rigidity of the structure. We plan to thoroughly analyze our top design to ensure it can surpass these problems. Basic analyses on the other two top concepts were also completed so that we had a backup if the analyses from the drum design proved it would fail rather than succeed. In addition, throughout our modeling and analysis, we chose to address any potential hazards of our concept. These identified hazards and our potential solutions can be found in Appendix I: Concept Design Hazard Identification Checklist.

Chapter 4: Final Design

Developing the Nonagon

Deviating from the conventional umbrella design, our drum designs were originally inspired by the AstroMesh design created by Northrop Grumman; however, as we attempted prototyping, it became clear that the complex linkage system utilized for AstroMesh provided too many challenges for our timeline. Already behind on our projected timeline, but desiring to stick with the drum concept, we began prototyping other small linkages and methods for creating an expanding truss structure. One of the early drum prototypes, Figure 24, consisted of square frames that could be collapsed into an accordion-like shape by bending the center joints of each square inward. While this configuration had a high deployed to stowed diameter ratio, the structure became unstable in the deployed phase due to excessive degrees of freedom. The structure would also collapse when a small load was applied to the perimeter of this drum configuration. It was determined that this type of drum structure could not be used for the purposes of our project.

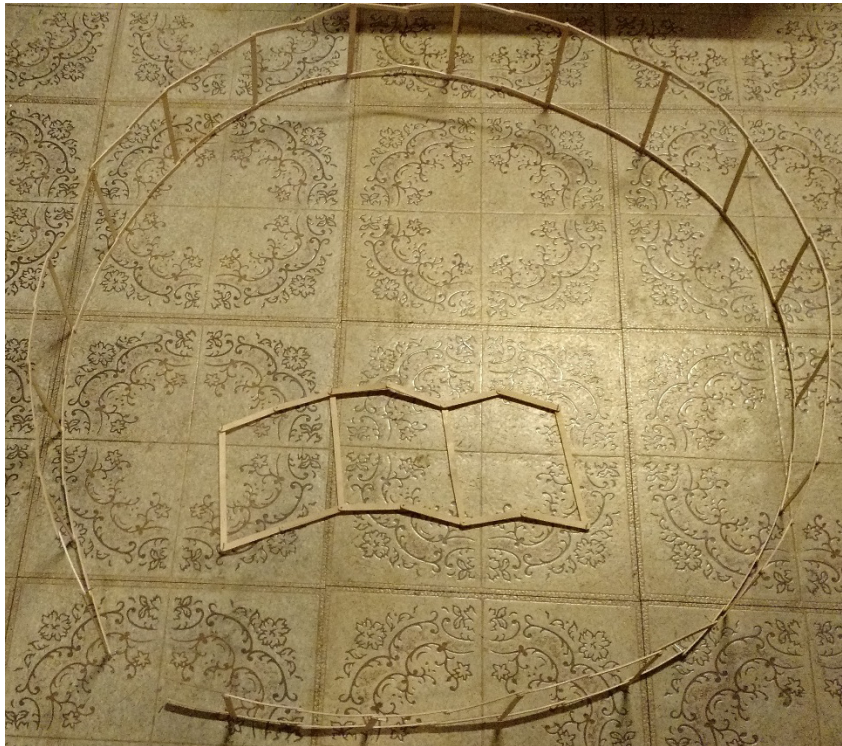


Figure 24: Collapsible square frame based truss structure.

Progressing from the square frame, another small truss prototype used a scissor configuration to expand and contract from a stowed position. This configuration utilized rubber bands set at equal intervals and strung between the top and bottom strut intersection points to simulate the vertical force of extension springs that cause the truss to deploy. This type of configuration proved to be much more stable than the square configuration in Figure 25. Also, there was no significant distortion in the frame as a load was applied to the vertices of the

structure. The scissor configuration prototype also had an excellent deployed to stowed diameter ratio, making this configuration the ideal choice for our final drum design.



Figure 25: An early prototype of the drum support using a collapsible scissor frame.

Based on the success of the small scale scissor prototype, we decided to build a large scale prototype of the scissor drum configuration to determine if the expansion ratio would be sufficient, how to deploy the truss the correct amount, and how to utilize springs in the deployment sequence. Using PVC pipe, thin wood molding, extension springs, and rapid prototype (RP) parts made by one of our team members, we created a working prototype. The prototype can be seen in its deployed and stowed state in Figure 26 and Figure 27 respectively.

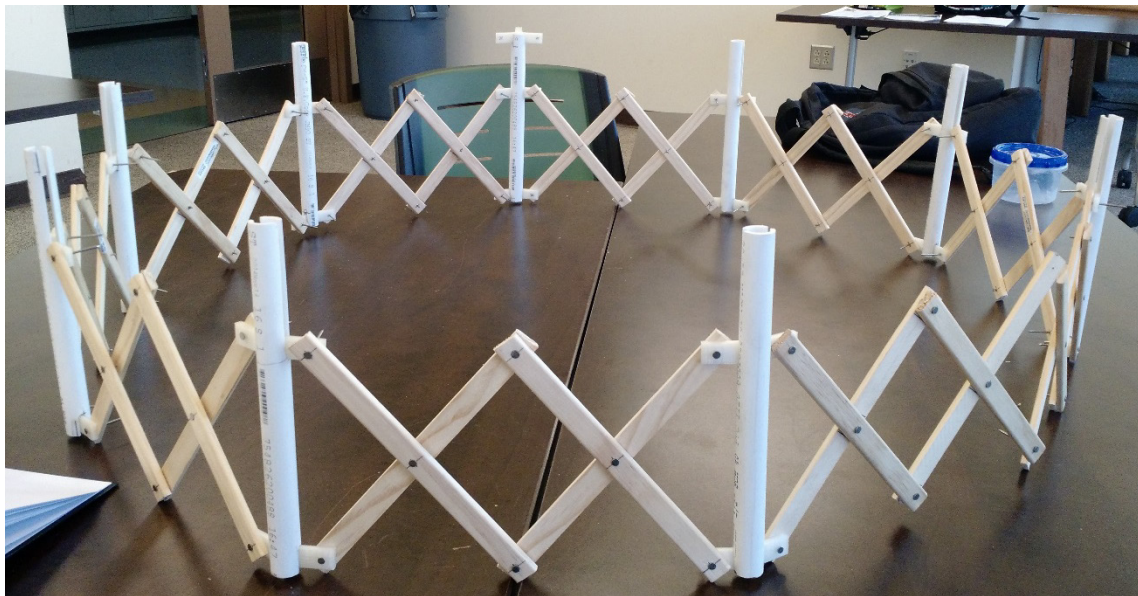


Figure 26: Drum prototype in the deployed configuration, scaled up with 1cm = 1in.



Figure 27: Drum prototype in the stowed configuration, scaled up with 1cm = 1in.

Slots were milled into the PVC vertices, and the rapid prototyped sliders were made to slide along the milled slots of the vertices. The wings of the sliders at each end of the PVC vertices connect to the ends of each scissor truss, where the bottom slider is fixed to the pipe while the top slider is allowed to move along the slot of the vertices. An extension spring located on the inside of each vertex pulls down on the top slider, forcing the scissor truss to extend horizontally. These extension springs remain in tension after the truss is fully deployed, holding the linkages in their fully extended positions. Each vertex contains this mechanism, allowing the entire drum to deploy simultaneously. Figure 28 below shows the more detail of the slider-spring mechanism.

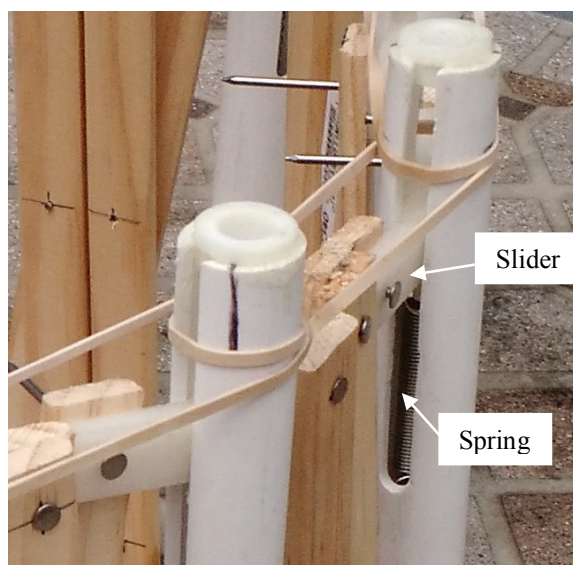


Figure 28: Close up view of the slider and spring mechanism.

The Nonagon

The Nonagon is a collapsible drum truss structure made up of nine identical sides, as seen in Figure 29. When fully deployed, the Nonagon is 500x500x141 mm; stowed, 141x91x94 mm. Overall, the structure has a mass of 0.4kg.

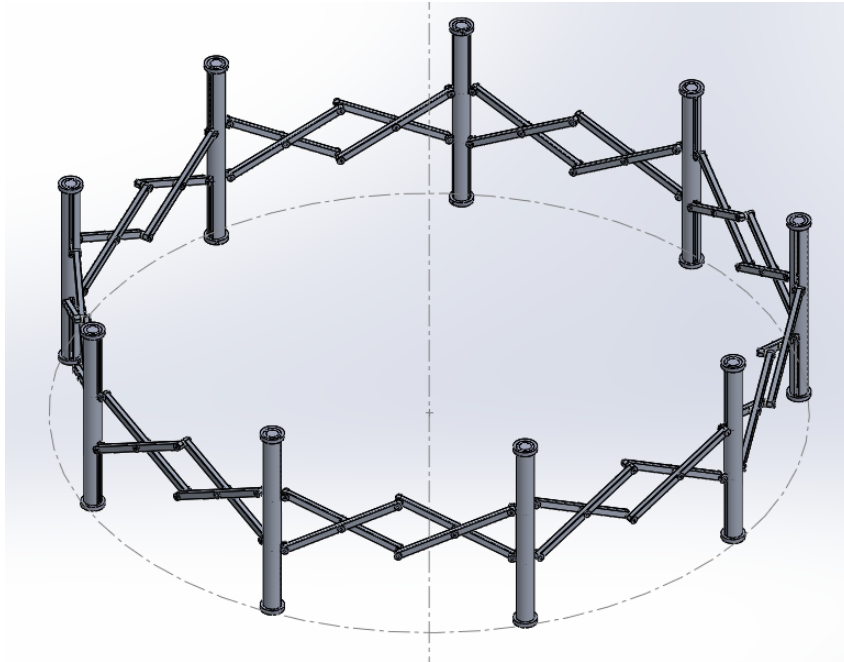


Figure 29: Nonagon when fully deployed.

Each side, Figure 30, consists of a vertex, two sliders, two extension springs, two hooks, two caps, four struts, four spacers, and eight rivets. The hooks are threaded and screw into the center hole of the sliders, one hook per slider, then the concentric springs attach to the hooks.

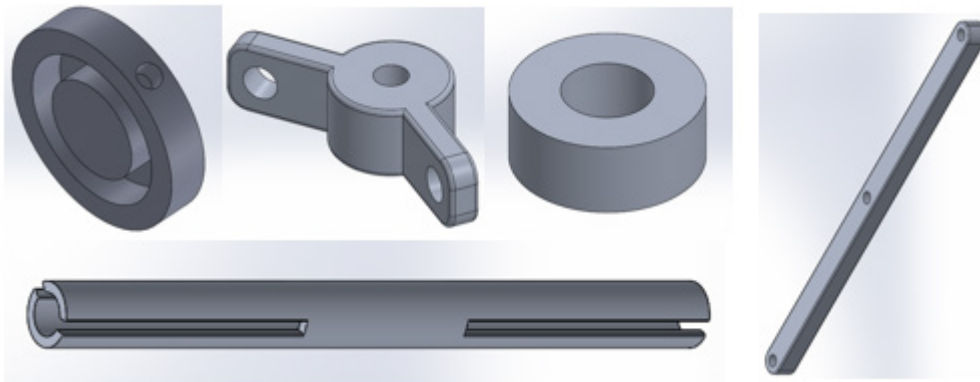


Figure 30: Models of Nonagon components (Top: cap, slider, spacer, strut. Bottom: vertex).

The entire slider and spring system is fit inside the vertex, the caps are press fit onto the ends of the vertex. A scissor truss is created with the four struts, four spacers, and eight rivets, then the scissor truss is connected to the two sliders nested in the slots of the vertex, Figure 31.

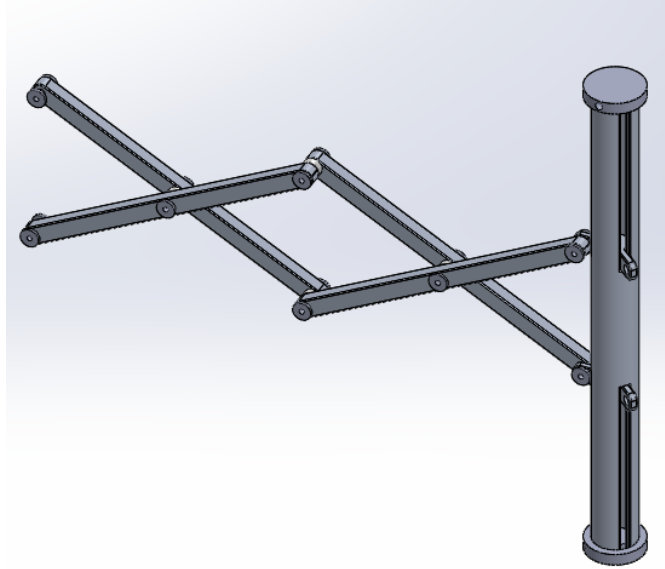


Figure 31: Singular side of the Nonagon.

When the full nine sided scissor truss is complete, the springs provide the deployment force while the slots in the vertex function as stops, limiting strut deployment. In the Nonagon's stowed position, Figure 32, the extension springs are stretched almost to their maximum, while in the deployed position, they are only slightly stretched.

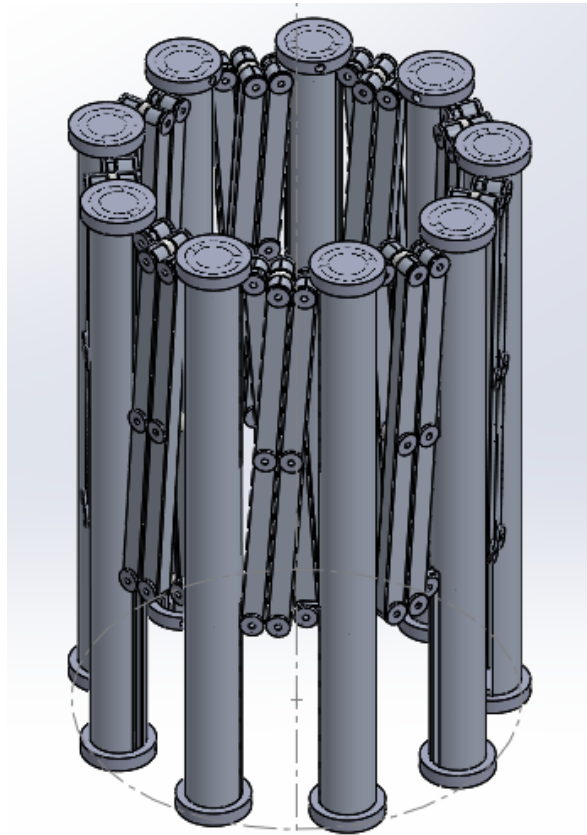


Figure 32: Stowed Nonagon truss model.

On each of the caps, there is a hole facing into the center of the Nonagon. These eighteen holes are utilized as connection points for the net which creates a parabolic shape through a geodesic design of planar approximations. The mesh is attached to this net and forced to match the parabolic shape. All detailed drawings pertaining to the scissor truss, as well as a Bill of Materials, are available in [Appendix B: Final Drawings](#).

During the manufacturing and assembly process, the design of the Nonagon changed slightly. The revisions to the SolidWorks parts and drawings can also be found in Appendix B.

Paraboloid: Mesh and Net Design

The tension net, or simply net, serves a critical purpose in the design. Two identical nets are attached to either side of the truss structure, and the reflector mesh is attached underneath the net on one side of the truss. To hold the reflective mesh in the required shape, tension ties are attached at every intersection point of both the front and rear nets. These ties are tensioned specifically to adjust the reflector into the correct paraboloid shape.

The mesh can take a variety of different forms depending on the required accuracy of the reflector required and the manufacturing methods used. The system currently in use is a geodesic net pattern as shown in Figure 33. This image clearly shows how this net type can produce any level of systematic error required simply by shortening the side lengths to better approximate the surface of the paraboloid.

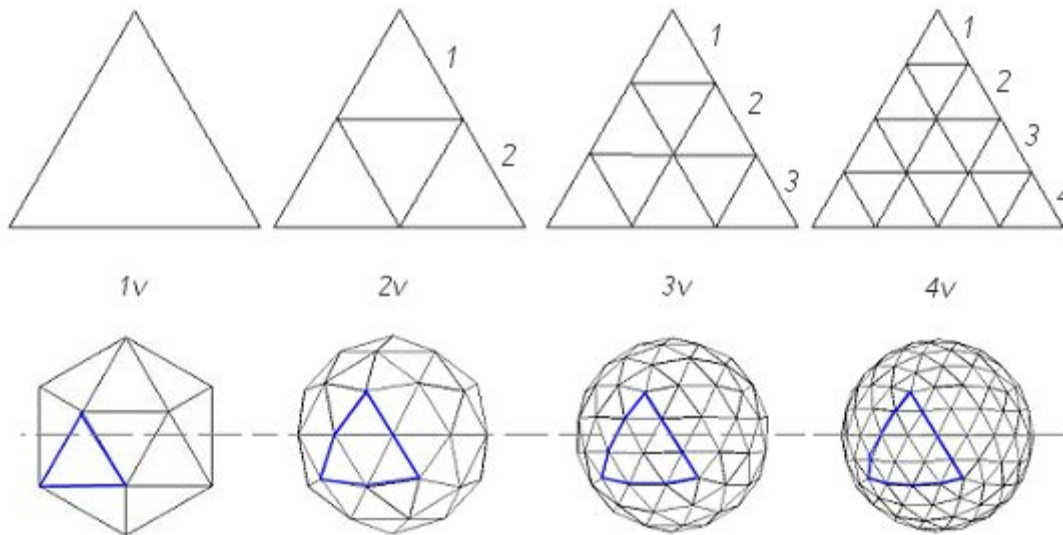


Figure 33: Geodesic net pattern of multiple surfaces.

However, this design is more difficult to manufacture since it requires the net to have a large number of soft connection points between different fibers. This adds another level of complexity and requires even more manufacturing research to produce reliably. In order to avoid this, a new net design is proposed, utilizing simplex patterns of the truss polygon. These constructions are often called complete graphs, because they are defined by a connection from each vertex to every other vertex in the polygon as shown below in Figure 34.

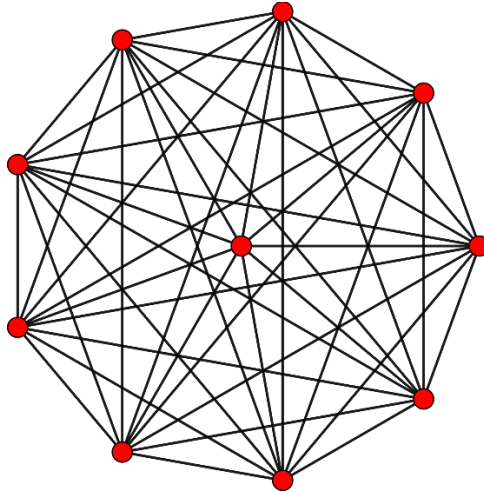


Figure 34: Complete graph of the nonagon net design.

This design allows the elimination of all soft connections between fibers and instead only connects the fibers to hard structures, simplifying manufacturing. Figure 34 does have one added vertex in the center however, that a normal 8 simplex nonagon would not have. This vertex represents the feed horn mast in the center of the reflector. The additional connections were added to better connect the two structures as well as further reduce systematic error introduced by this mesh.

Telescopic Mast

We mocked up a telescopic mast as a boundary condition for our truss and housing for our feed horn, without designing any signal receiving components per the edited requirements. A basic solid model of the mast can be seen in Figure 35. We envisioned that the mast will extend by the use of either internal compression springs or a motor.

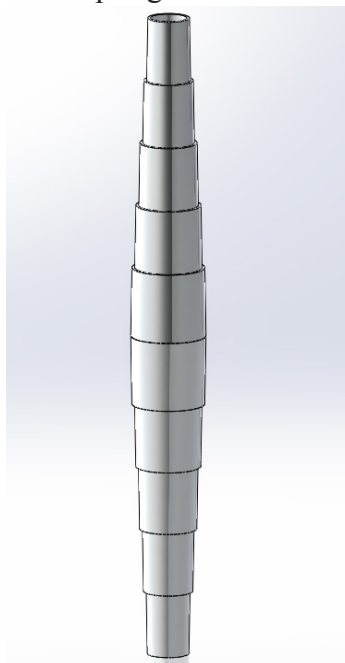


Figure 35: SolidWorks concept model of telescopic mast.

The mast, once deployed, will suspend our truss in space through the use of cables which connect from the top and bottom of the mast to the top and bottom of the truss's vertices. These cables will be symmetric on the top and the bottom as well as the mid plane of the truss, this aids in making sure that the truss structure will not be subjected to any torsion or unbalanced force that may cause excessive deformation. The bottom of the mast will be attached to the CubeSat housing.

Materials and Cost

The preferred material for the deployable CubeSat antenna is Aluminum 6061-T6. This material has a 1:1 ratio of thermal expansion in the x-y planes, which reduces the chance of warping due to thermal gradients. Aluminum is also relatively strong and light, compared to heavier metals like steel. Aluminum is also relatively easy to machine, which reduces the amount of time that must be spent cutting and post processing. All material and component data, along with suppliers and part numbers, can be found in Appendix C: Vendor List and Appendix D: Component Specifications and Data Sheets.

Truss Structure

The scissor truss structure consists of ten components: vertices, struts, two types of springs, rivets, sliders, spacers, threaded hooks, lock washers, and caps (small and large). Of these components, only the springs, spacers, and lock washers will not be Aluminum 6061-T6. Instead, the spacers are made of polytetrafluoroethylene (PTFE), commonly known as Teflon, the two springs are made of stainless steel (7mm) and music wire (4.5mm), and the lock washers are zinc plated steel. Teflon was chosen for the spacers due to its low friction and large working temperature range, which makes it a perfect material to align the struts while still allowing the truss to deploy with ease. The spring choice was predominantly driven by the inner diameter of the vertices (8mm), spring length, and then the spring constant. After finding extension springs that would fit inside our vertices, we then chose the spring with the highest spring constant in order to be certain the spring would exert enough force to deploy the truss structure. For the springs, stainless steel, spring steel, and music wire were all acceptable materials.

Parabolic Dish: Mesh and Netting

The net has been specified as being made of carbon fiber tow and the tension ties of Kevlar thread. These material choices stem from both thermal, RF, and manufacturing considerations. Carbon tow, or a strand of continuous carbon filaments, was chosen as the material for the net because of its low coefficient of thermal expansion, high specific strength, and high conductivity. The low rate of expansion is clearly advantageous for the rigorous accuracy requirements over a large thermal range. The specific strength is desirable because of the requirements for a low weight robust structure. The electrical conductivity has a less visible advantage, in that it should help prevent the buildup of static in any one area by more readily conducting between structures, and that it should also act as an RF reflector with no detriment to the mesh reflector.

Kevlar thread was also selected for its high specific strength and excellent thermal properties, but differs in that it is commonly made in very thin threads. This is a positive aspect

for manufacturing, since the Kevlar will be required to bind multiple small areas of the nets together, as well as small connections required for the tension ties.

After having attempted to create a net system with the carbon tow, we deemed the material unsatisfactory for our purposes. The tow would fray when exposed to the slightest bit of friction. Due to this, our team decided to move forward with a Kevlar only net system.

Cost Breakdown

Our final estimated cost to produce the Nonagon was significantly cheaper than expected, as seen in Table 10. This cheaper cost appears to be a function of the CubeSat dimensions, since very little material is needed to manufacture our parts; however, this price could increase based on outsourced machining costs. Currently, we have allotted for the maximum amount of machining costs, as we are expecting to machine a large portion of our components. This machining cost includes the purchasing of any special tools such as end or face mills. A downside to the small dimensions of our parts is that very few items can be bought commercially off the shelf.

Table 10: Complete cost breakdown of the project by part.

Item	Description	Supplier	Lead Time	Qty.	Total Item Price
3/32" x 0.224" Blind Rivet	Short Rivets	Grainger	2 days	500	22.55
3/32" x 0.500" Blind Rivet	Long Rivets	Grainger	12 days	500	20.25
1/2" x 12" Al Rod	Vertices	Grainger	7 days	20	23.34
4" x 1/4"x 1/4" Links Al 6061-T6	Struts	Misumi	21 days	40	800
1" x 1" Al Square Stock*	Sliders	N/A	N/A	20	N/A
3/4" x 1/2" Al 6061	End Caps	McMaster Carr	2 days	20	3.5
1/4"-20 x 36" Al 6061 Threaded Rod	Hooks	Grainger	7 days	1	3.75
3/16" PTFE Rod	Spacers	US Plastic Corp	7 days	40	0.8
7.010mm 302 Stainless Steel Spring	Large Spring	Lee Springs	7 days	10	64.5
4.495mm Music WireSpring	Small Spring	Lee Springs	7 days	10	64.5
Kevlar 69	Kevlar Thread	Thread Exchange	7 days	800 yds	46
Carbon 3K	Carbon Fiber Tow	Soller Composites	14 days	2 lbs	120
Molybdenum Mesh**	Mesh	JPL	N/A	1	N/A
Subtotal					1169.19
Est. Shipping & Tax					300
Est. Machining Cost					500
Total					1969.19

*We have allotted stock material for the sliders in case we need to switch manufacturing methods from casting to machining.

**For our prototyping purposes, we will be using a substitute for the mesh. Currently that substitute is tulle fabric, which has similar stretch and weight.

Analysis and Further Testing

A large portion of our analysis and testing was completed through the prototyping process. By creating a scaled truss prototype, we were able to prove that we could meet the size

and space limitations. In order to continue analysis via physical models, we intend to have a working prototype of the net system before the end of March. However, while models are incredibly useful, further analysis was necessary to be certain the design and materials selected would be able to withstand testing.

Truss Analysis

In order to determine the stowed diameter and the deployed diameter of the revised truss design, EES code was developed to automatically determine these values (see Appendix E: Detailed Supporting Analysis). The EES file took into account the dual strut geometry of each side and determined the angle at which the struts were offset from the vertical axis, this angle determined the side length which affected the diameter of the truss design. Using the EES code, we had the flexibility to modify the strut length, width, and depth dimensions, as well as sides, in order to iterate dimension combinations and optimize the stowed and deployed diameters. Once dimensions and number of sides were finalized, we created a SolidWorks model of the entire truss confirm that the design was feasible and components did not interfere with one another. Using the SolidWorks model and applying the correct materials to each components, the mass and area moment of inertia tensor of the entire design were calculated using the mass properties function of SolidWorks.

The EES code was then expanded to calculate the internal forces and axial stresses in each strut during launch. We had assumed the CubeSat would be subjected to a mean loading of five G's, typical of a rocket being launched. Following the General Environmental Verification Standard, we used a limit load at 97.72% probability with 50% confidence and applied an acceleration equivalent to ten G's. For our hand calculations on the EES code, we simplified the model by concentrating the weight of each component at its center of gravity. Due to the axisymmetric loading conditions and horizontal symmetry of each side, as shown in Figure 36, only half of a side of the truss was modeled. All other sides have the same internal forces and stresses.

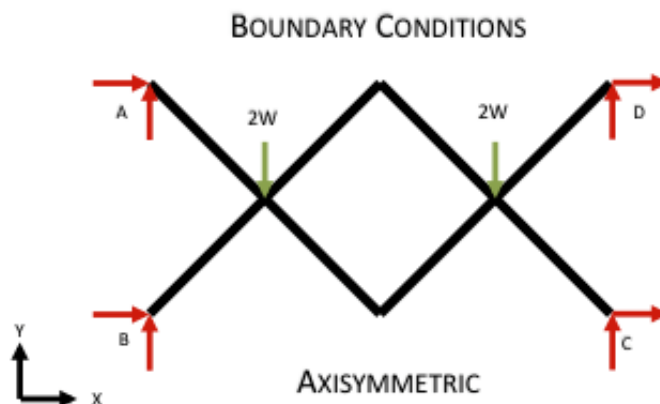


Figure 36: Boundary conditions for gravitational loading.

From the results, it was determined that the safety margin for the axial stresses in the struts was high and the maximum axial stress is 150 kPa. Structural results will be tested by

using 1.1 times the limit load to test yielding requirements and 1.25 times the limit load to test failure requirements. Structural testing will take place in the Composites Lab at Cal Poly using an Instron axial loading machine following the procedures and requirements of the Launch Services Program, Program Level Dispenser and CubeSat Requirements Documents Rev B.

The thermal deformation of the structure was modeled using the same symmetry assumptions as the structural analysis; analyzing a single pair of struts. Thermal expansion in the horizontal and vertical plane was proven to be a one-to-one ratio. This ratio results from using the same material for major components; therefore, any deformation will be uniform throughout the mesh. In order to determine if our truss design can withstand the operational temperature range, we thermally tested for acceptance requirements. Thermal testing consisted of heating our prototype to the operational maximum temperature and dwelling at the maximum temperature for one hour, then cooling down to the minimum temperature and dwelling at that temperature for an hour. This heating and cooling cycle repeated three times. Thermal testing will follow the procedures and requirements of the Launch Services Program, Program Level Dispenser and CubeSat Requirements Documents Rev B and occur in the Cal Poly CubeSat Lab via use of their thermal chamber.

The vibrational nodal modeling of the truss was not performed due to the limited computational memory in our school computers. Too many nodes were required to gain accurate results, and every attempt to run the nodal model with the required amount of nodes caused the computers to crash. As a result, we decided it would be best to experimentally test our truss design using the two generalized random noise profiles, from the General Environmental Verification Standard, for flight and workmanship approval. Each axis will be tested using the random noise profile for qualification and acceptance requirements. Vibrational testing will take place in the Mechanical Engineering Vibration Lab on the Cal Poly Campus.

Once completed, the prototype will be repetitively deployed and stowed to ensure the mesh does not catch on any components and that the joints do not require adjustment. In order to confirm if we meet our key engineering requirements from JPL, we had to confirm that the deployed mesh diameter, total mass, and surface tolerance all meet the requirements. We will measure these key parameters of our prototype to ensure we have met all key parameters stated in Table 4. The tests and measurements stated above are required for the prototype to be deemed acceptable.

Due to the limited testing equipment available at Cal Poly, measuring the parabolic surface tolerance of the mesh will not be conducted. Due to the limited functionality of the thermal chamber, thermal testing will not be conducted under vacuum. Signal strength cannot be tested due to the fact that the antenna is not electrically complete. Many tests were omitted or changed due to the equipment available and the nature of our prototype. In future design iterations, more thorough testing should be considered.

Paraboloid Systematic Error

Systematic error is any deviation from the desired paraboloid shape caused by the approximation methods used to make the reflector. Any error from the ideal reflector shape is important because it can cause the signal to interfere with itself destructively, lowering the gain of the antenna or even rendering it useless. The simplex polygon approach, while much simpler

to manufacture than the geodesic pattern, does suffer from slightly higher systematic error. Because of the limited time and resources of this student project, it was deemed a better approach to use the easier to manufacture, though not entirely ideal, simplex design.

To qualify the exact error of this design, a Matlab script, found in Appendix E: Detailed Supporting Analysis, was developed. This script takes as input the diameter and focal length of the desired reflector, as well as the number of sides and a vertex pairings for line generation of the actual reflector. The dynamic line pairing allows any simplex polygon to be constructed, connecting all vertices to each other, or only selectively connecting specific vertices. The code also allows for the generation of sub-vertices, like the one used in the center of the reflector of this project, and could also be used to evaluate the suitability of almost any geometric pattern as a paraboloidal approximation. The program uses Delaunay Triangulation to decompose all complex geometries generated by simplices, and then a planar model of every subsurface of the reflector to calculate the z height for any point on the reflector and calculate its error in relation to the perfect paraboloid. Results of a 250,000 point calculation of error for the reflector are shown below in Figure 37.

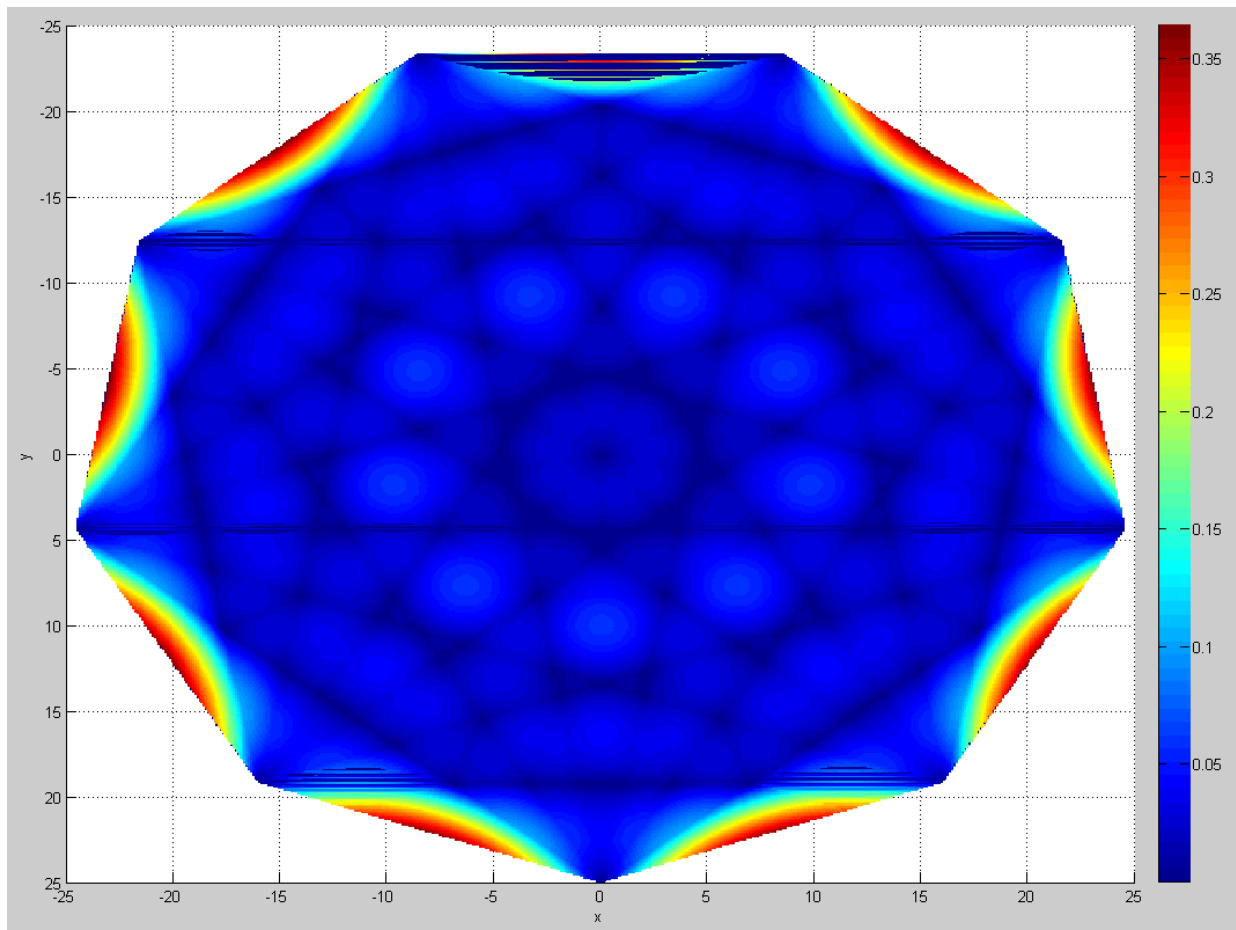


Figure 37: Graphical results of the paraboloid systematic error in centimeters derived from the nonagon net shape.

The bulk of the reflector produces systematic error at or below 0.5 mm, but the numerical average for the whole structure is 0.6 mm. Poor surface approximation between vertices likely

have a large effect on the calculation, as the error in these areas is on the order of 3 mm or more, six times greater than the error in most of the rest of the structure. Overall, this method of paraboloid approximation proves adequate for this application, especially where the positive aspects of its manufacture are considered. Additional investigations into this reflector design might do well to move to a geodesic design, or add supplementary vertices inside the reflector to eliminate high error areas while still maintaining a relative ease of manufacture.

Telescopic Tubes

Telescopic tubes are frequently used in space applications for the support of antennas or deployment of large sun shades such as the James Webb Space Telescope. The mechanisms are well understood and have been utilized in space exploration since the 1960's. A Northrop Grumman Telescopic Tubular Mast (TTM) is used as a primary example here of the possible characteristics of a mast for a parabolic reflector. Listed in Table 11 are some key size and expansion characteristics of the TTM compared to predicted values based on similar design performance for a CubeSat.

Table 11: Characteristics of the Telescopic Tubular Mast compared with predicted CubeSat values.

	No. of Segments	Stowed Length [m]	Deployed Length [m]	Total Percent Expansion [%]	Mean Expansion Percent per Segment [%]
Northrop TTM	17	2.16	34.3	1490	87
CubeSat	5	0.05	0.234	368	74

The TTM consists of 17 segments each 2.16 meters long. The deployed structure is 34.3 meters long which yields an effective length of 2.02 meters for each segment. This means that 6.6% of each segment's length is lost to overlap with the next segment. The proposed mast needed for the Nonagon deployable reflector requires a length of approximately 50 cm for symmetrical support of the reflector. To achieve this, the 15 cm allotted stow height is divided into three sections: 5 cm for the feed horn and RF assembly, 5 cm for a mast that deploys 25 cm in front of the reflector, and 5 cm for a mast that deploys 25 cm behind the reflector. This expansion from 5 to 25 cm is used for Table 11. The expanded length is calculated as 23.4 cm, with the difference accounted for by the 6.6% length lost per segment. This small shortcoming in length is acceptable however, since the 5 cm allotted for the RF assembly is more than adequate to reach the focal point. The table shows that the expansion ratios required to create such a mast are extremely possible, even with additional allowances for difficulties with miniaturizing the assembly.

In regards to the diameter of such a structure, the TTM has a mean decrease in diameter of 1.2 cm per segment. In the five segment deployable structure, this equates to a minimum diameter of 6 cm for the structure. While this would take up a significant portion of the 10 cm by

10 cm CubeSat structure, it is still considered feasible. A structure designed specifically for the application would likely use significantly thinner walls and the latching mechanism diameter would similarly be reduced. Though there are many hidden difficulties with extreme miniaturization of existing technologies, the assumed mast is feasible, though there is not enough time to fully define its design (Mobrem & Spier, 2012).

Design Verification Plan

In order to test and validate the design requirements set by JPL for the deployable antenna, a Design Verification Plan (DVP) was created to track the results of the testing phase and determine if the requirements were met satisfactorily.

Table 12 contains a complete list of the design requirements along with the test method, testing location, allowable parameter, team member responsible, and testing dates for each requirement. The DVP will be updated frequently to include test results of the design specifications when the testing phase is underway. Once all test results have been collected, they will be documented along with test procedures into the final Design Verification Plan and Report (DVP&R).

Table 12: Design Verification Plan of required design specifications

Specification	Test Description	Acceptance Criteria	Test Responsibility	TIMING	
				Start date	Finish date
Analysis					
Functional Force > 100%	Analysis, use load cell	>100%	Dom	5/7/2015	5/20/2015
Operation Thermal Range	Analysis, qualitative, simulate deployment conditions	-70°C to 110°C	Juan	5/7/2015	5/20/2015
Physical Model - Inspection					
Antenna Diameter	Inspection: Tape Measure	≥0.5m	Peter	5/7/2015	5/20/2015
Mass of antenna	Inspection: Scale	<1kg	Sarah	5/7/2015	5/20/2015
Feed hole at vertex of dish	Inspection: Dial Caliper	0.05m	Dom	5/7/2015	5/20/2015
Stow within 1.5U CubeSat housing	Inspection: Measuring tape, ensure lid closes	Fits in 1.5U space	Peter	5/7/2015	5/20/2015
Physical Model - Testing at Cal Poly					
Deployment Thermal Range	Thermal vacuum cycle	-15°C to 20°C	Juan	5/7/2015	5/20/2015

Random Vibration	Use accelerometers on 3 axes for 3 minutes	MPE + 6dB	Juan	5/7/2015	5/20/2015
Sine Vibration	Use accelerometers on 3 axes for 3 minutes	MPE + 6dB	Juan	5/7/2015	5/20/2015
Structural Testing-Yield	1.1X limit load with respect to yield strength, tensile test	No Yield	Peter	5/7/2015	5/20/2015
Structural Testing-Ultimate	1.25X limit load with respect to ultimate strength, tensile test	No Failure	Peter	5/7/2015	5/20/2015
Physical Model - Desired Testing at JPL					
Parabolic Surface Tolerance	Analysis of RMS from mftg./thermal/systematic error, use photogrammetry	<0.56mm	JPL (if available)	5/7/2015	5/20/2015
Ratio of focal point to dish diameter	RF Testing	0.5	JPL (if available)	5/7/2015	5/20/2015

Manufacturing, Assembly, and Maintenance

Our team took advantage of the resources available at Cal Poly to manufacture and assemble a large portion of the Nonagon in house. All vertices, sliders, caps, eye hooks, and spacers were machined at Cal Poly using the machine tools available through the two on campus shops and the Industrial and Manufacturing Department. None of our parts were dependent upon the others to be manufactured, which allows us to make multiple parts simultaneously.

Truss Manufacturing

The vertices, spacers, and end caps will be cut to length using a cold cut saw, and then machined using a Haas CNC Mill via tool paths generated in MasterCam to meet the exact specifications. For these parts, 1/16" and 3/32" center cutting end mills will be utilized, along with a face mill larger than 1" in diameter. The end mills must be center cutting because we will be required to plunge into the aluminum stock. We will be casting the sliders out of aluminum via a combination of investment casting and rubber plaster casting. Casting will allow us to create multiple sliders in a single, short session through the use of casting trees. We will be testing this method before the end of February to prove the tolerances and finish will work in practice and theory. If casting proves unpractical, then we will also be machining the sliders. CNC Milling and casting are preferred methods of manufacturing due to their accuracy and repeatability; we can achieve the same or very similar tolerance results for each component, which allows us to stay within specifications and mitigate human error.

The struts will be manufactured out of Aluminum 6061-T6 by Misumi to the exact specifications dictated in the strut drawing found in [Appendix B: Final Drawings](#). Having

the struts made out of house is very convenient because there are forty struts to be manufactured, which equates to a large amount of machining time.

Truss Assembly

The most crucial part of the truss assembly is the attachment of the springs to the sliders to the vertices; the next focus, recreating the same strut pattern on each individual side. Apart from those two challenges, the truss is a repeating pattern, so it should be easy to complete in an assembly line fashion. Similarly to the manufacturing, we can put together segments of the truss such as the nine sections of four struts linked with spacers and rivets for each side and the nine vertices with their sliders, springs, hooks, and end caps simultaneously. Then, once the strut sides and vertices have been assembled, we can connect each side and vertex to create the overall truss.

Paraboloid Mesh and Net Assembly

The net poses a significant manufacturing challenge because it is primarily a soft good and as such it is difficult to produce repeatable, accurate results. This can be mitigated however, through care in manufacturing, and allowing for the adjustment of the mesh in the final assembly. The first issue with the manufacture of the net, is producing the correct lengths of carbon tow for each line. This is accomplished by means of the systematic error Matlab program discussed previously in the report. It is critical that the lines be only very slightly shorter than the exact calculated value. This is because the carbon tow is extremely inelastic, and any additional tension required to achieve shape will cause undue loads on the truss structure. The code can also generate the specific profile for any of the lines in the net and the necessary length of the line. Now the line must be bound to the vertex. Because the net is paraboloidal, there will be no tension on the line during this process, which eases assembly. The line will be attached to the vertices by wrapping a loop of the carbon tow through an eye hook on the vertex, and then binding the loop with Kevlar thread in the manner shown in Figure 38. This joint may need to have a small amount of epoxy added to it to prevent slippage between the two materials. After the first loop is bound, its effective length will be measured to establish the exact location of the second vertex loop. After all lines on both nets have been bound to the structure, the tension ties must be put in place. The tension ties must be precisely adjusted to achieve the proper shape. The initial tensioning of the net will be achieved by use of simple plastic cable ties at all intersections. This will allow for gross adjustments during the initial connections. After gross adjustments are completed, each intersection will be re-tied using Kevlar thread and then the cable tie removed. Then the system will undergo measurement of the intersection points. After measurement, all out of spec intersection points will be re-tied, and then the whole net measured. This process will be iterated until the final shape is achieved.

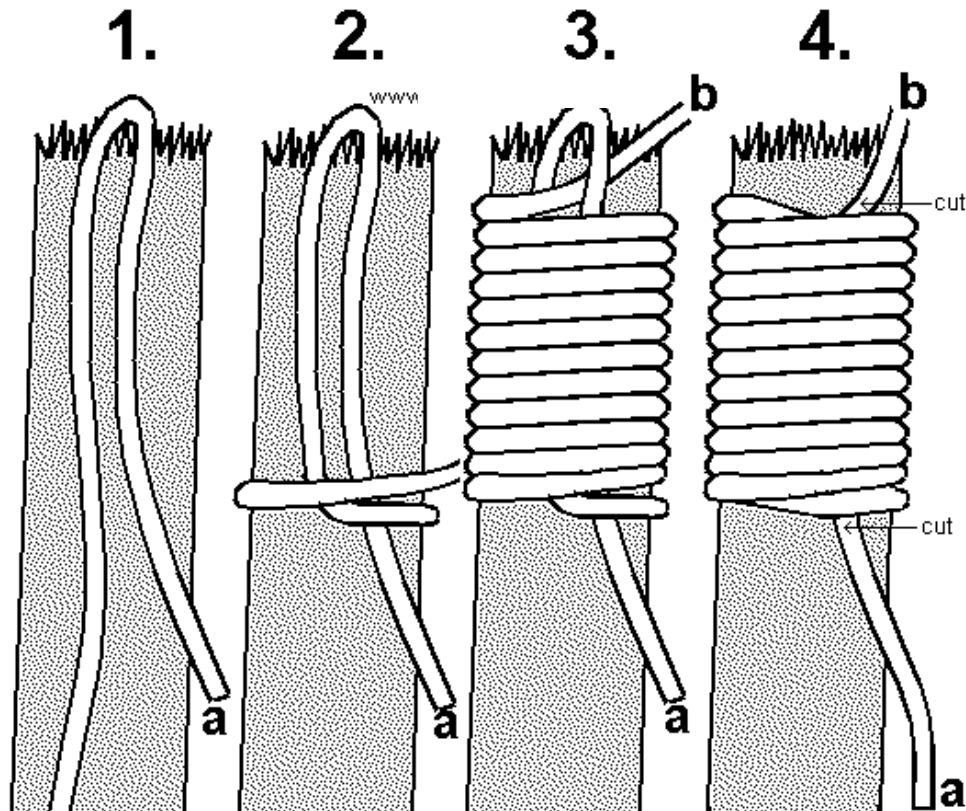


Figure 38: Binding pattern for the Kevlar thread and carbon tow.

Maintenance

The deployable CubeSat antenna is meant to operate in space and orbit the Earth, making it impossible to retrieve the unit for maintenance or repair. For this reason, thorough testing must be performed before launch in order to maximize the effectiveness of the antenna. Testing in conditions that simulate the space environment will help improve the design and lifespan of the antenna after it is launched into space.

Failure Modes and Safety

Throughout our manufacturing, assembly, and testing, we will mitigate any potential and realized hazards of our concept. These identified hazards and our potential solutions can be found in **Error! Reference source not found.** However, we must also attempt to diminish not only safety hazards, but also potential failure modes.

In order to identify critical design aspects of our design, a Design Failure Modes and Effects Analysis (DFMEA) was performed. In this analysis, potential failure modes were first classified and then tabulated against their respective potential cause and effect of failure. A recommended action was also listed with each failure mode in order to help prevent such failure from occurring.

Each potential *effect* of failure was rated with a level of severity between 1 and 10, 1 being the least severe and 10 being the most severe. In addition, each potential *cause* of failure was rated with a level of occurrence between 1 and 10, 1 being most unlikely to occur and 10 being highly likely to occur. Once the levels of severity and occurrence were determined for all

possible failure modes, these numbers were then multiplied by each other to yield the critical number of each failure mode. Critical numbers for all failure modes were then compared and ranked, labeling modes with the highest critical number to have the most importance for the design specifications of the drum antenna.

Many possible causes and effects of failure for the deployable antenna were considered in the DFMEA, and it was necessary to envision the different phases of operation of the satellite. Areas that were studied for potential failure modes include stowed position of the antenna, transport during spaceflight, ejection of the unit from the housing, and full deployment of the antenna in space. Operation errors of manufacturing and assembly were also considered for in the analysis. Upon request, the DFMEA and a complete detailed list of the failure modes considered for the deployable CubeSat antenna can be sent. It will not be included within this report due to its size and repetitive nature; the most relevant information from the DFMEA has been included in Table 13. Upon completion, the DFMEA yielded six potential causes of failure with a considerable critical numbers, all of which were at or above the set threshold of 60. This threshold was chosen because most of the failure modes under this threshold contribute to the modes with a critical number at or above 60; therefore, in accounting for the modes over 60, we were also able to account for many less critical modes.

Table 13: Potential failure modes with critical numbers at or over a threshold of 60.

Potential Failure Mode	Potential Cause of Failure	Critical Number
Poor signal strength	Inaccurate shape of dish	90
Jamming of Components (tangled, locked)	Parts are loose and interfere with rest of assembly	90
Mesh material tears/jams	Loose mesh gets caught with other components	90
Parabolic dish does not transmit RF effectively	Dish surface tolerance is inadequate	80
Parabolic dish does not deploy	Insufficient truss rigidity for mesh tensioning	80
	Deployment hinge fails to activate	70

Poor signal strength, jamming of components, and tearing of the mesh material were noted as the three most critical potential failure modes of the eight chosen for the analysis and testing of this project. These three modes will take priority, following with the remaining five modes of failure.

Poor signal strength due to inaccurate shape of the dish is critical to the design of the antenna dish since it defeats the primary purpose of the overall project. For example, distortion of the deployed antenna dish may cause the reflected signal beams to focus off-center of the focal point of the signal receiver. Poor focus of these reflected signals reduces the quality of signal transmission, making the dish ineffective. Other causes of inaccurate shape of the dish

include factors like thermal expansion/contraction of materials, inaccurate manufacturing of components, poor assembly of the antenna unit, or an unequal force distribution in the members of the dish support. Testing, including thermal cycling, vibration testing, and stress analysis as previously discussed, will be completed on materials and the final assembly in order to keep these problem factors at a minimum. Manufacturing of the satellite components will include close monitoring during machining, and multiple dimension checks that can be verified by different team members. Sub-assemblies will be used to facilitate and control the assembly process, and different team members will monitor and verify assembly of the final prototype.

Jamming of components due to loose parts is the second potential failure mode that is being considered in the design of the final antenna prototype. Vibrations during the rocket launch may cause fasteners of the antenna unit to become loose. Hinged components could potentially detach from one another, cause interference with adjacent components, and possibly render the mechanism useless. This failure mode will be mitigated via vibrational testing performed on subassemblies and the final antenna assembly to ensure that fastener joints can withstand these conditions without losing rigidity and function. Also, collapsing and deployment of the antenna will be performed respectively by team members to ensure fasteners and joints do not loosen over time.

The mesh material used to form the parabolic dish is relatively delicate, and it is crucial that the mesh is installed in a manner where it will not interfere with moving parts during the deployment phase. Excessive interference may cause the mesh material to pinch, catch, or even tear, reducing the effectiveness of the deployed mesh dish for RF transmission. The mesh will be in close proximity to moving parts during the stowed and deployed phases of the antenna, and the design of the mesh location and points of attachment should minimize entanglement of the mesh as much as possible. The collapsing and deployment sequences of the antenna will be performed multiple times, and team members will check the mesh for possible damage after each sequence.

RF transmission has a direct relationship with dish surface tolerance, and a poor surface tolerance will affect the ability of the dish to effectively transmit RF signals. The parabolic dish serves as a reflector that focuses RF waves to a focal point, where a transmitter can then pick up these frequencies. A dish with a poor surface tolerance reduces the amount of RF that is focused on the transmitter, thereby weakening the signal being transmitted thru the antenna. Since a flexible mesh will be used to form the dish, the support frame of the mesh should allow for a mesh shape that meets or exceeds the required standard set for this project. Surface tolerance is difficult to perform without specialized instrumentation, and Cal Poly does not have the equipment necessary for this type of testing.

In order to form the deployed parabolic dish, the support structure of the mesh should have sufficient tension to keep the dish shape taut. Insufficient tension in the drum support structure may cause the mesh to sag, affecting the surface tolerance of the dish shape thereby reducing RF transmission. The design of the mesh attachment points should be integrated with the current drum structure at locations where tensioning is easiest to achieve and keep uniform. Tensioning of the dish support structure will be tested with multiple deployment sequences, checking for loosening or sag of the mesh material. The deployment mechanism that initiates the final deployment of the drum could also fail to trigger, so testing of this release lock with multiple test runs will be performed to ensure that it releases the drum when desired.

Chapter 5: Product Realization

Manufacturing

Moving into the manufacturing phase of the project required careful planning in order to meet the required specifications of the antenna design and also facilitate the final assembly of the antenna components. Due to the small size and relatively complex features of the antenna components, it was crucial to also maintain proper tolerances for fixed and moving parts. It became apparent early on that manufacturing would take longer than what was expected, so the approach was to make as many parts in the least possible number of tool set ups and operations.

Sliders

Manufacturing of the sliders proved to be the most challenging of all the components used in the drum support structure. Due to its complex and angled features, the slider required multiple tool operations and milling orientations to achieve the desired dimensions of slider design. CNC machining was chosen as the method of manufacturing for the sliders, and an add-on program to SolidWorks called HSM Works was used generate the tool paths and CNC codes for the sliders. Figure 39 depicts a snapshot during the material removal simulation from the original bar stock. A summary of the tools used for this setup can be found in Table 14.

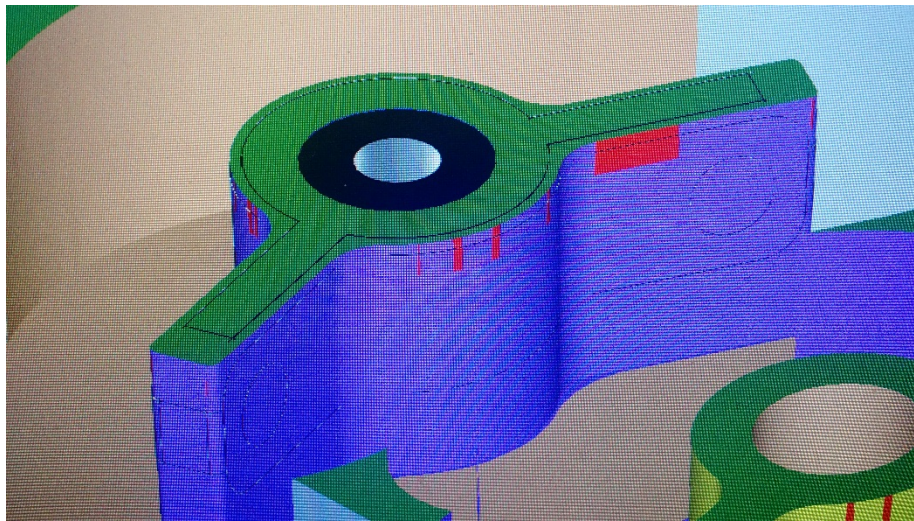


Figure 39: CAM image of the slider during CNC code generation

Table 14: Tools used to CNC Mill sliders

Tool	Tool Path
1.5" Flat End Mill	Facing
1/4" Flat End Mill	Rough Profile
1/8" Flat End Mill	Finish Profile
#7 (0.2010 inch) Drill Bit	Center Hole
1/4"-20 Tap Drill Bit	Hole Threads

Eighteen sliders were required for the antenna design, but extras were added to be used solely for testing purposes. To avoid manufacturing sliders one at a time, a machining pattern was created to yield eight sliders from a single piece of aluminum bar stock. This lowered manufacturing cycle times and ensured consistent dimensions. The features cut in this setup include the profile, center hole, and threads of the slider, which can all be seen in Figure 40.

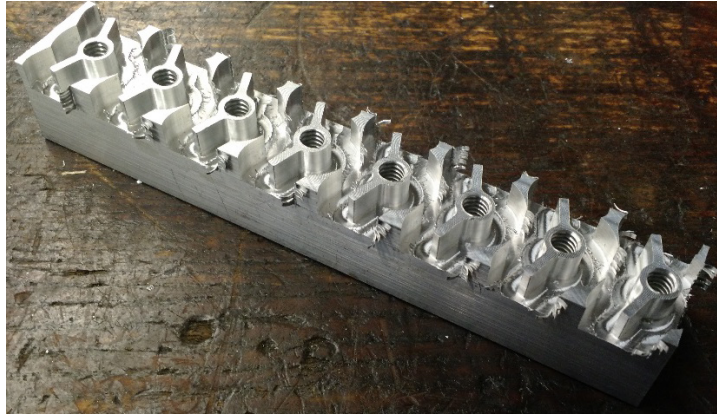


Figure 40: Pattern of sliders after CNC machining

Once the operation was complete, the sliders were carefully cut from the aluminum stock with a band saw. To compensate for the thickness of the band saw and human error, an allowance was added to the height of the slider which can be seen in Figure 39. To achieve the correct slider thickness, the fixture depicted Figure 41 was created to face the sliders. The fixture was designed to provide support for the thin winglets of the sliders to prevent any change in angle due to forces exerted by the vise.

Table 15 lists the tool used to make the fixture. For the second setup, the sliders were placed in the fixture with the sawed surface facing up and a 1.5" face end mill was used to face the top surfaces of the sliders.



Figure 41: Soft jaw fixture used to face sliders to correct height

Table 15: Tooling used to CNC facing fixture

Tool	Tool Path
1/8" Flat End Mill	Profile

A second fixture depicted in Figure 42, was created to hold the sliders during the drilling operation on the winglets. For this third set up, the sliders sat in a “cradled” position in the fixture, allowing easy rotation of the slider in order to drill the opposite winglet. The second setup can be seen in Figure 43.



Figure 42: Fixture used to drill holes in winglets of sliders.

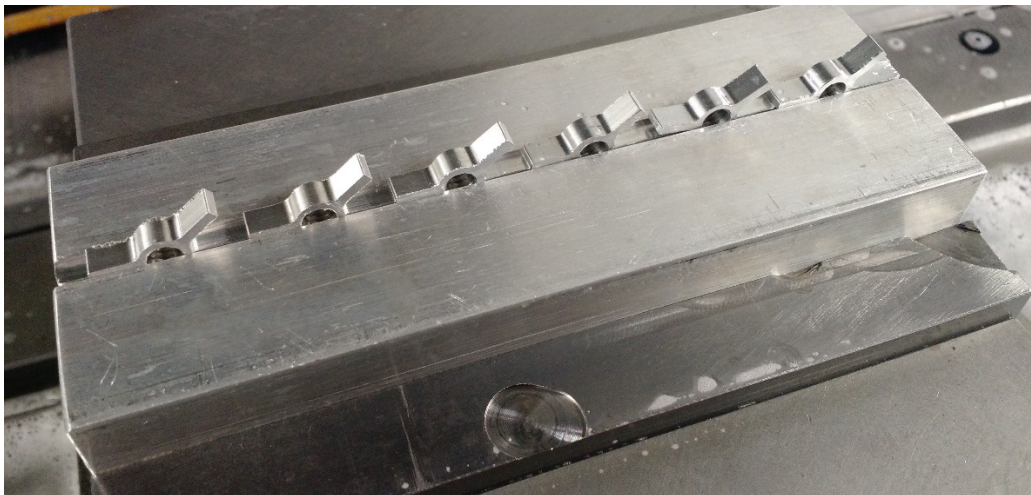


Figure 43: Sliders mounted in vise of CNC machine

A CNC sequence was created to drill the holes in the winglets, and the opposite winglet holes were drilled by flipping the sliders and repeating the same drilling sequence. A 3/32" drill bit was used to make the holes in the winglets as depicted in Figure 44.



Figure 44: Sliders with holes after completion of CNC drilling operation

Other challenges faced with machining the sliders was achieving adequate clamping force on the sliders in the fixtures, and not being able to machine sharp corners due to round cutting tools. The filleted edges of the slider as seen in Figure 39, cause interference and tighter fits between mating components during the assembly process. This necessitates time-consuming post processing to obtain proper fits.

Future iterations of the fixtures would include deeper contours in the fixtures to increase the clamping surface area, and reduced winglet thickness to compensate for the fillets created by round tools.

Vertices

Despite having a relatively simple geometry, the vertices were the second most challenging component to manufacture for the drum support structure. The slots on the vertices must be extremely accurate to prevent the sliders binding. CNC machining was chosen due to the accuracy, consistency, and cycle time that can be achieved.



Figure 45: Tube stock cut to design length of vertices

As shown in Figure 45: Tube stock cut to design length of vertices, tube stock was used to make the nine vertices required for the drum design. The first challenge to manufacture the vertices was coming up with a way to hold multiple tubes to increase productivity without interfering with cutting operations. This was achieved with the fixture in Figure 46. The tools used to make the fixture are listed in Table 16.

Table 16: List of CNC tools used to make fixture for vertices

Tool	Tool Path
1/4" Face End Mill	Rough Profile
1/8" Face End Mill	Finish Profile
5/64" Face End Mill	Slots



Figure 46: Fixture used to mill slots of vertices

The second challenge of manufacturing the vertices was providing enough support along the length of the tubes. In order to minimize the deflection of the tubes as the cutting tool approached the center of the tube, solid cores were turned down (Figure 47) and inserted thru the tubes to improve rigidity of the set up and help the tubes resist deflection. Figure 48 shows the set up as seen right before running the milling sequence in the CNC machine.



Figure 47: Stock milled down and used as support cores for vertices

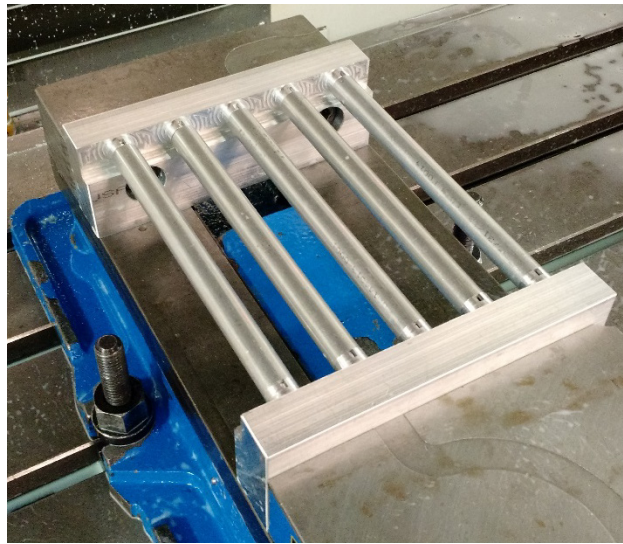


Figure 48: Vertices mounted in vise of CNC machine

The support cores were made longer than the vertices to provide extra support against deflection. The bores in the fixture were also made deeper to accommodate for the longer support cores. Figure 49 shows the deep bores for the cores and the “ring” surfaces that serve as rests for the tubes.



Figure 49: Fixture designed with deep bores for support cores. Two locating slots assist in aligning stock

The third challenge with making the vertices was finding a way to accurately locate the position of the angled slots relative to one another. This was achieved by milling two slots with the desired angle between them (Figure 49). The tool used to mill the slots was a 5/64" Flat end mill. Once one set of slots were milled, the vice was loosened to rotate the tubes to match the angled slot. The second set of slots could be milled as shown in Figure 50.

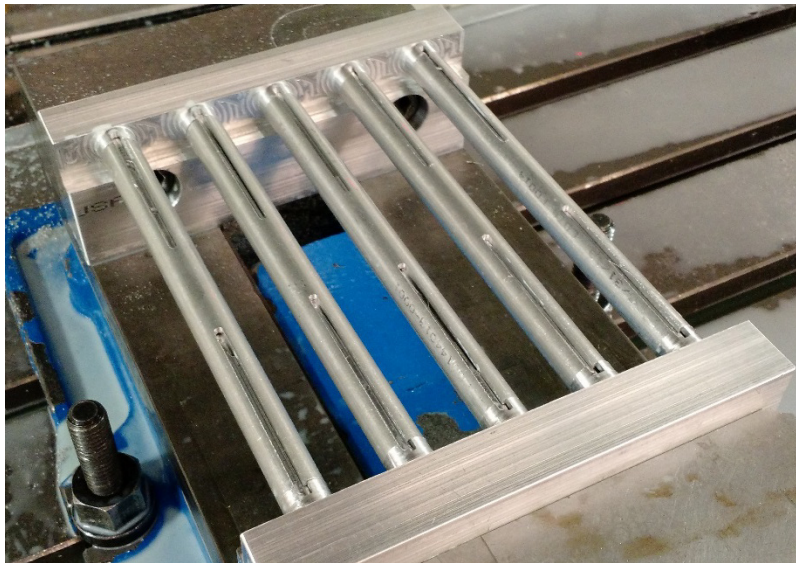


Figure 50: Vertices with slots after completion of CNC milling operation

The completed vertices were checked to ensure that slots lined up and that that the angle between the slots was sufficient to allow movement of the sliders. Once all the sliders and vertices were completed, the components were checked for proper fit and manufacturing defects as seen in Figure 51.

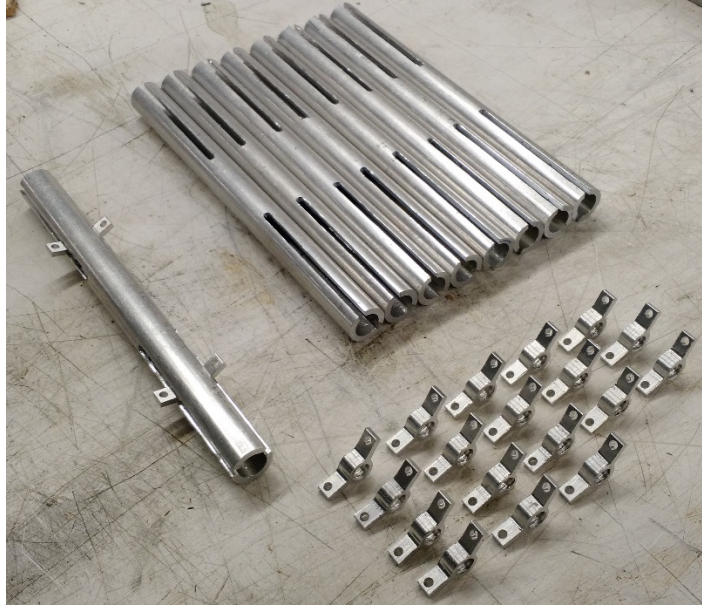


Figure 51: Fit check of sliders and vertices

Considerations for future iterations of the fixture should include a design that keeps the soft jaws aligned to one another. Any misalignment of the soft jaws will yield crooked slots in the vertices. Additionally, electro discharge machining should be examined as a superior way to manufacture the slots to require less deburring, which we used as a way to ensure the sliders would function as intended in the vertex slots.

Struts:



Figure 52: Struts used for the final antenna prototype

The struts were used to link the nine vertices of the drum support, and served as the basis of the scissor mechanism that deployed the structure. Due to time constraints and the large quantity required for the drum support, the struts were sourced from Anvil Fabrication and Manufacturing, a local machine shop near the Cal Poly campus. These struts can be seen in Figure 52.

A few testing struts were manufactured in-house for testing while the final struts were being made. A block of aluminum stock was used to CNC the strut profiles and drill holes for the rivets (Figure 53). The tools used for the test struts are listed in

Table 17.

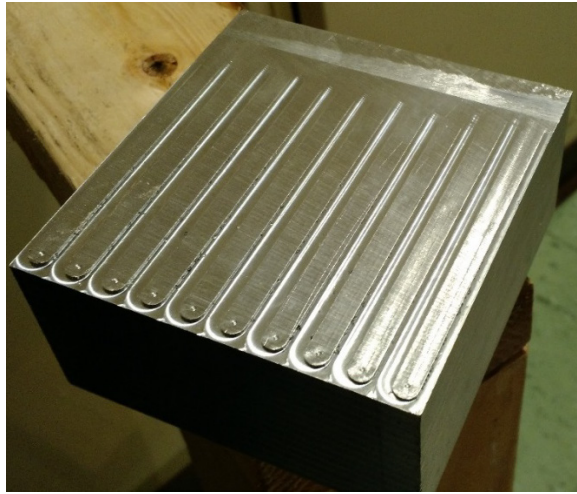


Figure 53: Stock used to mill testing struts in CNC machine. Here, struts have already been cut off from stock

Table 17: List of tools used to make test struts

Tool	Tool Path
1.5" Face Mill	Facing
1/8" Face End Mill	Profile
3/32" Drill Bit	Holes

Figure 54 shows the fixture used to face down the test struts to the design thickness. Once the test struts were removed from the stock with a band saw, five were placed next to each other in the fixture and with the rough cut face upward and milled to thickness.



Figure 54: Fixture used to face down testing struts to the correct thickness

With sufficient time and stock material, the struts could be made in-house. However, because the scissor motion of the struts depends on the surface finish of the struts, careful consideration must be given to machining variables and de-burring processes.

Spacers:

The spacers were made from PTFE stock. The stock was cut with a razor as all available saws had too large a kerf.



Figure 55: Jig used to drill holes in spacers

To drill the holes in the spacers, a piece of wood was used to make a jig that could hold the spacers during drilling, as seen in Figure 55. The jig was then covered with tape to keep the spacers from rotating as the center holes were drilled.

Future iterations for the spacers could consider using different materials that are more malleable than PTFE. Materials that have lower melting temperatures could also facilitate manufacturing, but these materials could run the risk of early failure due to the harsh conditions and temperatures of outer space.

Eye Hooks:

The eyehook seen in Figure 56 was used to connect the springs and sliders within the vertices. These hooks were cut from a threaded aluminum rod and ground at one end to provide a flat to drill the holes.



Figure 56: Stages of manufacturing (left to right) for the threaded eye hooks

The main advantage of this design is that the threads allow adjustment of the tension in the springs. Due to its small size, grinding and drilling becomes tedious and inaccurate. Later iterations of the hook could be implemented as part of the slider body, reducing the number of parts and assembly time. Additionally, casting could be reconsidered as a method to produce the slider, eye hook, and lock washer in a single component.

Cap Plugs:

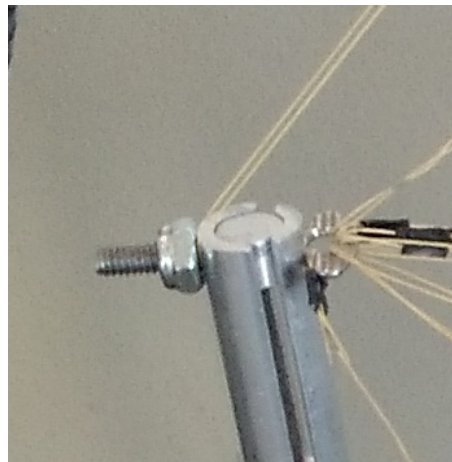


Figure 57: Cap plugs inserted in vertices

The cap plugs were made from the support cores used to machine the slots in the vertices. Since these rods were turned to fit the inner diameter of the vertices, it was only necessary to cut the rods to the design length of the cap plugs. There are two types of plugs, one short and one long. The long plugs keep the bottom sliders from moving, while the short plugs allow the top sliders to freely move up and down the vertex slots. As seen in Figure 57, the cap plug was attached to the vertex by match drilling a hole thru the cap and vertex, then using a thumb screw fastener and nylon insert nut to keep the parts together.

Although this cap design yields a rigid connection, the nut and bolt approach increases the space required for storage of the collapsed drum structure. A different design should be considered where the fastener will not project too far from the surface of the vertices.

Assembly

Truss Assembly

In order to create the scissoring truss motivated by springs, we had to insert the springs, sliders, eye hooks, and lock washers into the vertices. Once all of those components were in place, we were able to fasten one long and one short cap plug in each vertex. The vertex assembly process consisted of the components mentioned above, a table clamp, two pairs of needle nose pliers, a long wire hook, and Loctite. To prepare for the assembly process, each component was thoroughly cleaned using Simple Green, then dried. Next sliders and eye hooks were paired with vertices. Each threaded segment of the eyehooks were covered in Loctite, then screwed into the sliders until the top of the slider and the top of the eye hook were co-planar. By placing the smaller diameter spring inside the larger one, we made the springs concentric. To assemble a vertex, the following process, seen in Figure 58, was used. Additionally, Figure 59 displays the internal view of the components of the vertex assembly and the SolidWorks assembly.

1. One slider and eye hook pair was attached to one pair of concentric springs with a lock washer. The washer is opened, pushed through the spring hooks and the eye hook, and then closed with the pliers.
2. The unattached side of the spring hooks (from the slider and spring assembly in part 1) is then caught with the wire hook and pulled down into the vertex until the slider rests on the bottom of the slot and the wire hook can be seen dangling out the bottom of the vertex.
3. A long plug in then inserted into the vertex top to prevent the slider from moving, then the vertex is clamped horizontally in place along the plug with the table clamp.
4. The wire hook is used to stretch the concentric springs until a lock washer can be pushed through the two spring hooks and the other slider and eye hook combination.
5. The lock washer is closed using pliers, the slider is held outside of the vertex until the wire hook is released, and then the slider is slowly allowed to be pulled down the vertex slots until it comes to rest at the bottom of the slot.
6. The vertex assembly is then removed from the clamp and tested by pulling the movable slider up and down the slot length. At this point in time, dry lubrication can be sprayed inside the vertex to assist with movement.

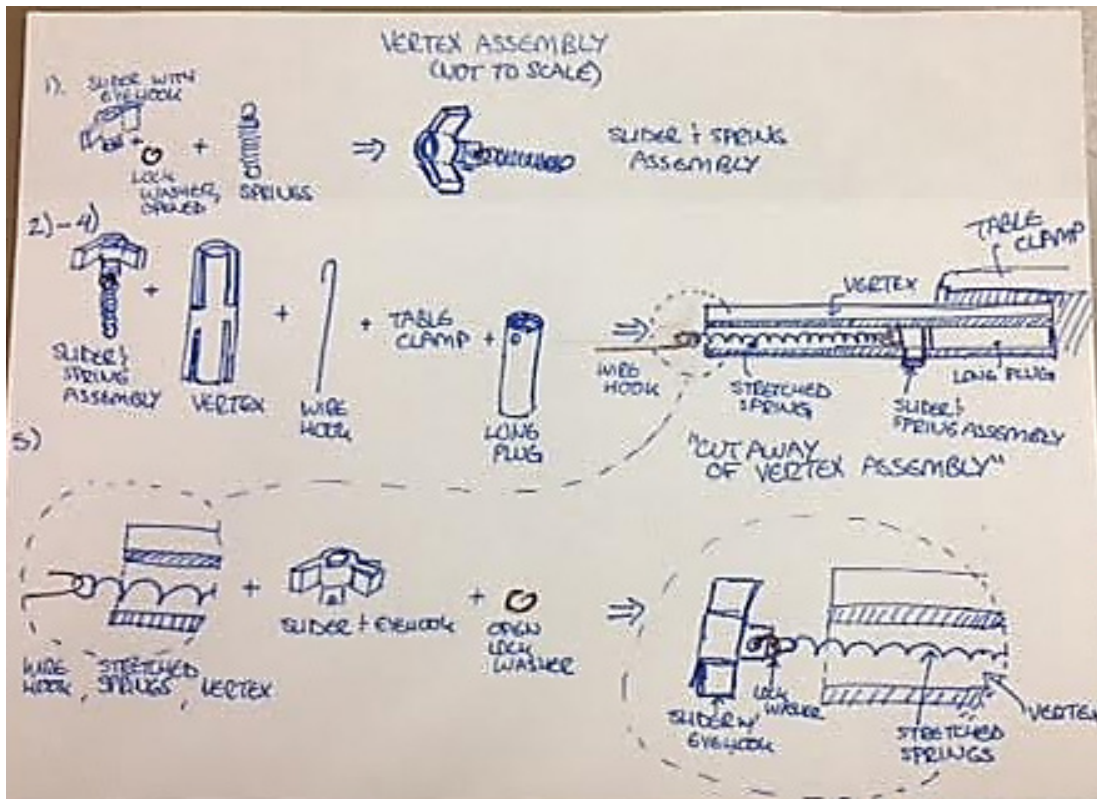


Figure 58: Outline of vertex assembly steps (not to scale).

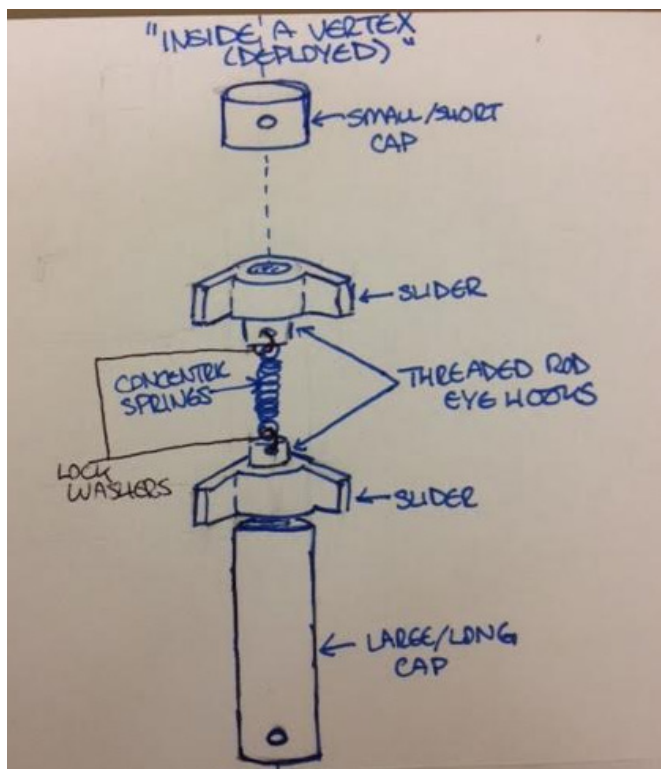
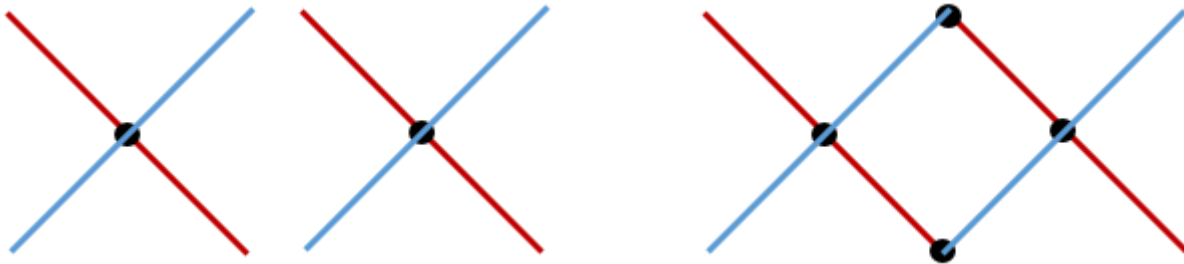


Figure 59: Left: Internal look at a vertex when truss is deployed (not to scale) Right: SolidWorks assembly of vertex and components..

The scissoring struts were assembled simultaneously with the vertices. To assemble a single strut side the following components and tools were required: 4 struts, 4 spacers, 4 rivets, and a rivet gun. Initially, two “x” shapes are formed, each with a spacer placed in the center of the “x” between the two struts. Rivet the center of each “x.” Next, the two “x” shapes are placed next to each other so that the two struts above the center spacers point in the same direction, and the two struts below the center spacers face the same direction. There should be a visible diamond where the two “x” shapes meet, place a spacer between the struts and the top and bottom of the diamond, then rivet the top and bottom of the diamond. This process is seen in Figure 60 and Figure 61.



*Figure 60: Scissor truss side assembly.
Black circles are spacers with rivets, blue lines the top struts, and red lines the bottom struts.*

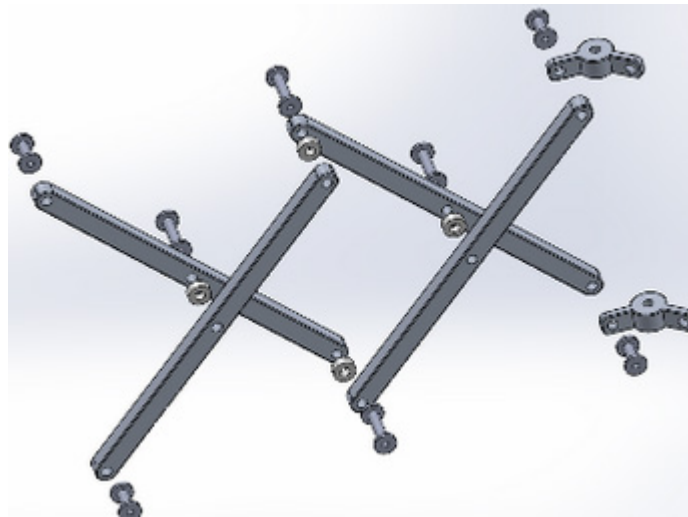


Figure 61: SolidWorks side strut assembly.

Once each of the vertices and sides were completed, the truss was able to be fully assembled. Working in a circle, and ensuring that each of the strut segments all collapsed the same direction, rivets were inserted at each slider and strut connection, but not engaged. After completing the full nine sides and double checking the expansion and contraction capability, each rivet was engaged using a rivet gun.

Net Assembly

The net manufacturing method was established through a series of small scale tests. This proved worthwhile as we discovered a number of failures and bottlenecks in the manufacturing process.

The design called for carbon tow to be bound using Kevlar thread in a small wrap knot. Multiple issues arose during initial testing of this arrangement, the first of which is shown in Figure 62. The carbon tow proved to be especially susceptible to fraying. Impromptu testing using a variety of lubricants and mandrels showed that abrasion, not the diameter of the bight, was the culprit for the fraying. The carbon tow was abandoned in favor of an all Kevlar net.

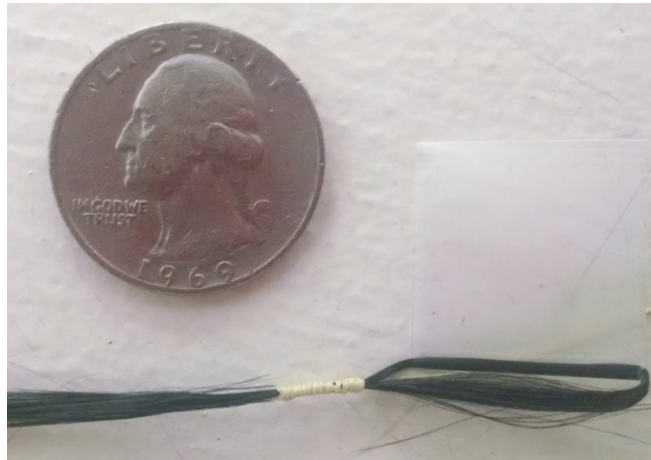


Figure 62: Carbon tied with Kevlar, initial test. Quarter provided for scale.

The Kevlar net had its own share of problems. The first was that the knot would slip easily on the line, providing easy adjustment of line lengths but no permanent solution for deployment. This was solved by wicking cyanoacrylate glue into the knot after adjustment was completed. An example of the joint is shown in Figure 63.



Figure 63: Kevlar tied with Kevlar. Quarter background for scale.

This joint proved acceptable from a design standpoint, but inordinately difficult to manufacture. The net requires more than 500 of these joints, so any gains in efficiency result in massive improvements overall. Through a brainstorming session, we came to a new idea of using heat shrink instead of a knot. This was significantly easier than tying knots by hand, but still allowed manual adjustment of the ties before being locked in place with cyanoacrylate. Tensile testing results for the heat shrink based joints can be seen in Chapter 6: Design Verification.



Figure 64: Test of single net line with tension ties

Figure 64 **Error! Reference source not found.** shows a net section jig that was used to test initial manufacturing methods. Initial tests of the tension ties were not sufficient to indicate the tedium of the knotting method, so the test section was extremely valuable in refining the ties.



Figure 65: Net manufacturing jig

The final manufacturing method for the net involved the development of a new jig. The jig pictured in Figure 65 serves multiple purposes. First it allows the net to be built in parallel with the truss structure, shortening the overall manufacturing timeline. Second it allows the net threads to be pulled tight during manufacturing, which aids in keeping the structure clear. After the net is completed on the jig, it can be transferred to the truss and adjusted in place.

Originally, our manufacturing plan was to use two circular jigs to create two nets. The nets would then be laid on top of each other, allowing the installation of the tension ties while the net is tight and easily manipulated away from the truss. Once the nets and tension ties are completed, all the lines can be adjusted to pre-calculated lengths, which will yield an initial shape when transferred to the truss. The net shape can then be measured in place on the truss and adjusted iteratively till the exact shape is reached. Due to time constraints, only the nets were completed and the tension ties were never installed.

Realized Design

While we were able to complete the perimeter truss structure and the two Kelvar nets, our team was unable to create the full parabolic shape using tension ties between the nets. To assist our audience in visualizing how the Nonagon would appear when deployed, we created a stand and some rapid prototyped attachments for the placebo mast and tension ties. Figure 66 displays a rendering of the Nonagon as it would appear with the telescoping mast. Additionally, Figure 67 shows our realized, suspended version of the Nonagon from multiple angles.

Throughout the manufacturing and assembly period, the team kept careful accounting records to minimize our budget. The updated budgets for entire project can be found in Appendix H: Detailed Budgets. Additionally, since our realized version of the Nonagon does not function as a completed CubeSat would, we have provided handling guidelines and suggestions for future teams that may continue this project that can be found in Appendix G: Operators Manual with Safety Guidelines and Appendix J: Future Work and Recommendations respectively.



Figure 66: Render of the Nonagon with telescoping mast.



Figure 67: The final assembled design with placebo mast and Kevlar tension ties connecting the truss to the mast.

Chapter 6: Design Verification

Based on the testing breakdown discussed in Table 12, the Design Verification Plan, our team was prepared to dedicate multiple weeks to testing and verification. However, as the manufacturing and assembly timeline was pushed further back, our testing time shortened drastically. The summarized results of the tests we were able to complete can be found in Table 18; however, full discussion of these tests, their results, and any improvements can be found below.

Table 18: Testing results for realized Nonagon.

Test Type	Criteria	Tooling/Description	Result
Inspections			
Dish Diameter	$\geq 50\text{cm}$	Tape Measure	48cm
Feed Horn Diameter	$\geq 5\text{cm}$	Dial Calipers	6.4cm
Mass*	$\leq 1\text{kg}$	Scale	485g
Fit	Stows in 1.5U	1.5U Model	Pass
Physical Model – Testing as Cal Poly			
Cable Tie	Failure	Fish Scale Tensile test to failure load	33 lbs
Structural Testing – Yield	No Yield	Instron Machine Tensile test to 1.1 yield load	Pass
Structural Testing – Ultimate	No Failure	Instron Machine Tensile test to 1.25 ultimate load	Pass
Deployment Thermal Range	-15°C to 20°C	Thermal Chamber Test Stand	Pass
Random Vibration	MPE + 6dB	Vibes Table Accelerometers on 3 axes for 3 minutes	N/A
Sine Vibration	MPE + 6dB		N/A

We learned quite a bit throughout the design verification and testing period. The primary lesson we learned was that when designing the model, we need to think about testing. If we are not able to accurately test each section with the correct boundary and loading conditions, then we cannot fully validate our preliminary analysis. Similarly, if we cannot produce a fixture to hold our design in place, we cannot test. Much like manufacturing, testing required more time than we had allotted. In the future, more time will be allocated for testing. For our team, the time crunch was due to unanticipated testing machine issues, errors, incorrect procedures, and a lack of time to analyze the data retrieved.

Physical Inspections

Diameter:

From the list of specifications for the deployable antenna, a dish diameter of at least 50cm was required for the design. Using a ruler, the dish diameter of the final prototype measured 48cm, two centimeters short of the design requirement. After closer inspection, it was noted that the springs were unable to fully retract the sliders towards the center of the vertices. As a result, the scissor mechanisms could not fully extend to the intended length, hence slightly reducing the overall diameter of the antenna. Possible reasons for the incomplete extension of the antenna may include poor lubrication leading to excessive friction as the sliders moved within the barrel of the vertices, insufficient tensile strength in the springs, and/or uneven slots in the vertices which cause the sliders to jam.

Mass:

The list of requirements specified a mass of less than a 1kg for the antenna design. Using a digital scale, the mass of the antenna prototype measured 485g. It should be noted that this mass accounts for the drum support only. Since the mesh for the dish design could not be completed in time, it was omitted from the final weigh in. Also, this mass does not account for the bolts used to fasten the cap plugs with the vertices. The mass of the antenna should be weighed once all components have been assembled.

Stow Size:

A 10cm x 10cm x 15cm stowing space was specified for the antenna design. Using a wooden box that was manufactured to these dimensions, the size of the collapsed antenna was checked for fit. The antenna did fit inside the box in the stowed position, therefore meeting the design requirement. Things to note is that the bolts used to attach the net were not yet assembled, so the size of the stowed antenna should be rechecked once the bolts are assembled. The height of the stowed antenna should also be rechecked once an ejection mechanism is implemented. The mechanism will add height to the antenna, so it's important to check that the lid of the CubeSat housing will still be able to close.

Thermal Testing:

Due to the space applications of the antenna, a thermal-vacuum test was the ideal test for this design. A thermal-vacuum test can be used to simulate the harsh environments of space where satellites operate. Due to time constraints however, testing was resorted to using a thermal oven only. The antenna prototype was cycled between -62 C and 120 C, with a soak time (dwelling) of about 10 minutes at each of the extreme temperatures. Soaking was to allow the temperature of the prototype to reach equilibrium with the temperature of the oven.

Below is a list of test parameters that should be considered when using the thermal vacuum test for the deployable antenna. Thorough testing can help ensure that the antenna design will last for its intended lifetime.

Requirements: -70 to 110 C, 3 thermal cycles, with dwell time at the cold and hot extremes

Temperature Sensors: two thermocouples, one at the top and bottom of a vertex

Tolerances: 2.0 C

Fixtures: none

Ramp Rate: <5 C/min

Thermal soaking: Payloads will dwell at the extreme temperatures of a cycle

Dwell Time: Twelve hours

Typically 2-3 thermal cycles are sufficient to demonstrate that the hardware can survive the predicted thermal environment without damage or degradation in performance.

Record Temperatures in Thermal Testing Log every 20 minutes and write your initials.

Procedures:

1. 4 thermocouples will be used on the Nonagon. A thermocouple will be mounted at the bottom and top of a vertex. The other two shall be mounted in the same manner on the opposite vertex of the nonagon. Determine which thermocouples shall be called T1, T2, T3, and T4. These temperatures will be recorded and must be kept in the same manner.
2. Ensure that the sensors are properly mounted.
3. Confirm that CubeSat thermal oven temperature matches the sensor temperature by comparing steady state temperatures.
4. Ramp up to the maximum temperature, and at maximum temperature, stabilize for the required dwell time. Ensure that the ramp rate does not exceed stated maximum ramp rates.
5. Ramp down to the minimum temperature, and at minimum temperature, stabilize for the required dwell time. Ensure that ramp rate does not exceed stated minimum ramp rate.
6. Begin cycling phase by ramping up to maximum temperature and the ramping down to the minimum temperature and repeating until 3 cycles. Ensure that ramp rate does not exceed stated maximum.
7. Once 3 cycles are completed, ramp back to the ambient temperature.
8. Once at ambient temperature, identify if any differences arises. If any problems arise, attempt to identify the cause of failure.
9. If the initial inspection is approved, attempt to deploy structure.
10. If structure deploys, no further steps are needed.
11. If structure fails to deploy, determine the cause of failure.
12. Determine if the cause of failure could be fixed by modifying the Nonagon's design.

Key Things to Confirm:

Did the springs compress to desired length?

Did any components jam?

Did mesh deploy?

Test Temperature Sensor Location – Temperatures recorded during a thermal vacuum soak shall be based on the temperatures at selected locations, or the average temperatures in a set of locations. The locations shall be selected in accordance with an assessment to ensure that

components and/or critical parts of the payload achieve the desired temperature for the required time during the testing cycle. In some cases, the temperature sensors shall be attached to the component base plate or heat sink on which the component is mounted, if the temperature requirement is defined at the mounting interface. Temperature soaks and dwells shall begin when the “control” temperature is within $\pm 2^{\circ}\text{C}$ of the proposed test temperature. The “control” temperature criterion for cryogenic systems should be determined by the thermal engineer and the project as it may be significantly more stringent than 2°C .

Subsystem/Instrument – Subsystems and instruments shall dwell for a minimum of twelve hours at each temperature extreme of a cycle. The duration of thermal soaking must be of sufficient to allow completion of performance tests for all modes of operation including safehold and survival.

Payloads/Spacecraft – Payloads shall be exposed for a minimum of 24 hours at each extreme of each temperature cycle. The duration of thermal soaking must be sufficient to allow completion of the required performance tests (functional, comprehensive, etc.) for all modes of operations including safehold and survival at the hot and cold extremes. Projects seeking to reduce durations or the number of cycles must submit deviations and receive approval from AETD prior to PDR. The test plan for units, subsystems, and instruments should then be adjusted to ensure 12 cycles before flight of all units.

Return to Ambient – If the mission includes a requirement for the test item to remain in an operational mode during the descent and landing phases, an additional test segment will be added to verify that capability. If possible, the test unit should be kept warmer than the surroundings to protect against contamination from the test facility. Before the chamber is returned to atmospheric conditions, all sensors should read above the dew point to insure that water does not condense on the payload.

Structural Testing:

Requirements: Equivalent loading is 60 G's

Strain Gages: One at the top and bottom of a vertex, one on each strut

Tolerances: 0.005 in/in

Safety Factors: 1.1 yield, 1.25 ultimate

Fixtures: See document S1 and S2

Ramp Rate: 0.01 in/min

Procedures:

1. Determine the limit forces required to test yield strengths and ultimate strengths.
2. Ensure that the strain gages are properly mounted.
3. Place test sample in fixture and check that it is mounted correctly.
4. Place fixture in bottom portion of Instron.
5. Place rivets in a second fixture and check that they are mounted correctly.
6. Place fixture in top portion of Instron.
7. Confirm that the Instron is operating with the correct ramp rate and that the LabView software has the correct calibration values for the strain gages.

8. If any yielding or failure occurs during testing, stop the test.
9. Begin to record data, then start the Instron machine
10. Continue to ramp up until the Instron has reached the yield force determined with a safety factor.
11. Stabilize for 10 minutes. If no yielding occurs, continue until the Instron has reached the ultimate force determined with a safety factor.
12. Stabilize for 10 minutes. If no failure occurs, unload the structure.
13. Save all data to a flash drive.

Cable Tie Testing:

Requirements: Test cable ties until failure

Tolerances: 0.005 in/in

Fixtures: Modified “eye-hooks” to attach cable ties to Instron fixtures

Ramp Rate: 0.01 in/min

Sample Size: 20 cable ties

Procedures:

1. Ensure Instron has correct ramp rate and correct ramping function.
2. Place fixture in the bottom section of the Instron.
3. Place cable tie in the bottom fixture.
4. Place second fixture in top portion of the Instron.
5. Attach cable tie to the top fixture.
6. Begin to record data in LabView, then start the Instron machine.
7. Save all data to a flash drive. Label data files according to the test number.
8. Analyze data using B-based analysis (See Mil-Hdbk-5J).

Key Things to Confirm:

Were failure loads consistent for a sample size?

How did the cable ties fail? Was it a cable or knot that failed?

Vibrational Testing:

Requirements: Equivalent loading is 60 G's

Equipment: Accelerometer? Will depend on speed of oscillation

Location: One accelerometer at the top and bottom of a vertex

Sweep Rate: 4 octaves per minute

Fixtures: Fixed to the base of the test station

Procedures:

1. Ensure that the base is properly mounted and fastened.
2. Displace the vertex, then release.
3. Count oscillations and record duration of oscillations.
4. If oscillations are too rapid to count with naked eye, use an oscilloscope to measure the frequency.

Chapter 7: Conclusions

A miniaturized version of normal satellites, CubeSats provide a low cost test platform for academic research in space. Currently CubeSats are limited to LEO flight by their low frequency, low gain communications systems, which do not have enough throughput to support long distance missions. An antenna system is needed that will allow CubeSats to transmit more data at longer distances than is currently possible. The Jet Propulsion Laboratory proposed the design of a collapsible parabolic reflector that would produce high gain in the Ka radio band.

In order to accomplish this design proposal, the problem was fully defined for the team, key requirements were determined, and the organization and project methodology were discussed to demonstrate how the team expects to develop and deliver a useful product to the sponsor on time. Past implementations of designs of this type were explored, including a solution specifically for CubeSats developed by USC. Other types of antennas were also explored in order to understand the problem more thoroughly. Material properties of commonly used aerospace grade materials were also explored and compared. The House of Quality method was used to determine the relative importance of system requirements and specific numerical goals were set. From the background research and engineering requirements, ideas were generated. Through decision matrices and eliminating unusable concepts, the gathered ideas were narrowed down into a set of five detailed designs. These five designs were then further narrowed down via decision matrix to a singular, top concept – the Nonagon. This top concept was then fully designed with detail drawings, analysis, materials and component selection, and manufacturing and assembly plans. Finally, the Nonagon was manufactured, assembled, and tested to determine if the realized design was able to meet the key requirements, or if it was unable to meet the requirements what could have caused the failure. Design improvements were noted, and future work was catalogued.

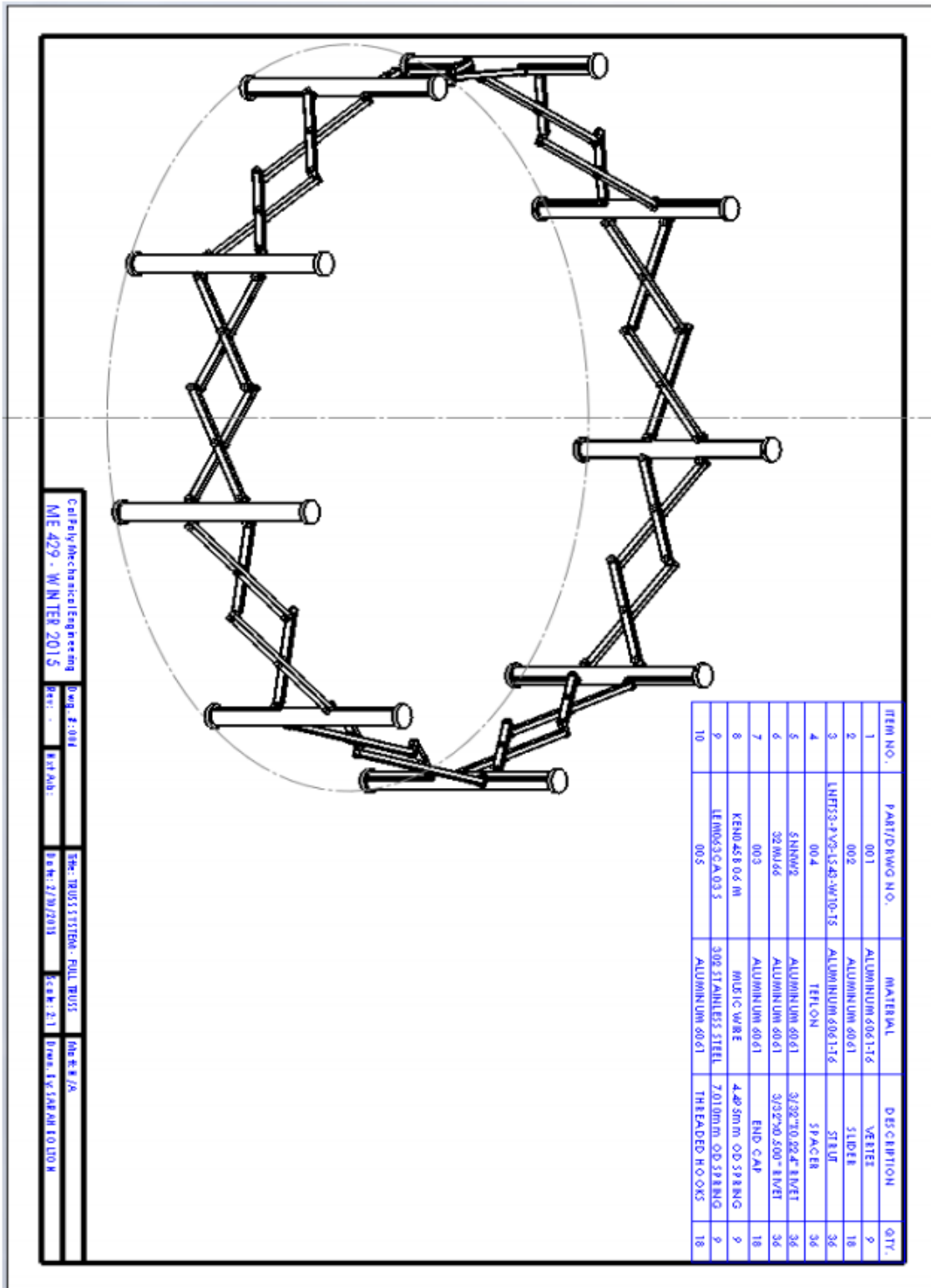
References

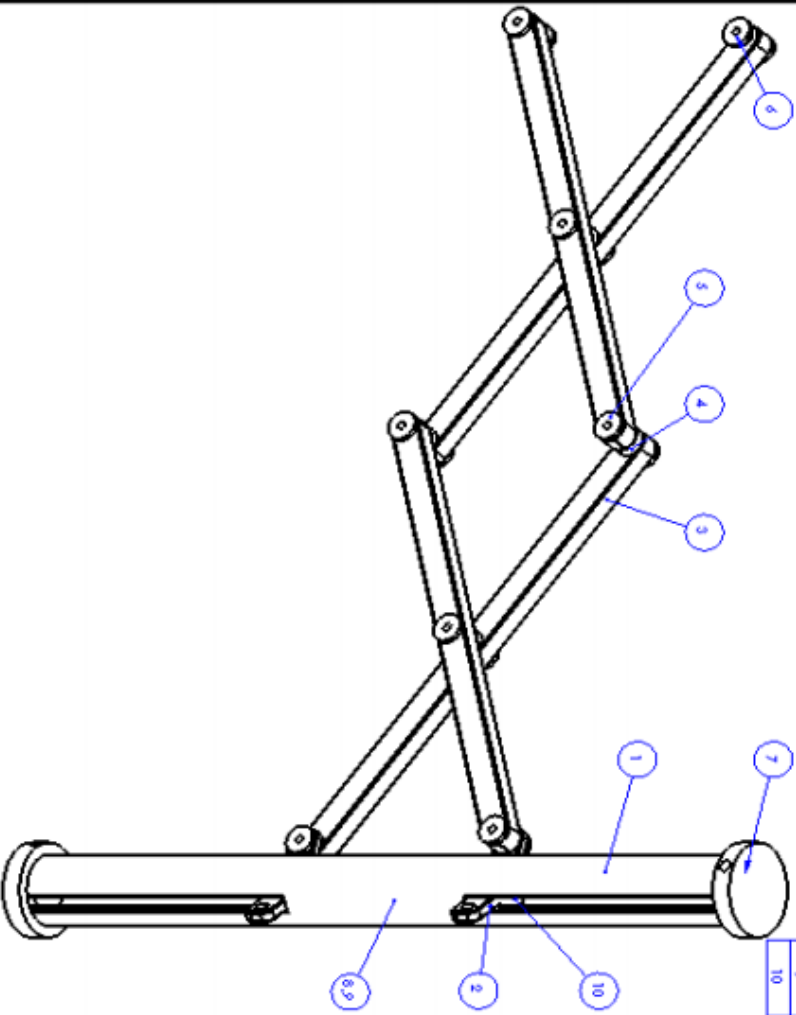
- Computers in Theory and Practice*. (2013, April 26). Retrieved from World Architecture: <http://www.worldarchitecture.org/authors-links/pgc/vn/computers-in-theory-and-practice.html>
- Davis, J. (2014, September 24). *LightSail Sails through Day-in-the-Life Test*. Retrieved from The Planetary Society: <http://www.planetary.org/blogs/jason-davis/2014/20140924-lightsail-sails-ditl.html>
- del Rio Bocio, C. (2009). *High Performance Horn Antenna Design (II)*. Pamplona, Spain: Public University of Navarra.
- DuPont. (2011). *DuPont Kapton HN: Polyimide Film*. Retrieved from <http://www.dupont.com/content/dam/assets/products-and-services/membranes-films/assets/DEC-Kapton-HN-datasheet.pdf>
- Hoberman Associates, Inc. (2014, November). *Hoberman Sphere (product)*. Retrieved from Hoberman: Transformable Design: <http://www.hoberman.com/portfolio/hobermansphere-toy.php?rev=0&onEnterFrame=%5Btype+Function%5D&myNum=14&category=&projectname=Hoberman+Sphere+%28product%29>
- Hoberman, C. (1990). *U.S. Patent No. 5024031A*.
- Kramer, H. J. (2012, October). *Aeneas*. Retrieved from eoPortal Directory: Sharing Earth Observation Resources: <https://directory.eoportal.org/web/eoportal/satellite-missions/a/aeneas>
- Love, A. W., Rudge, A. W., & Olver, A. D. (1982). Primary feed antennas. In A. W. Rudge, K. Milne, A. D. Olver, & P. Knight, *The Handbook of Antenna Design, Volume 1* (p. 339). London, UK: Peter Peregrinus Ltd.
- Marks, G., Keay, E., Kuehn, S., Fedyk, M., & Laraway, P. (2012, January 1). *Performance of the Astromesh Deployable Mesh Reflector at KA-Band Frequencies and Above*. Retrieved from Northrop Grumman: Astro Aerospace: <http://www.northropgrumman.com/BusinessVentures/AstroAerospace/Pages/TechnicalPapers.aspx>
- MatWeb. (2014). Retrieved from MatWeb: Material Property Data: <http://www.matweb.com/index.aspx>
- Mobrem, M., & Spier, C. (2012). Design and Performance of the Telescopic Tubular Mast. *Aerospace Mechanisms Symposium*. Carpinteria, CA: Astro Aerospace - Northrop Grumman Aerospace Systems.
- NASA Goddard Space Flight Center. (2013, April 22). General Environmental Verification Standard (GEVS). Greenbelt, Maryland.

- NASA: Launch Services Program. (2014). *Launch Services Program: Program Level Dispenser and CubeSat Requirements Document* (Revision B ed.).
- Overbye, D. (2009, November 9). *Settling Sail Into Space, Propelled by Sunshine*. Retrieved from The New York Times: http://www.nytimes.com/2009/11/10/science/space/10solar.html?pagewanted=1&_r=1&
- Poole, I. (2014). *Parabolic Reflector Antenna Feed Systems*. Retrieved from Radio-Electronics.com: <http://www.radio-electronics.com/info/antennas/parabolic/parabolic-reflector-dish-feed-systems.php>
- Poole, I. (2014). *Parabolic Reflector Antenna Gain*. Retrieved from Radio-Electronics.com: <http://www.radio-electronics.com/info/antennas/parabolic/parabolic-reflector-antenna-gain.php>
- Poole, I. (2014). *Yagi Antenna/Yagi-Uda Antenna*. Retrieved from Radio-Electronics.com: <http://www.radio-electronics.com/info/antennas/parabolic/parabolic-reflector-antenna-gain.php>
- TEMBO Deployable Structures*. (2014). Retrieved from Composite Technology Development: http://www.ctd-materials.com/wordpress/?page_id=76
- The Library of Manufacturing. (2015, January). *Investment Casting*. Retrieved from The Library of Manufacturing: http://thelibraryofmanufacturing.com/investment_casting.html
- Veldman, S., & Vermeeren, C. (2001). Inflation Structures in Aerospace Engineering - An Overview. *European Space Agency*, 93.
- Xact Wire EDM Corporation. (2015, January). *EDM Capabilities: Wire EDM*. Retrieved from Xact Wire EDM Corporation: <http://www.xactedm.com/edm-capabilities/wire-edm/>

Appendix B: Final Drawings

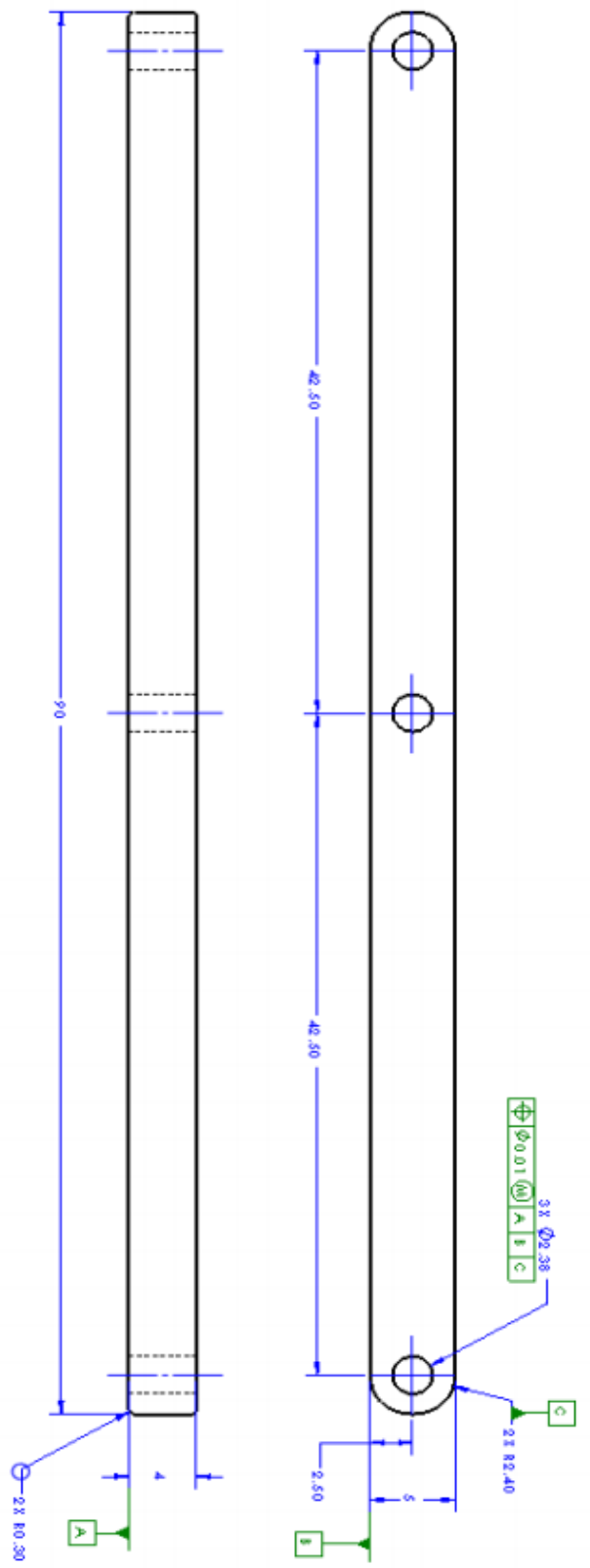
Revision A Drawings – From Detailed Design



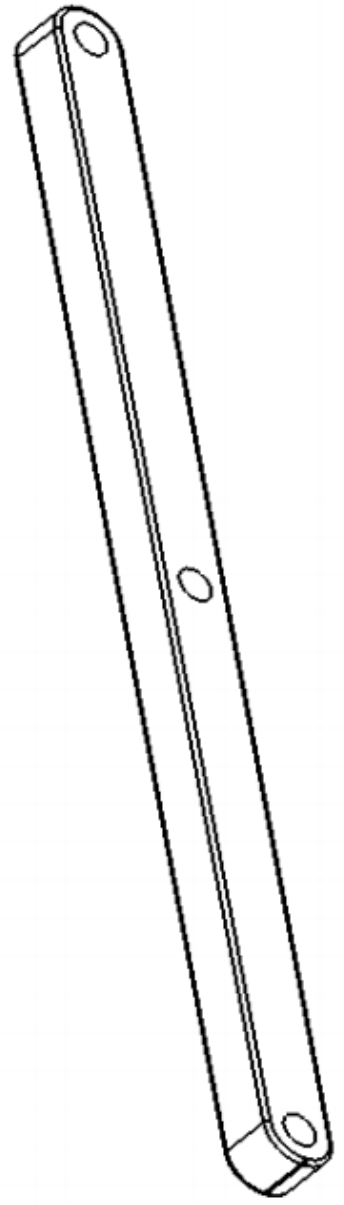


ITEM NO.	PART NUMBER	MATERIAL	DESCRIPTION	QTY
1	001	ALUMINIUM 6061-T6	VERTER	1
2	002	ALUMINIUM 6061	SLIDER	2
3	ENF53-P-VG-US43-WT0-T5	ALUMINIUM 6061-T6	STUB	4
4	004	TEFLON	SPACER	4
5	SHHW2	ALUMINIUM 6061	3/32"X0.284" RIVET	4
6	32M16	ALUMINIUM 6061	3/32"X0.500" RIVET	4
7	003	ALUMINIUM 6061	END CAP	2
8	KEN0438 06 M	MUSIC WIRE	4.40 5MM OD SPRING	1
9	LEND063 CA 00 5	302 STAINLESS STEEL	7.01 0MM OD SPRING	1
10	107782	ALUMINIUM 6061	THREADED HOOPS	2

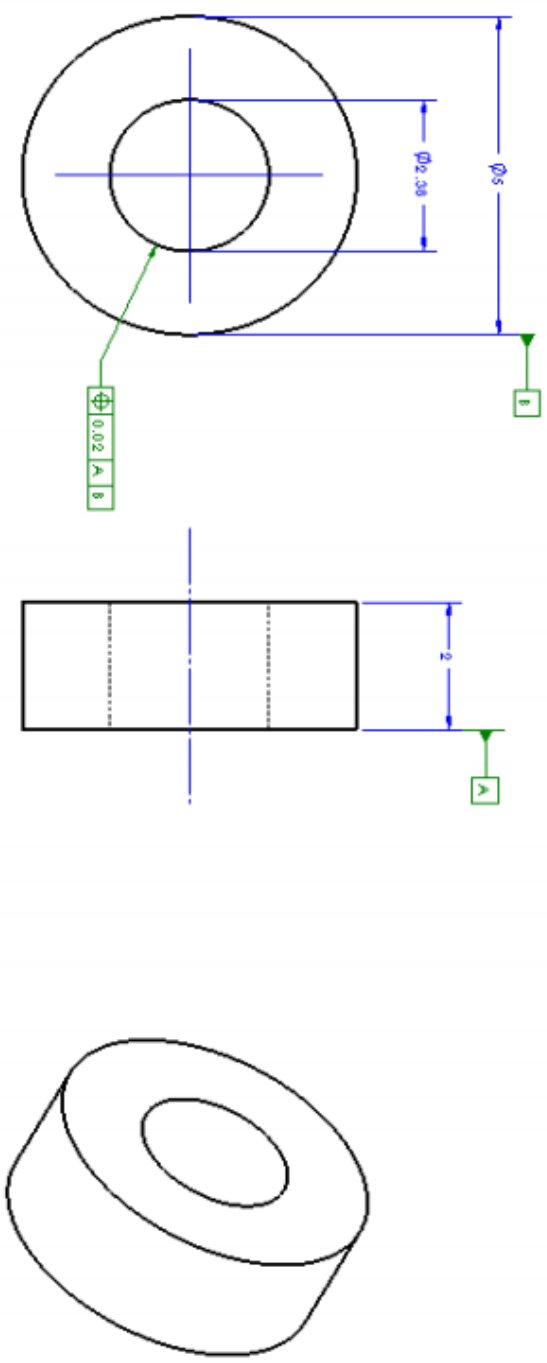
Cal Poly Mechanical Engineering
 ME 429 - WINTER 2015
 Prof. F. 001
 Ext. 007
 Date: 2/10/2015
 Page: 2/3
 Dimension: 1200x1000



- NOTE: OTHERWISE SPECIFIED:
 1. ALL DIMS. IN MILLIMETERS
 2. TOLERANCES:
 X.XX = 00.05
 X.X = 00.2
 ANGLES = 21°
 3. INSIDE TOOL RADIUS 0.5 MM AS
 4. BREAK SHARP EDGES 0.5
 5. ✓ FAO 1/8

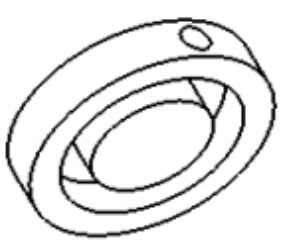
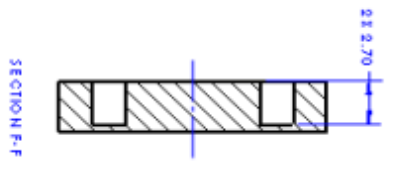
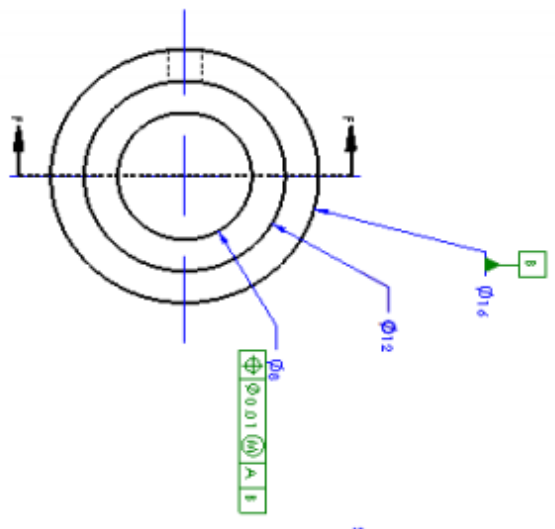
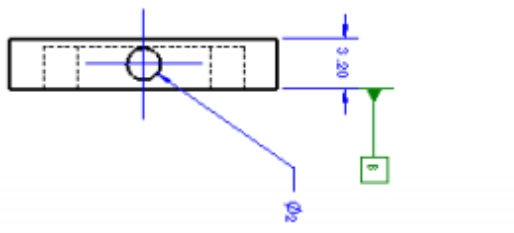


CalPolyMechanicalEngineering	DATE: 8/16/2015, REV: 5/15/15, W: 10-11	DATE: 2/10/2015	DATE: 1/1/2015	DATE: 1/1/2015
ME 429 - WINTER 2015	DRW: Z/10/2015	SCR: 1-1	DRW: 1/1/2015	DRW: 1/1/2015



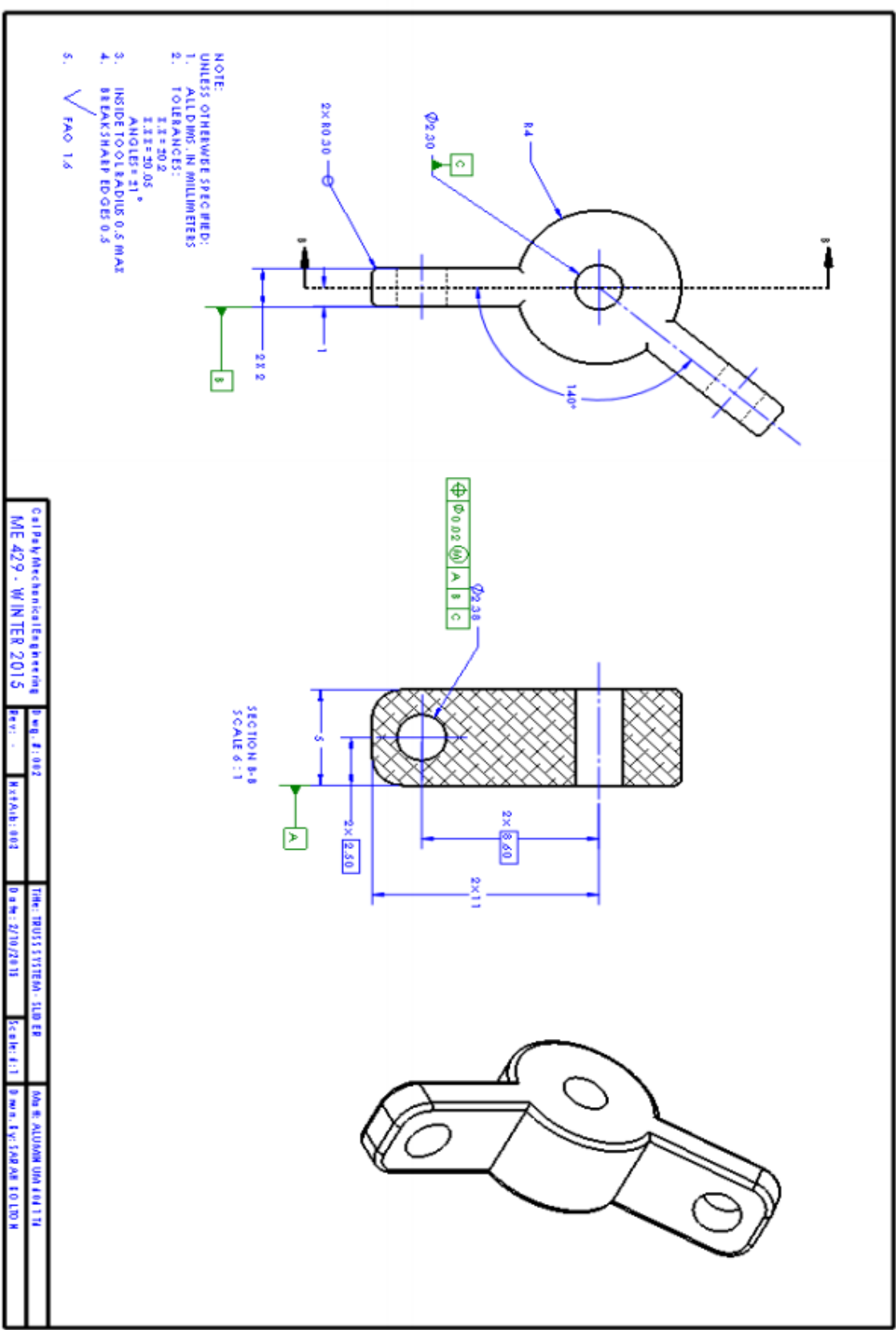
- NOTE:
 UNLESS OTHERWISE SPECIFIED:
 1. ALL DIMS. IN MILLIMETERS
 2. TOLERANCES:
 X.X = ±0.2
 X.XX = ±0.05
 ANGLES = 11°
 3. INSIDE TOOL RADIUS 0.5 MAX
 4. BREAK SHARP EDGES 0.5
 5. ✓ FAO 1.6

ColPalyMechanicalEngineering	Drawn: J. 034	Title: MECH 51 SYSTEM - SPACER	Drawn: TEFLO H
ME 429 - WINTER 2015	Rev: 1	Date: 27/07/2015	Drawn: EYASBAH ELLIOM

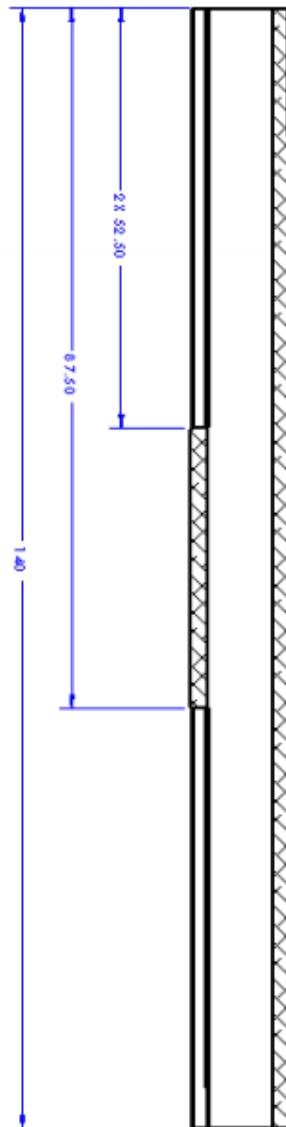
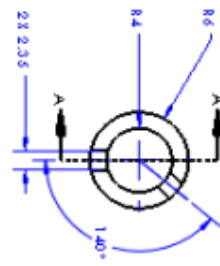


- NOTE:
UNLESS OTHERWISE SPECIFIED:
1. ALL DIMS. IN MILLIMETERS
2. TOLERANCES:
 XX = ±0.05
 XX = ±0.05
 ANGLES = ±1°
3. INSIDE TOOL EDGES 0.5 MAX
4. BREAKSHARP EDGES 0.5
5. FAO 1.6

California Mechanical Engineering	Page # : 002	Date: 2/10/2015	Scale: 1:1	Mr. H. ALUMBI USM 0411 M
ME 429 - WINTER 2015	Part: -	Order: 2/10/2015	Order: 2/10/2015	Order: 2/10/2015

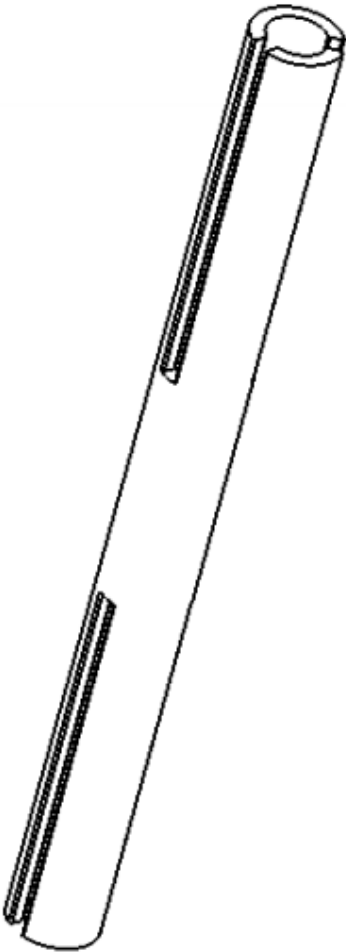


Cal Poly Mechanical Engineering	Des. #: 002	Title: TRUSS SYSTEM - STUD EB	DRW. R. ALUMINUM DIA 484.174
ME 429 - WINTER 2015	Rev.:	EXTRA: 002	DATE: 2/10/2013
			SCALE: 1:1
			DATE: 11/13/2012



SECTION A-A
SCALE: 1:1

- NOTE:
UNLESS OTHERWISE SPECIFIED:
1. ALL DIMS. IN MILLIMETERS
2. TOLERANCES:
 X.X = 0.2
 X.XX = 0.05
 ANGLES = 31°
3. INSIDE TOOL RADIUS 0.5 MAX
4. BREAK SHARP EDGES 0.3
5. ✓ FAO 1.6



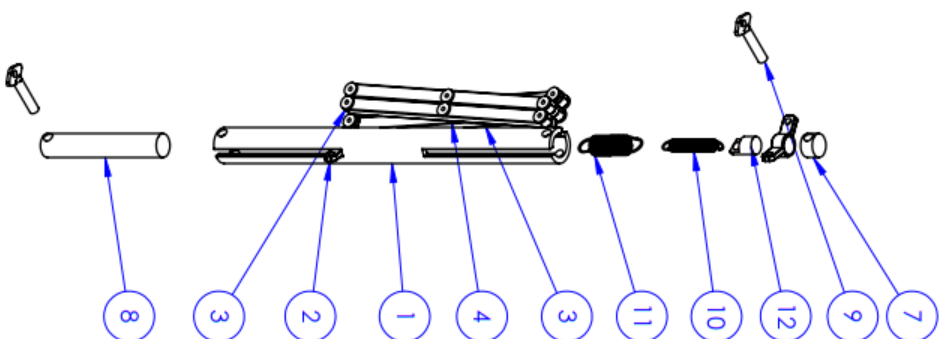
C:\paly\mechanical\Engineering
ME 429 - WINTER 2015

Draw: 2:001
Rev: .

REVISED: 002

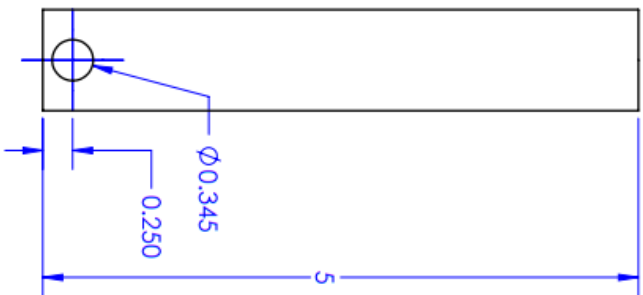
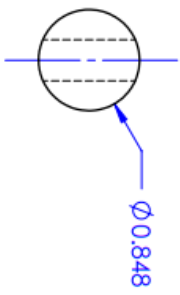
TEMP. MISC. SYSTEM: VERT 1
DATE: 2/10/2015
Scale: 2:1

DRN: EY SARAB KOLTO H



ITEM NO.	DESCRIPTION	PART NUMBER	QTY.
1	Vertex	006	1
2	Slider	001	2
3	Strut	005	4
4	Spacer	004	4
5	Long Rivet	N/A	4
6	Short Rivet	N/A	4
7	Top Cap	002	1
8	Bottom Cap	003	1
9	Thumbscrew	N/A	2
10	LeeSpring- LEM045B06M	LEM045B06M	1
11	LeeSpring- LEM063CA03S	LEM063CA03S	1
12	Hook	1/4" - 20 Aluminum	2

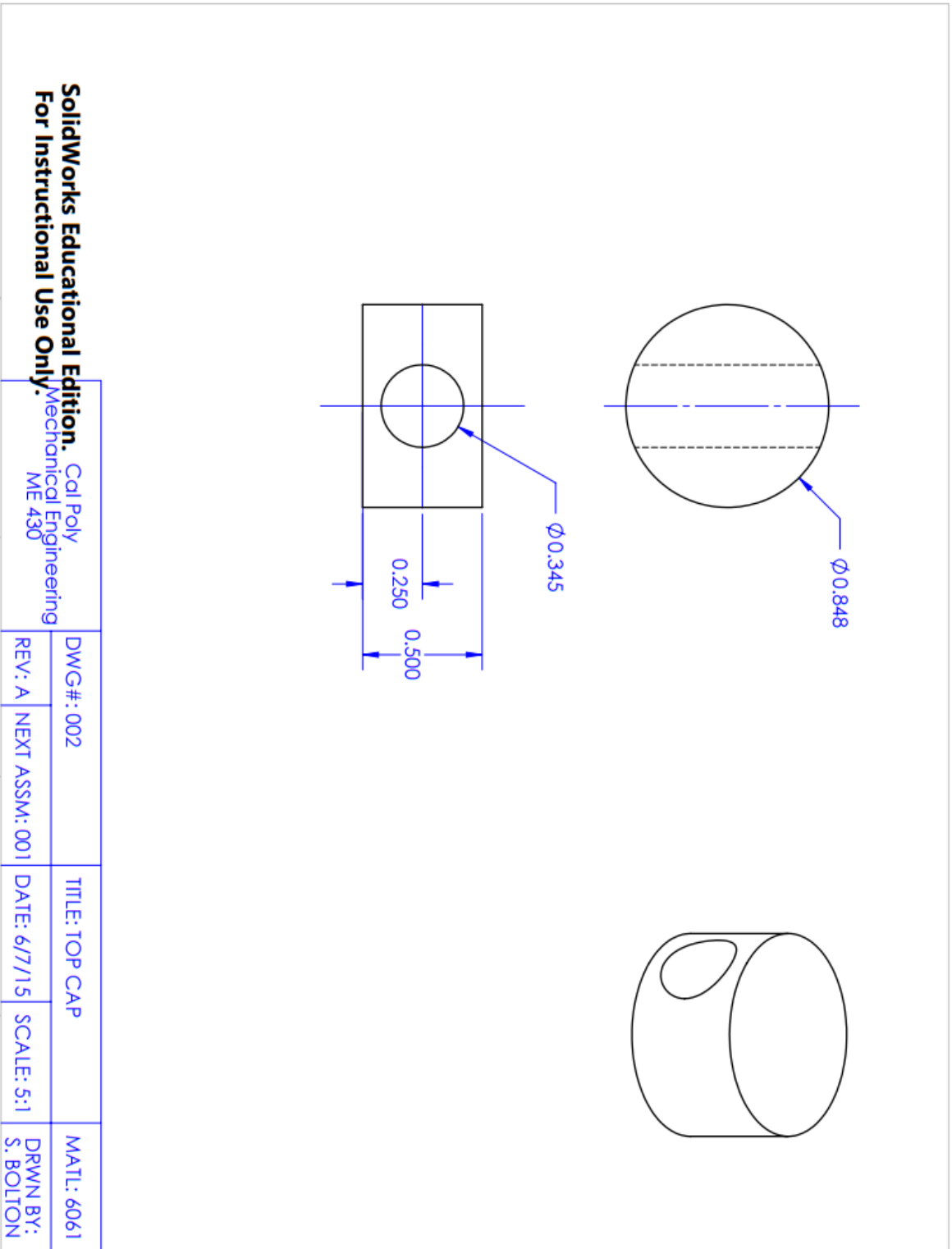
SolidWorks Educational Edition. Cal Poly For Instructional Use Only. Mechanical Engineering ME 430		ASSM#: 001	TITLE: SINGLE WALL ASSEM	MATL: N/A
REV: B	NEXT ASSM: N/A	DATE: 6/7/15	SCALE: 1:2	DRWN BY: S. BOLTON



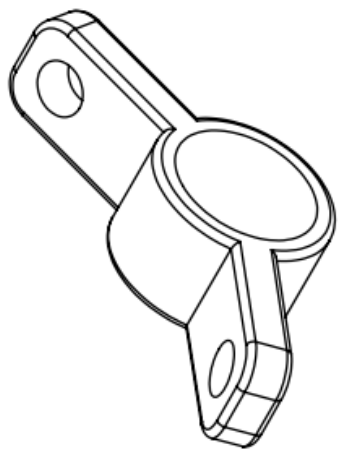
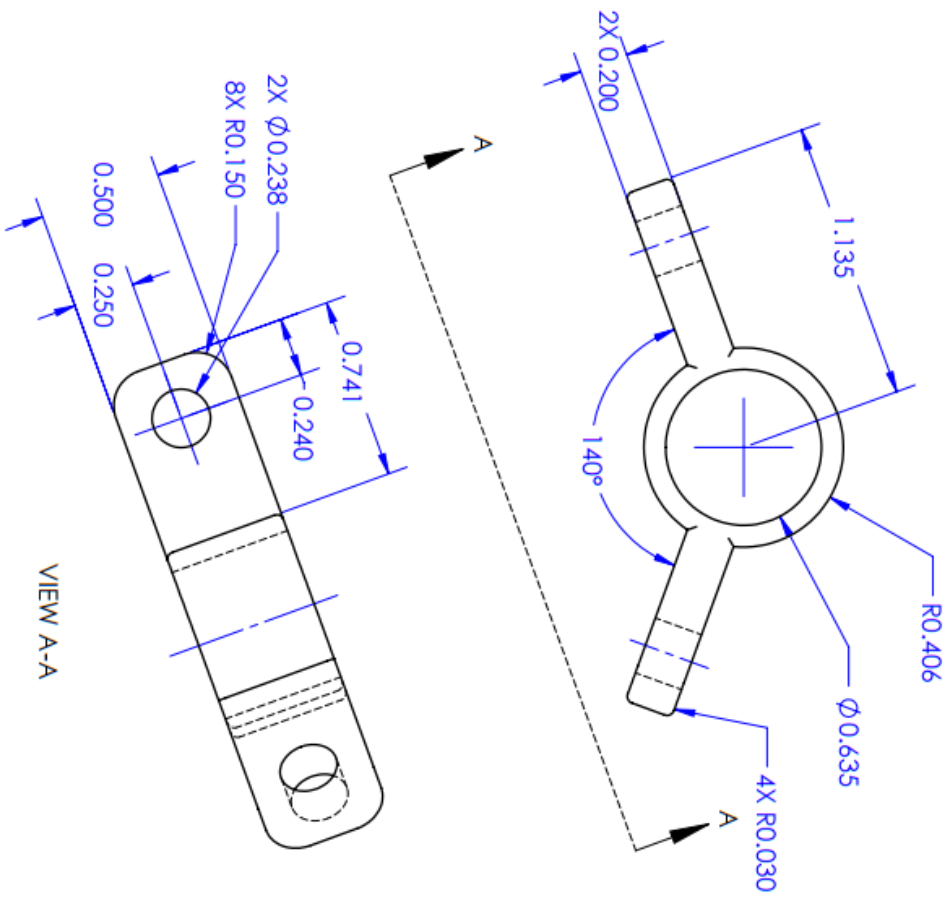
SolidWorks Educational Edition. Cal Poly
 Mechanical Engineering
 ME 430
For Instructional Use Only.

DWG#: 003	TITLE: BOTTOM CAP	MATL: 6061
REV: A	NEXT ASSM: 001	DATE: 6/7/15
	SCALE: 2:1	DRWN BY: S. BOLTON

5 4 3 2 1



SolidWorks Educational Edition. Cal Poly
Mechanical Engineering
ME 430
For Instructional Use Only.



SolidWorks Educational Edition.
 For Instructional Use Only.

Cal Poly
 Mechanical Engineering
 ME 430

DWG#: 001

TITLE: SLIDER

MATL: 6061

REV: B

NEXT ASSM: 001

DATE: 6/7/15

SCALE: 4:1

DRWN BY:
 S. BOLTON

5

1

4

1

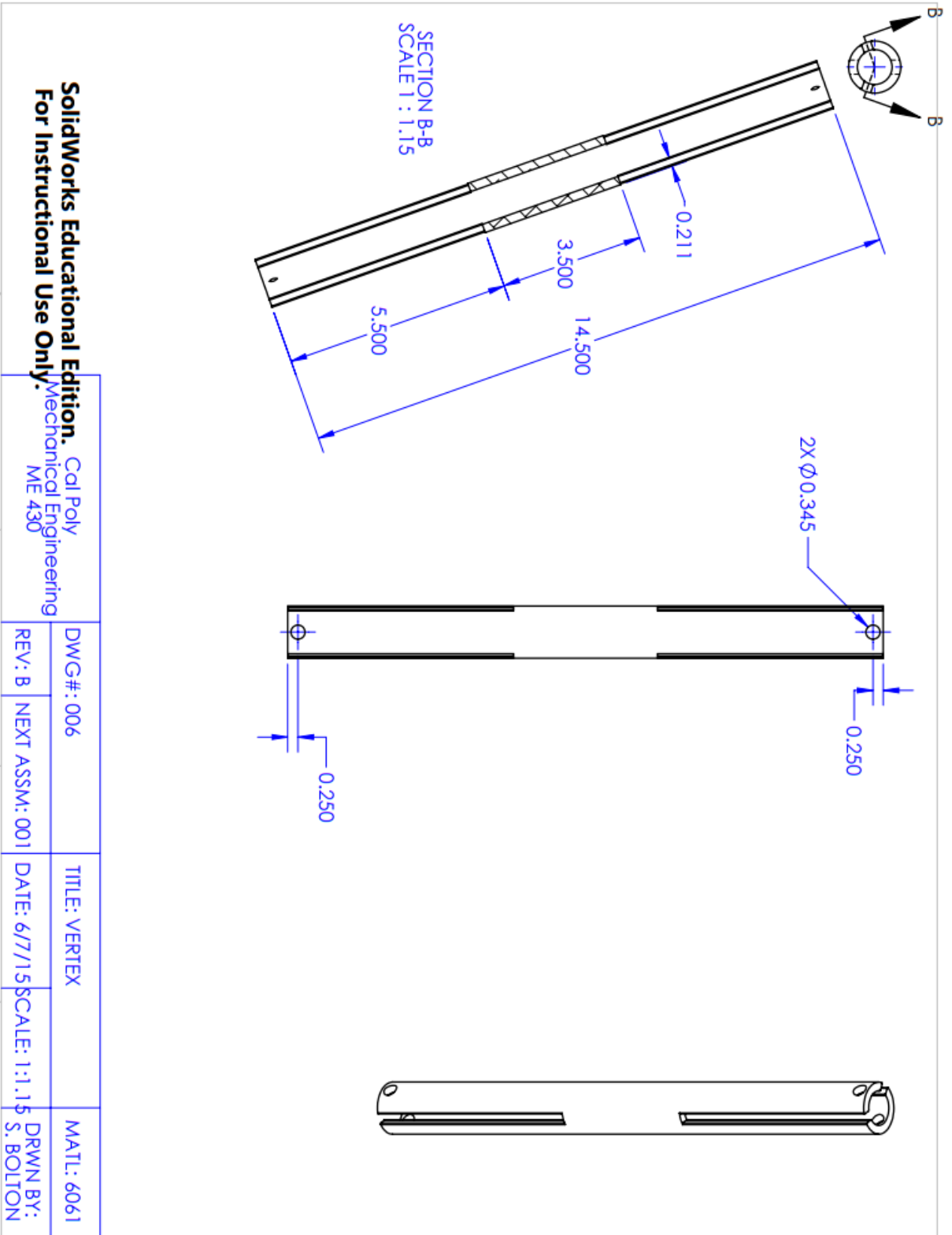
3

1

2

1

1



SolidWorks Educational Edition. Cal Poly Mechanical Engineering ME 430

For Instructional Use Only.

Appendix C: Vendor List

Vendor	Contact Information	Pricing
Anvil Fab. & Mfg	Rich Crooks (r.crooks@anvilfm.com)	\$780.00
AutoZone	autozone.com	\$
Beverly's	805-543-6433	\$
Cal Poly University Store	805-756-5322	
Dollar Tree	805-542-9457	\$
Fastenal	www.fastenal.com	\$\$*
Grainger	www.grainger.com	\$\$*
Home Depot	www.homedepot.com	\$
Kroegers (Ace Hardware)	www.acehardware.com	\$
Lee Springs	www.leespring.com	\$178.74
McMaster-Carr	www.mcmaster.com	\$\$*
Metals Depot	www.metalsdepot.com	\$
Miners (Ace Hardware)	www.acehardware.com	\$
Online Metals	www.onlinemetals.com	\$
Soller Composites	www.sollercomposites.com	\$60
Staples	www.staples.com	\$16
The Thread Exchange	www.thethreadexchange.com	\$15
U.S. Plastic Corp	www.usplastic.com	\$11.52
Walmart	www.walmart.com	\$

Appendix D: Component Specifications and Data Sheets

Aluminum 6061-T6

6061-T6 Aluminum Material Notes

Component	Wt. %	Component	Wt. %	Component	Wt. %
Al	95.8 - 98.6	Mg	0.8 - 1.2	Si	0.4 - 0.8
Cr	0.04 - 0.35	Mn	Max 0.15	Ti	Max 0.15
Cu	0.15 - 0.4	Other, each	Max 0.05	Zn	Max 0.25
Fe	Max 0.7	Other, total	Max 0.15		

Physical Properties	Metric	English	Comments
Density	2.7 g/cc	0.0975 lb/in ³	AA; Typical
Mechanical Properties			
Hardness, Rockwell B	60	60	Converted from Brinell Hardness Value
Hardness, Vickers	107	107	Converted from Brinell Hardness Value
Ultimate Tensile Strength	310 MPa	45000 psi	AA; Typical
Tensile Yield Strength	276 MPa	40000 psi	AA; Typical
Elongation at Break	12 %	12 %	AA; Typical; 1/16 in. (1.6 mm) Thickness
Modulus of Elasticity	68.9 GPa	10000 ksi	AA; Typical; Average of tension and compression. Compression modulus is about 2% greater than tensile modulus.
Poisson's Ratio	0.33	0.33	Estimated from trends in similar Al alloys.
Fatigue Strength	96.5 MPa	14000 psi	AA; 500,000,000 cycles completely reversed stress; RR Moore machine/specimen
Fracture Toughness	29 MPa-m ^{1/2}	26.4 ksi-in ^{1/2}	KIC; TL orientation.
Shear Strength	207 MPa	30000 psi	AA; Typical
Electrical Properties			
Electrical Resistivity	3.99e-006 ohm-cm	3.99e-006 ohm-cm	AA; Typical at 68°F
Thermal Properties			
CTE, linear 68°F	23.6 µm/m-°C	13.1 µin/in-°F	AA; Typical; Average over 68-212°F range.
CTE, linear 250°C	25.2 µm/m-°C	14 µin/in-°F	Estimated from trends in similar Al alloys. 20-300°C.
Thermal Conductivity	167 W/m-K	1160 BTU-in/hr-ft ² -°F	AA; Typical at 77°F
Melting Point	582 - 652 °C	1080 - 1205 °F	AA; Typical range based on typical composition for wrought products 1/4 inch thickness or greater; Eutectic melting can be completely eliminated by homogenization.
Solidus	582 °C	1080 °F	AA; Typical
Liquidus	652 °C	1205 °F	AA; Typical

½” 6061 Aluminum Rod (Vertices) – Grainger (PN: 16NH51)

Technical Specs			
Item	Round Rod	Diameter Tolerance	+/-0.003"
Type	General Purpose	Length Tolerance	+/- 0.032"
Material	Alum	Typical Tensile Strength (PSI)	Min 47
Alloy Type	6061-T6	Typical Yield Strength (PSI)	Min 44
Diameter	1/2"	Typical Hardness	F85
Length	12"	Hardness Scale	Rockwell
Finish	Mill	Standards	ASTM B221
Temper	Extruded		

1x1in Aluminum Stock Square (Sliders) – Grainger (PN: 2EZV9)

Technical Specs			
Item	Square Stock	Thickness Tolerance	+/-0.012"
Type	Corrosion Resistant	Width Tolerance	+/-0.012"
Material	Aluminum	Length Tolerance	+/-1.000"
Alloy Type	6061	Typical Tensile Strength (PSI)	45,000
Thickness	1"	Typical Yield Strength (PSI)	40,000
Width	1"	Typical Hardness	95
Length	1 Ft	Hardness Scale	BHN
Finish	Unpolished	Standards	ASTM B221, AMS-QQ-A-200
Temper	Extruded		

3/32”x0.224” Rivet – Grainger (PN: 5NNW2)

Technical Specs			
Item	Blind Rivet	Core	Solid
Head Type	Button	Head Dia.	0.187"
Rivet Material	Aluminum	Head Height	0.031"
Mandrel Material	Aluminum	Drill Size	#41
Rivet Dia.	3/32 (0.094)"	Hole Size	0.097 to 0.100"
Rivet Length	0.224"	Single Shear Strength (Lbs.)	54
Grip Range	0.032 to 0.125"	Tensile Strength (Lb.)	72

3/32"x0.500" Rivet – Grainger (PN: 32MJ66)

Technical Specs			
Item	Blind Rivet	Grip Range	0.251" to 0.375"
Head Type	Dome	Head Dia.	0.178" to 0.198"
Rivet Type	Open	Head Height	0.032"
Rivet Material	5052 Aluminum	Drill Size	#41
Mandrel Material	Aluminum	Hole Size	0.097" to 0.100"
Rivet Dia.	3/32 (0.094)"	Single Shear Strength (Lbs.)	70
Rivet Length	0.500"	Tensile Strength (Lb.)	80

3/4" 6061 Aluminum Rod (Caps) – McMaster Carr (PN: 8974K11)

Alloy	6061
Shape	Rod
Finish	Unpolished
Diameter	3/4"
Diameter Tolerance	±0.006"
Yield Strength	35,000 psi
Hardness	Soft (95 Brinell)
Material Condition	Heat Treated
Temper	T6511
Specifications Met	ASTM B221
Material Composition	
Silicon	0.4-0.8%
Iron	0-0.7%
Copper	0.05-0.4%
Manganese	0-0.15%
Magnesium	0.8-1.2%
Chromium	0.4-0.8%
Nickel	0-0.05%
Zinc	0-0.25%
Titanium	0-0.15%
Zirconium	0-0.25%
Other	0.15%
Aluminum	95.1-98.2%
Nominal Density	0.097-0.1 lbs./cu. in.
Modulus of Elasticity	10.0 ksi × 10 ³
Elongation	8-17%
Melting Range	1,080° to 1,205° F
Thermal Conductivity	1390 Btu/hr × in./sq.ft. @ 75° to 77° F
Electrical Resistivity	24 Ohm-Cir. Mil/ft. @ 68° F

#8 Zinc Plated Steel Lock Washers

SPECIFICATIONS

■ DIMENSIONS

Inside Diameter	0.164 in	Product Height (in.)*	0.293
Inside Diameter	1/8 in	Product Width (in.)	0.293
Outside Diameter	1/4 in	Washer Size	#8
Outside diameter (in.)	0.293	Washer Thickness	0.049 in
Product Depth (in.)	0.04		

■ DETAILS

Fastener Plating	Zinc	Measurement Standard	USS
Fastener Type	Split Lock Washer	Package Quantity	30
Finish Family	Metallic	Product Weight (lb.)	0.01587312 lb
Material	Steel	Returnable	90-Day

Lee Springs: General Tolerances and Specifications

TOLERANCES EXTENSION DIAMETERS*			
.063" to .098"	O.D. ± .004"	1.60mm to 2.50mm	± .10mm
.109" to .299"	O.D. ± .005"	2.77mm to 7.59mm	± .13mm
.300" to .500"	O.D. ± .010"	7.62mm to 12.70mm	± .25mm
.501" to .850"	O.D. ± .015"	12.73mm to 21.59mm	± .38mm
.851" to 1.125"	O.D. ± .020"	21.62mm to 28.58mm	± .51mm
1.126" to 1.250"	O.D. ± .030"	28.60mm to 31.75mm	± .76mm
1.251" to 1.500"	O.D. ± .040"	31.78mm to 38.10mm	± 1.02mm
1.501" to 1.750"	O.D. ± .050"	38.13mm to 44.45mm	± 1.27mm
1.751" to 2.000"	O.D. ± .055"	44.48mm to 50.80mm	± 1.40mm

Spring rate: ± 10%

***Except where noted to meet DIN 2097**

EXTENSION SPRINGS

To find the load at any working length, when the free length, rate and initial tension are given, use the formula: $P = (R \times F) + I.T.$

where P is the load in lbs.; R is the rate in lbs. per inch; F is the deflection from free length; I.T. is the initial tension.

Example: (Lee Stock Spring Catalog #LE-031C-1) – Given a free length of 1", a rate of 6.9 pounds per inch, and .7 pounds initial tension, find the load at 1.500".

$$P = (6.9 \times .500) + .7 = 3.45 + .7 = 4.15 \text{ lbs.}$$

7mm OD 302 Stainless Steel Spring – Lee Spring (PN: LEM063CA 03 S)

Part Number	LEM063CA 03 S
Outside Diameter	7.010 mm
Wire Diameter	0.635 mm
Maximum Load	10.141 N
Free Length	25.603 mm
Rate	0.21 N/mm
Maximum Length	67.208 mm
Initial Tension	1.392 N
Material	SS
Total Coils	25.0
Number of Coils	25.0
Finish	PASSIVATE PER ASTM A967

4.5mm OD Music Wire Spring – Lee Spring (PN: LEM045B 06 M)

Part Number	LEM045B 06 M
Outside Diameter	4.495 mm
Wire Diameter	0.457 mm
Maximum Load	6.849 N
Free Length	24.993 mm
Rate	0.16 N/mm
Maximum Length	62.331 mm
Initial Tension	0.622 N
Material	MW
Total Coils	41.2
Number of Coils	41.2
Finish	ZINC PLATE AND BAKE PER ASTM B633

3/16" PTFE Rod (Spacers) – US Plastic Corporation (PN: 47501)



PTFE Rod

PTFE is a low friction fluoropolymer with outstanding chemical and weathering resistance. The working temp range is -20°F to 500°F. It has the lowest coefficient of any solid. It has no slip-stick characteristics; static and dynamic coefficients are equal. Nothing sticks with any strength to unheated surfaces. Both virgin and mechanical grades are UV stabilized. Virgin material meets FDA standards and is USDA approved. Mechanical grade is 5% reprocessed material.

Description	Standard Length	Sold By	Stock Grade	Stock	Price	Description	Standard Length	Sold By	Stock Grade	Stock	Price
3/16" PTFE Rod	6"	1'	Mechanical	47501	\$0.80	1-1/4" PTFE Rod	6"	1'	Mechanical	47508	\$22.88
1/4" PTFE Rod	6"	1'	Mechanical	47502	\$1.18	1-1/2" PTFE Rod	6"	1'	Mechanical	47509	\$28.83
3/8" PTFE Rod	6"	1'	Mechanical	47503	\$2.40	1-3/4" PTFE Rod	6"	1'	Mechanical	47510	\$46.77
1/2" PTFE Rod	6"	1'	Mechanical	47504	\$4.05	2" PTFE Rod	6"	1'	Mechanical	47511	\$61.13
5/8" PTFE Rod	6"	1'	Mechanical	47505	\$6.15	2-1/4" PTFE Rod	1'	1'	Virgin	47512*	\$93.55
3/4" PTFE Rod	6"	1'	Mechanical	47506	\$8.75	2-1/2" PTFE Rod	1'	1'	Virgin	47513*	\$118.81
1" PTFE Rod	6"	1'	Mechanical	47507	\$15.49	2-3/4" PTFE Rod	1'	1'	Virgin	47514*	\$139.49
						3" PTFE Rod	1'	1'	Virgin	47515*	\$154.03

Discount: less 5% in 12'; less 10% in 24'; less 15% in 72'. *Available in 1' lengths only.



Kevlar 69 Thread – Thread Exchange (PN: KEV069NATL02B)

Kevlar Specifications

Sizes

Commercial	15	23	46	69	92	138	207	346	415	693	800
Tex	16	21	40	60	80	120	210	400	500	700	800
Government	A	A	B	E	F	FF	3 Cord	5 Cord	6 Cord	N/A	N/A
U.S.											
Tensile strength (Lbs)	4	6	14	23	30	45	64	135	150	175	225
Yards per pound	28,000	25,000	10,000	6,700	5,000	3,350	2,100	1,050	900	780	500
Diameter (Inches)	4/1000	6/1000	8/1000	10/1000	11/1000	14/1000	18/1000	26/1000	27/1000	33/1000	45/1000
Metric											
Tensile strength (kg)	1.8	2.7	6.3	10.4	13.6	20.3	29.0	61.2	68.0	79.2	102.9
Diameter (mm)	0.10	0.15	0.21	0.25	0.29	0.36	0.46	0.65	0.69	0.82	1.14

8-32 x 6' Aluminum Threaded Rod – Fastenal (PN: 47518)

Compliance:  

3TG: Does not contain 3TG

Contract Catalog Item: Y

Diameter: #8

Diameter-Thread Size: #8-32

Finish: Plain

Grade: 6061

Hardness: Rockwell B40 - B50

Length: 6 ft

Material: Aluminum

REACH: Y

RoHS: Y

Specification: ASTM F468

System of Measurement: Imperial (Inch)

Tensile Strength: 37000 - 52000 psi

Thread: Coarse

Thread Requirement: 1A

Thread Size: 32

Type: Threaded Rod

Yield Strength: 31000 psi

Product Weight: 0.0001 lbs.

8-32 x 1", P Type Thumb Screw – Ace Miner

Technical Specs			
Item	Thumb Screw, Type P	Head Width	0.49 to 0.51"
Head Type	Spade	Head Height	0.30 to 0.32"
Thread Size	8-32	Head Material	Steel,Zinc
Length	1"	Rockwell Hardness	Brinell Min 137
Material	Steel	Package Quantity	25
Finish	Zinc Plated		

8-32 Nylon Insert Lock Nuts – Ace Miner

Technical Specs			
Item	Hex Locknut	Width	11/32"
Type	With Nylon Insert	Height	7/32"
Material	18-8 Stainless Steel	Temp. (F)	Up to 250
Finish	Waxed	For Use With	18-8 Bolts and Screws
Thread Size	8-32	Application	Resists Vibration
Thread Type	UNC	Meets/Exceeds	IFI 100/107
Thread Direction	Right Hand	Package Quantity	100

Appendix E: Detailed Supporting Analysis

Matlab Script – Finding Systematic Error

```
function vertex = findvertex()
%% vertices = findvertex()
% Given Diameter, number of sides, and focal ratio, findvertex calculates
% the XYZ coordinates of every vertex of the paraboloid frame polygon.

global D FoverD number_of_sides

r = D/2;
f = FoverD*D;
z_of_vertices = (r^2)/(4*f);
theta = 360/number_of_sides;

vertex = zeros(number_of_sides +1,3); % extra +1 for [0,0,0]
for i = [0:number_of_sides-1]
    %Calculate the xy distro of every vertex, find its z, and store it in a
    %matrix
    vertex(i+1,:) = [r*cosd(i*theta),r*sind(i*theta),z_of_vertices];
end
% Append a point at zero zero zero since we can always have that attached
% to the feedhorn
vertex(length(vertex),:) = [0,0,0];
end
```

```

function [fincoordinates] = intersections(pairs)
% [ fincoordinates ] = intersections(D,foverD,number_of_sides,pairs)
% intersections takes diameter, focal ratio, number of sides of
% approximating regular polygon, and vertex pairings for the net
% structure in the form [x,y;x,y;x,y]. It returns a matrix of
% [X,Y,Z;X,Y,Z;X,Y,Z] intersection coordinates.

global D FoverD number_of_sides

%% Calculate Vertices
% and focal length
f = FoverD*D;
vertices = findvertex();

%% Check for bad pairs
% Duplicate pairings, vertices paired with themselves, and values that
% don't correspond to a vertex
for i = [1:length(pairs)]
    if max(pairs(i,:)) > length(vertices)
        fprintf('ERROR - ')
        fprintf('A pair refers to a value larger than the number of vertices\n')
        fprintf('Check row %0.0f\n',i)
        return
    elseif min(pairs(i,:)) <= 0
        fprintf('ERROR - ')
        fprintf('A pair refers to a vertex value less than zero\n')
        fprintf('Numbering starts at zero in MATLAB land\n')
        fprintf('Check row %0.0f\n',i)
        return
    elseif pairs(i,1) == pairs(i,2)
        fprintf('ERROR - ')
        fprintf('A vertex cannot be paired with itself\n')
        fprintf('Check row %0.0f\n',i)
        return
    end
    for j = [i+1:length(pairs)]
        if pairs(i,:)- pairs(j,:) == [0,0]
            fprintf('ERROR - ')
            fprintf('Duplicate pairing\n')
            fprintf('Check row %0.0f\n',i)
            return
        end
    end
end
end
end

```

```

%% Find the intersections of each Vertex pair line
% Using polyxpoly, find the intersection of every line with all other lines
% return these intersections of the form
% [x1,x1,x1,x1;y1,y1,y1,y1;x2,x2,x2,x2;y2,y2,y2,y2] horizontal rows are
% either x or y coordinates of intersections for one line. Each two rows is
% one lines intersections with all others
for i = [1:length(pairs)]
    % Put the first vertex in the output, even though this isn't usually
    % necessary, as any lines starting at the same vertex will be counted
    % as an intersection and will thus show up. But this is left in just in
    % case of a lone line from any vertex
    rawcoordinates(2*i-1,:) = [vertices(pairs(i,1),1)];
    rawcoordinates(2*i,:) = [vertices(pairs(i,1),2)];
    for j = [1:length(pairs)]
        % i represents the line of interest, j the lines it is being
        % compared to.
        if j~=i
            % this checks that the line is not being checked for
            % intersections with itself, because that would be nuts.
            % These 'temp' names are xy pairs of vertices for use with
            % polyxpoly. Makes it easier to keep straight whats happening
            tempx1 = [vertices(pairs(i,1),1),vertices(pairs(i,2),1)];
            tempy1 = [vertices(pairs(i,1),2),vertices(pairs(i,2),2)];
            tempx2 = [vertices(pairs(j,1),1),vertices(pairs(j,2),1)];
            tempy2 = [vertices(pairs(j,1),2),vertices(pairs(j,2),2)];
            % Magic, polyxpoly finds the intersection of two lines and
            % returns the xy coordinates of any found intersections, [xi,yi]
            [xi,yi] = polyxpoly(tempx1,tempy1,tempx2,tempy2);
            if isempty([xi,yi]) == 0
                % polyxpoly returns an 'empty' matrix if it finds no
                % intersections. These are matrices with dims 0x1 or 1x0
                rawcoordinates(2*i -1,j) = xi; % since it isn't empty, we append it to the output
                rawcoordinates(2*i,j) = yi;
            end
        end
    end
end
[H,W] = size(rawcoordinates);
% Append the last vertex to the end of the output for the same reasons
% the first is appended.
rawcoordinates(H+1,:) = [vertices(pairs(i,2),1)];
rawcoordinates(H+2,:) = [vertices(pairs(i,2),2)];
end

```



```

%% Remove duplicate intersection coordinates
[H,W] = size(rawcoordinates);
% We naturally have a lot of duplicate intersections by virtue of multiple
% lines starting at the same point. These are all removed and replaced with
% a NaN
for i = [1:2:H]
    for j = [2:W]
        if rawcoordinates([i:i+1],j-1) == rawcoordinates([i:i+1],j)
            RepeatOffender = rawcoordinates([i:i+1],j);
            rawcoordinates([i:i+1],j) = [NaN;NaN];
        elseif rawcoordinates([i:i+1],j) == RepeatOffender
            rawcoordinates([i:i+1],j) = [NaN;NaN];
        elseif rawcoordinates([i:i+1],j) == [0;0]
            rawcoordinates([i:i+1],j) = [NaN;NaN];
        end
    end
end

%% Condense into one matrix, removing NaNs [X,Y,Z]
[H,W] = size(rawcoordinates);
% This now moves the coordinates into a final matrix of a nicer form, and
% leaves all the NaN's out. Also calculates Z while were here.
k = 1;
% k represents how far down the matrix we are writing, since there is no
% way of knowing how many good coordinates will be in the matrix at any one
% time.
for i = [1:2:H]
    for j = [1:W]
        if isnan(rawcoordinates(i,j)) % if it isn't NaN, (is a ≠) write it to the final
        else
            fincoordinates(k,1) = rawcoordinates(i,j);
            fincoordinates(k,2) = rawcoordinates(i+1,j);
            fincoordinates(k,3) = (fincoordinates(k,1)^2 + fincoordinates(k,2)^2)/(4*f);
            k = k+1;
        end
    end
end

% round all the coordinates to 5 decimal places. Matlab tends to have
% things as 1e-15 as a random round off error, and then refuse to treat
% them as zero. This forces all minute differences to resolve
Ndecimals = 5;
Npower = 10.^Ndecimals;
fincoordinates = round(Npower*fincoordinates)/Npower;

```

```

% Unique drops all duplicate rows just to keep it squeaky clean
% it also sorts them based on x value.
fincoordinates = unique(fincoordinates, 'rows');
end

function Z = paraboloid(X, Y)
%[z] = paraboloid(x, y)
% Returns the z value of any point on the paraboloid reflector with
% diameter D and focal ratio f/D

global D FoverD

f = FoverD*D;
Z = (X.^2 + Y.^2)/(f*4);

end

function zq = planarinterp(p1, p2, p3, xq, yq)
%zq = planarinterp(p1, p2, p3, xq, yq)
% interpolation by defining a plane through three given points and
% finding the z value of any given point on that plane.

normalvect = cross(p3-p1, p2-p1);
normalvect = (normalvect/norm(normalvect));%.*[1,1,-1]

zq = (-normalvect(1)*xq - normalvect(2)*yq + normalvect*p1')/normalvect(3);

end

```

```

function [error] = VertextoError(vertices,xaxis,yaxis)
%[surfmesh] = VertextoSurf(vertices,xaxis,yaxis)
% This function takes an input of a lot of vertices in [X,Y,Z] and x and
% y axis arrays that determine the limits and resolution of the
% resolution of the resulting mesh.

%% Input Error Checking
[xH,xW] = size(xaxis);
if xH > 1
    display 'xaxis is too tall, must be row vector'
    return
elseif xW < 2
    display 'xaxis is too narrow, must be a row with more than one element'
    return
end

[yH,yW] = size(yaxis);
if yH > 1
    display 'yaxis is too tall, must be row vector'
    return
elseif yW < 2
    display 'yaxis is too narrow, must be a row with more than one element'
    return
end

[vH,vW] = size(vertices);
if vH < 3
    display 'vertices needs at least three points'
    return
elseif vW ~= 3
    display 'vertices must be 3 wide [X,Y,Z]'
    return
end

%% Delaunay Triangulation
triangulation = delaunayTriangulation(vertices(:,1),vertices(:,2));
figure
trimesh(triangulation,vertices(:,1),vertices(:,2))
axis equal

```

```

%% Calculate Error
% Check the matrix of points and calculate their error from the perfect
% paraboloid

xres = abs(xaxis(2)-xaxis(1));
yres = abs(yaxis(2)-yaxis(1));

error = zeros(length(xaxis),length(yaxis));
xq = min(xaxis);
for i = [1:length(xaxis)]
    yq = min(yaxis);
    for j = [1:length(yaxis)]
        triholding = pointLocation(triangulation,[xq,yq]);
        if isnan(triholding)
            % any points outside the triangulation are set to zero error
            error(i,j) = NaN;
        else
            % inside the triangulation, the plane representing that
            % triangle is found and the z of that particular point is
            % calculated. Its error from the perfect paraboloid is then
            % found and stored
            p1 = vertices(triangulation.ConnectivityList(triholding,1),:);
            p2 = vertices(triangulation.ConnectivityList(triholding,2),:);
            p3 = vertices(triangulation.ConnectivityList(triholding,3),:);

            error(i,j) = (planarinterp(p1,p2,p3,xq,yq) - paraboloid(xq,yq))/2;

        end
        yq = yq + yres;
    end
    xq = xq + xres;
end

end

```

```

%% Net Systematic Error Calculator
% Given a number of sides, antenna quantities f/D and D, and vertices to
% connect with net members, this program calculates the systematic error of
% the surface approximation produced by the net. It also calculates the
% length of each net member for manufacturing. Renders the net approximated
% paraboloid surface.

%% Housekeeping
clear all
close all
clc
global D FoverD number_of_sides

%% User Run Options
plot_surf = false;

%% User Input Values
number_of_sides = 9;
D = 50;
FoverD = .5;
RESOLUTION = .1;
% Connection Lines between vertexes, numbered clockwise
% This is for every pair in 9 sides
pairs = [1,2;1,3;1,4;1,5;1,6;1,7;1,8;1,9;
         2,3;2,4;2,5;2,6;2,7;2,8;2,9;
         3,4;3,5;3,6;3,7;3,8;3,9;
         4,5;4,6;4,7;4,8;4,9;
         5,6;5,7;5,8;5,9;
         6,7;6,8;6,9;
         7,8;7,9;
         8,9;
         1,10;2,10;3,10;4,10;5,10;6,10;7,10;8,10;9,10;]; % Connect to center, pt 10

%% Calculate Focal Length
f = FoverD*D;

```

```

%% Plot Paraboloid
if plot_surf == true
    [X,Y] = meshgrid(-25:RESOLUTION:25);
    Z = (X.^2 + Y.^2)/(f*4);
    figure
    surf(X,Y,Z, 'EdgeColor', 'none')
end

%% Find Vertices
vertices = findvertex();

%% Find Net Intersection Points
[coordinates] = intersections(pairs);
figure
scatter3(coordinates(:,1),coordinates(:,2),coordinates(:,3))
axis equal

%% Vertices Conversion to Nets
[error] = VertextoError(coordinates, (-25:RESOLUTION:25), (-25:RESOLUTION:25));

%% Plot the Error
[xq,yq] = meshgrid(-25:RESOLUTION:25);
figure
surf(xq,yq,error, 'LineStyle', 'none')
% mesh(xq,yq,error)
xlabel('x')
ylabel('y')
zlabel('z')
display 'Mean Error is: '
disp(nanmean(nanmean(error)))

```

EES Script – Dimensional and Structural Analysis

*CubeSat Antenna
Senior Project 2015
Appendix F*

*Creator: Juan Togual
Date Created: 1/27/2015
Date Modified: 2/15/2015*

The following function determines the radius of the base circle to assist in determine the base circle's outer diameter. The function is the summation of the sides at a angle from the horizontal axis. See logbook entry 1/31/2015 regarding BASE CIRCLE OUTER DIAMETER

Function **BaseRadius** (num_{length}, L_{section}, θ_{circle})

i := 0

Length := 0 [mm]

Units for Theta & Length must be set manually in the BaseRadius solution tab, must be in same units as the inputs, Theta will always be in [deg] but L_{side} & Length may be in any unit of length. Confirm that L_{side} & Length is in the same units as L_{strut} & W_{strut}

Repeat

i := i + 1 Serves as a counter to stop the function at desired iteration

For Loop to determine the correct angle from the horizontal axis

If [i < 2] Then $\theta := 90 \text{ [deg]} - \frac{\theta_{circle}}{2}$ Else $\theta := \theta - \theta_{circle}$

Endif

Length := Length + L_{section} · cos [θ]

Until [i = num_{length}] The Stopping requirement

BaseRadius := Length

End **BaseRadius**

Design Constraints

$L_{\text{strut}} = 85$ [mm] *Distance between center of strut bolts' holes*

$W_{\text{strut}} = 5$ [mm] *Width of the strut*

$\text{Thick}_{\text{strut}} = 4$ [mm] *Thickness of the strut*

$\text{Height}_{\text{deployed}} = 40$ [mm]

$L_{\text{slider}} = 8.6$ [mm] *sliders' tab length from slider's center to tab's bolt hole center*

$$\text{num}_{\text{sides}} = 9$$

$$\text{OD}_{\text{rod}} = 12 \text{ [mm] Outer Diameter of rod}$$

$$\text{ID}_{\text{rod}} = 8 \text{ [mm] Inner Diameter of rod}$$

The following section of the code is to determine the length of a side based off the geometry of a strut

Length Geometry Analysis

System of Equations from geometry

$$\beta_{\text{strut,undeployed}} = 90 \text{ [deg]} - \theta_{\text{strut,undeployed}}$$

Theta is measured from the Horizontal Axis, Beta is measured from the Vertical Axis

$$L_{\text{strut}} \cdot \cos [\theta_{\text{strut,undeployed}}] = \frac{W_{\text{strut}}}{\cos [\beta_{\text{strut,undeployed}}]}$$

$$L_{\text{side,undeployed}} = 2 \cdot \frac{W_{\text{strut}}}{\cos [\beta_{\text{strut,undeployed}}]}$$

Length of one side, distance between center of sliders' bolt hole, does not take into account the sliders' tab length from slider's center to tab's bolt hole center

$$L_{\text{section,undeployed}} = 2 \cdot L_{\text{slider}} + L_{\text{side,undeployed}} \quad \text{Length of one complete section; 4-bar linkage, 2 sliders (one on each end)}$$

$$\text{Height}_{\text{undeployed}} = L_{\text{strut}} \cdot \sin [\theta_{\text{strut,undeployed}}]$$

The following section of the code is to determine the distance from one side to the opposite side based off the amount of struts

Base Circle Geometry Analysis

System of Equations from Undeployed geometry

$$\theta_{\text{circle}} = \frac{360 \text{ [deg]}}{\text{num}_{\text{sides}}} \quad \text{Theta is measured from a horizontal line on top of circle, aligned with a side}$$

$$\text{num}_{\text{length}} = \frac{\text{num}_{\text{sides}}}{2}$$

Ignores the bottom half of the circle, only calculates sides that have a displacement in the x-axis for a quarter model of the base circle. See logbook entry 1/31/2015 regarding base circle

System of Equations from Deployed geometry

$$\text{Height}_{\text{deployed}} = L_{\text{strut}} \cdot \sin \left[\theta_{\text{strut,deployed}} \right]$$

$$L_{\text{side,deployed,half}} = L_{\text{strut}} \cdot \cos \left[\theta_{\text{strut,deployed}} \right]$$

The following section of the code is to determine the forces and stresses in the struts

Structural Analysis

Design Constraints

$$G_{\text{forces}} = 10$$

$$\text{Gravity} = 9.81 \text{ [m/s}^2\text{]}$$

$$\text{Yield}_{\text{SF}} = 1.5$$

$$\text{Ultimate}_{\text{SF}} = 1.2$$

$$\text{num}_{\text{strut}} = 4 \cdot \text{num}_{\text{sides}}$$

$$\text{num}_{\text{rod}} = \text{num}_{\text{sides}}$$

Material Properties for Aluminum 6061-T6

$$\text{Yield}_{\text{Strength}} = 9.5 \times 10^7 \text{ [Pa]}$$

$$\text{Ultimate}_{\text{Strength}} = 1.1 \times 10^8 \text{ [Pa]}$$

$$\text{Shear}_{\text{Mod}} = 2.4 \times 10^{10} \text{ [Pa]}$$

$$\text{Young}_{\text{Mod}} = 6.9 \times 10^{10} \text{ [Pa]}$$

$$\text{density} = \frac{2,700 \text{ [kg/mm}^3\text{]}}{1,000^3}$$

System of Equations from geometry

$$\text{Mass} = L_{\text{strut}} \cdot W_{\text{strut}} \cdot \text{Thick}_{\text{strut}} \cdot \text{num}_{\text{strut}} \cdot \text{density}$$

$$\text{Weight}_{\text{perstrut}} = \text{Mass} \cdot \text{Gravity} \cdot \frac{G_{\text{forces}}}{\text{num}_{\text{strut}}}$$

$$\text{Weight}_{\text{total}} = \text{Weight}_{\text{perstrut}} \cdot \frac{\text{num}_{\text{strut}}}{G_{\text{forces}}}$$

$$\text{Total}_{\text{Accel}} = \text{Gravity} \cdot G_{\text{forces}}$$

$$\text{Force} = \text{Mass} \cdot \text{Total}_{\text{Accel}}$$

$$\text{Area} = W_{\text{strut}} \cdot \text{Thick}_{\text{strut}} \cdot 0.001 \text{ [m/mm]}^2$$

Symmetry Model about middle vertical axis

$$R_{ay} + R_{by} - 2 \cdot \text{Weight}_{\text{perstrut}} = 0 \text{ Sum of the Forces, y-axis}$$

$$R_{ax} + R_{bx} - R_{DL} + R_{CL} = 0 \text{ Sum of the Forces, x-axis}$$

$$- [R_{ay} + R_{by}] \cdot \frac{\cos [\theta_{\text{strut,deployed}}]}{2} - R_{ax} \cdot \frac{\sin [\theta_{\text{strut,deployed}}]}{2} + R_{bx} \cdot \frac{\sin [\theta_{\text{strut,deployed}}]}{2} + R_{DL} \cdot \frac{\sin [\theta_{\text{strut,deployed}}]}{2} + R_{CL} \cdot \frac{\sin [\theta_{\text{strut,deployed}}]}{2} = 0$$

Sum of the Moments, z-axis about point G

$$[R_{DL} + R_{bx}] \cdot \frac{\sin [\theta_{\text{strut,deployed}}]}{2} - R_{by} \cdot \frac{\cos [\theta_{\text{strut,deployed}}]}{2} = 0$$

$$[R_{CL} - R_{ax}] \cdot \frac{\sin [\theta_{\text{strut,deployed}}]}{2} - R_{ay} \cdot \frac{\cos [\theta_{\text{strut,deployed}}]}{2} = 0$$

$$R_{bx} \cdot \cos [\theta_{\text{strut,deployed}}] + R_{by} \cdot \sin [\theta_{\text{strut,deployed}}] = R_{ax} \cdot \cos [\theta_{\text{strut,deployed}}] - R_{ay} \cdot \sin [\theta_{\text{strut,deployed}}]$$

System of Equations to Find Stresses

$$\text{Stress}_{bL} = \frac{R_{bx} \cdot \cos [\theta_{\text{strut,deployed}}] + R_{by} \cdot \sin [\theta_{\text{strut,deployed}}]}{\text{Area}}$$

$$\text{Stress}_{tL} = \frac{R_{ax} \cdot \cos [\theta_{\text{strut,deployed}}] - R_{ay} \cdot \sin [\theta_{\text{strut,deployed}}]}{\text{Area}}$$

$$\text{Stress}_{bR} = \frac{R_{DL} \cdot \cos [\theta_{\text{strut,deployed}}]}{\text{Area}}$$

$$\text{Stress}_{tR} = \frac{-R_{CL} \cdot \cos [\theta_{\text{strut,deployed}}]}{\text{Area}}$$

SOLUTION

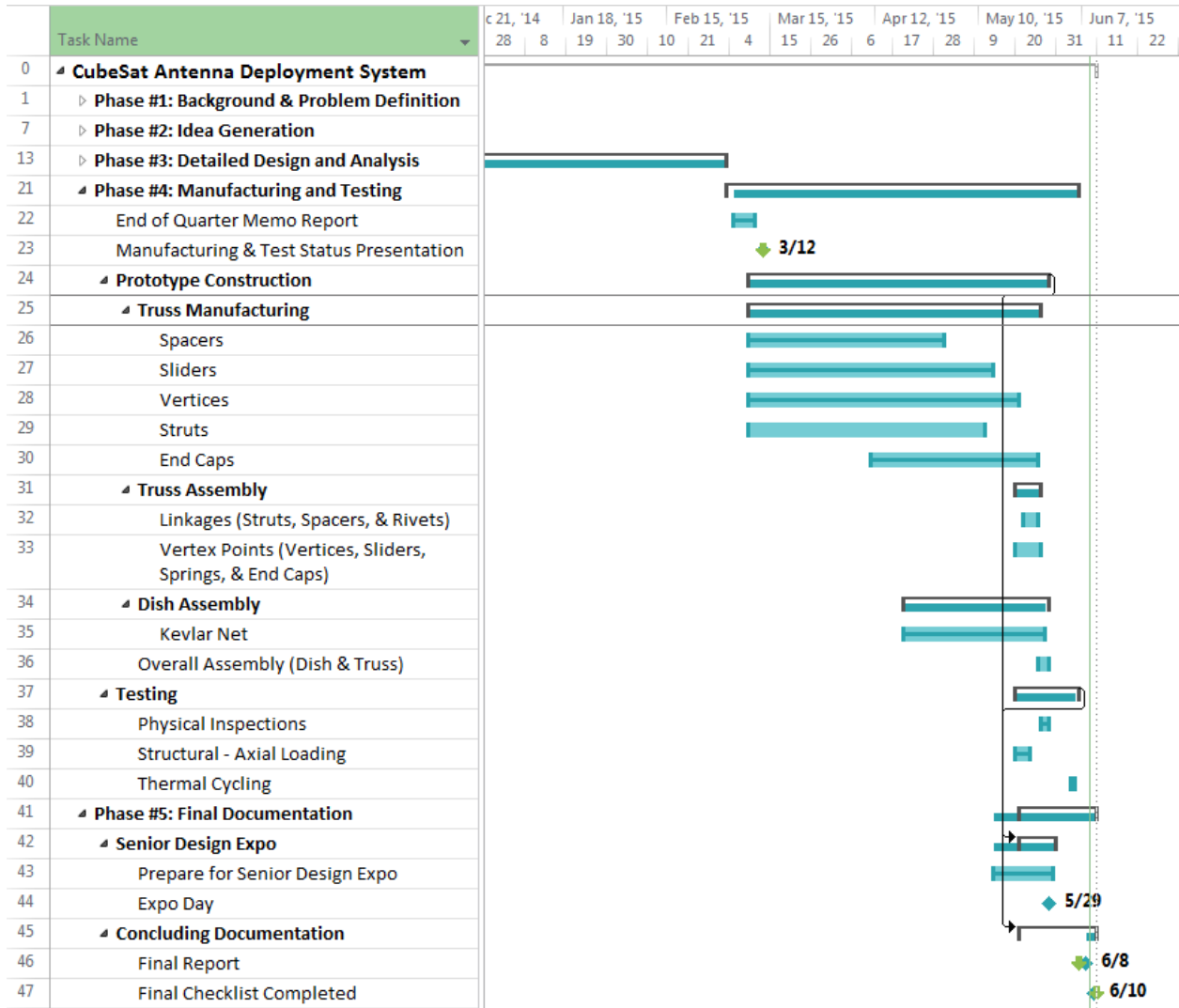
Unit Settings: SI C kPa kJ mass deg

Area = 0.00002 [m²]
beta_strut_undeployed = 3.378 [deg]
density = 0.0000027 [kg/mm³]
Force = 16.21 [kg-m/s²]
Gravity = 9.81 [m/s²]
Gforces = 10
Height_deployed = 40 [mm]
Height_undeployed = 84.85 [mm]
ID_rod = 8 [mm]
L_section_deployed = 167.2 [mm]
L_section_undeployed = 27.22 [mm]
L_side_deployed = 150 [mm]
L_side_deployed_half = 75 [mm]
L_side_undeployed = 10.02 [mm]
L_slider = 8.6 [mm]
L_strut = 85 [mm]
Mass = 0.1652 [kg]
numlength = 4.5
numrod = 9
numsides = 9
numstrut = 36
OD_rod = 12 [mm]
R_ax = 2.402 [kg-m/s²]
R_ay = -1.856 [kg-m/s²]
R_bx = 1.922 [kg-m/s²]
R_by = 2.757 [kg-m/s²]
R_CL = -1.078 [kg-m/s²]
R_DL = 3.247 [kg-m/s²]
ShearMod = 2.400E+10 [Pa]
Stress_bL = 149,659 [kg-m/s²]
Stress_bR = 143,234 [kg-m/s²]
Stress_tL = 149,659 [kg-m/s²]
Stress_tR = 47,549 [kg-m/s²]
theta_circle = 40 [deg]
theta_strut_deployed = 28.07 [deg]
theta_strut_undeployed = 86.62 [deg]
Thickstrut = 4 [mm]
TotalAccel = 98.1 [m/s²]
UltimateSF = 1.2
UltimateStrength = 1.100E+08 [Pa]
Weightperstrut = 0.4503 [kg-m/s²]
Weighttotal = 1.621 [kg-m/s²]
Wstrut = 5 [mm]
YieldSF = 1.5
YieldStrength = 9.500E+07 [Pa]
YoungMod = 6.900E+10 [Pa]

No unit problems were detected.

EES suggested units (shown in purple) for Area beta_strut_undeployed density Force L_section_deployed L_section_undeployed .

Appendix F: Gantt Chart



	Task Name	Duration	Start	Finish	Predecessors
0	▸ CubeSat Antenna Deployment System	254 days	Tue 9/30/14	Wed 6/10/15	
1	▸ Phase #1: Background & Problem Definition	22 days	Tue 9/30/14	Tue 10/21/14	
7	▸ Phase #2: Idea Generation	45 days	Wed 10/22/14	Fri 12/5/14	
13	▸ Phase #3: Detailed Design and Analysis	87 days	Sat 12/6/14	Mon 3/2/15	11,12
21	▸ Phase #4: Manufacturing and Testing	88 days	Tue 3/3/15	Fri 5/29/15	20,19
22	End of Quarter Memo Report	6 days	Thu 3/5/15	Tue 3/10/15	
23	Manufacturing & Test Status Presentation	1 day	Thu 3/12/15	Thu 3/12/15	
24	▸ Prototype Construction	81 days	Mon 3/9/15	Thu 5/28/15	
25	▸ Truss Manufacturing	79 days	Mon 3/9/15	Tue 5/26/15	
26	Spacers	53 days	Mon 3/9/15	Thu 4/30/15	
27	Sliders	66 days	Mon 3/9/15	Wed 5/13/15	
28	Vertices	73 days	Mon 3/9/15	Wed 5/20/15	
29	Struts	64 days	Mon 3/9/15	Mon 5/11/15	
30	End Caps	45 days	Sat 4/11/15	Mon 5/25/15	
31	▸ Truss Assembly	7 days	Wed 5/20/15	Tue 5/26/15	
32	Linkages (Struts, Spacers, & Rivets)	4 days	Fri 5/22/15	Mon 5/25/15	
33	Vertex Points (Vertices, Sliders, Springs, & End Caps)	7 days	Wed 5/20/15	Tue 5/26/15	
34	▸ Dish Assembly	39 days	Mon 4/20/15	Thu 5/28/15	
35	Kevlar Net	38 days	Mon 4/20/15	Wed 5/27/15	
36	Overall Assembly (Dish & Truss)	3 days	Tue 5/26/15	Thu 5/28/15	
37	▸ Testing	17 days	Wed 5/20/15	Fri 6/5/15	
38	Physical Inspections	2 days	Wed 5/27/15	Thu 5/28/15	
39	Structural - Axial Loading	4 days	Wed 5/20/15	Sat 5/23/15	
40	Thermal Cycling	1 day	Thu 6/4/15	Thu 6/4/15	
41	▸ Phase #5: Final Documentation	21 days	Thu 5/21/15	Wed 6/10/15	
42	▸ Senior Design Expo	10 days	Thu 5/21/15	Sat 5/30/15	24,37
43	Prepare for Senior Design Expo	16 days	Thu 5/14/15	Fri 5/29/15	
44	Expo Day	0 days	Fri 5/29/15	Fri 5/29/15	
45	▸ Concluding Documentation	21 days	Thu 5/21/15	Wed 6/10/15	19,24,37
46	Final Report	0 days	Mon 6/8/15	Mon 6/8/15	
47	Final Checklist Completed	0 days	Wed 6/10/15	Wed 6/10/15	

Appendix G: Operators Manual with Safety Guidelines

Currently, our antenna consists of purely mechanical systems; however, there are still some rather specific requirements in order to operate or move the truss and net system. Due to the system being spring loaded, opening and closing the truss requires either multiple people or a cam strap. Although it was the team's intent to create a nichrome restraining system, our lack of time made that impossible. Instead the truss is held with twisted baling wire. The following procedures outline how to deploy, stow, and adjust the net of the antenna in its current state.

Deployment:

1. Remove antenna from 1.5U housing and place on an unobstructed, flat surface.
2. Place hand over the top of the antenna in such a way that prevents motion.
3. Untwist restraining wire with unoccupied hand.
4. Once restraining wire falls away, without allowing the truss to move, maneuver hands until they encircle the antenna.
5. Slowly move hands away from antenna structure. The springs will cause the truss to begin expanding. The expansion rate is related to how quickly hands release the structure.
6. Once antenna and truss appear fully deployed check all Kevlar net connections and lines to ensure they aren't tangled or interfering with expansion.

Note: Antenna deployment can also be achieved by use of a cam strap that is slowly loosened. In this case, the strap can function as the restraining wire and the hands controlling the rate of deployment.

Stowing:

1. Place antenna on an unobstructed, flat surface.
2. Encircle outer perimeter of antenna with a cam strap, slowly tighten the strap until it can rest in the middle of each vertex without slipping down.
3. Ratchet or pull the strap tighter. This causes each side of the antenna to collapse the same amount.
4. As the strap is being pulled, examine struts, sliders, and vertices to determine if any are jamming. In the case of jamming, try to expand and collapse the truss again, or have another person attempt to correct the issue (probable issues include: slider jamming, struts locked, or net caught).
5. Once the antenna is fully collapsed, either lock cam strap in place or use restraining wire to keep structure in a stowed position.
6. Place stowed structure back into the 1.5U housing.

Adjusting the Net:

1. Ensure antenna is in its fully deployed state.
2. Determine which line of the net requires adjustment and find the end of the line which has excess Kevlar.
3. Using needle nose pliers or tweezers, pull excess Kevlar through the heat shrink joint to loosen or tighten Kevlar line to the required amount.

Safety Concerns:

1. Pinching a finger between struts when the antenna is expanding or collapsing antenna, or while adjusting sliders.
2. Restraining strap or wire breaks causing violent deployment.
3. Breaking components due to excessive force in deployment or stowage.

Appendix H: Detailed Budgets

Items purchased with JPL grant

Part Number	Item	Description	Supplier	Qty.	Total
5NNW2	3/32" x 0.224" Blind Rivet	Short Rivets	Grainger	500	27.18
32MJ66	3/32" x 0.500" Blind Rivet	Long Rivets	Grainger	500	29.08
8974K28	1/2" x 12" Al Rod	Vertices	Online Metals	10	54.26
9008K14	1" x 1" Al Square Stock	Sliders	McMaster Carr	20	15.49
R334	3/4" x 12" Al 6061	End Caps	Metals Depot	20	20.72
N/A	1/4"-20 x 36" Al 6061	Hooks	Fastenal	1	11.34
47501	3/16" PTFE Rod	Spacers	US Plastic Corp	40	11.52
LEM063CA 03 S	7.010mm Spring	Large Spring	Lee Springs	10	90.9
LEM045B 06 M	4.495mm Spring	Small Spring	Lee Springs	10	87.84
SQ314	1/4" x 1/4" x 6" Square Stock	Material for	Online Metals	6	14.52
KEV069NATL0	Kevlar 69	Kevlar Thread	Thread Exchange	800	15
CAR-3K-TOW	Carbon 3K	Carbon Fiber	Soller	2 lbs	60
N/A	1.9" OD 1.61" ID AL 6061-T6	Pseudo Mast	Online Metals	2 ft	31.21
47518	1/4"-20 x 36" Al 6061 Thrd	Hooks	Grainger	1	17.79
N/A	Tooling material	Tooling material	Home Depot	N/A	54.55
N/A	Fixture material	Fixture material	Online Metals	N/A	43.56
N/A	Tooling material	Tooling Material	Home Depot	N/A	4.33
N/A	Drill bits	Tooling	Miners	1	8.74
N/A	Steel and Aluminum plate	Plating	Online Metals	1	38.48
N/A	Split Lock Washer	Split Lock	Home Depot	1	1.27
N/A	150 Grit Sandpaper	Sandpaper	Home Depot	1	4.29
N/A	32"X40" Foamboard 3/16	Foamboard	University Store	1	5.32
N/A	Fasteners	Fasteners	Miners	1	9.02
N/A	Spacer Drill bits	Drill bits	Miners	3	12.5
N/A	Drill bit and saw	Tooling	Miners	1	19.42
N/A	Struts machine shop	Struts	Anvil Fab &	1	780
Subtotal (w/Tax)					1468.33
Machining					780
Total					2248.33

Items purchased with Cal Poly ME Dept. grant

Part Number	Part Description	Vendor	Quantity	Total Cost
079946148367	Foamboard 30X40 WH	Staples	2	\$16
N/A	Clear Tape	Dollar Tree	1	\$1
N/A	Toothpicks		1	\$1
N/A	Plastic Straws		1	\$1
N/A	Steel Wire Rolls		1	\$1
008179788034	1 yard Fabric		Walmart	1
0007287928518	Pins	1		\$2
338301 30953	Window Shade	AutoZone	1	\$9
151839 30954	Window Shade	AutoZone	1	\$11
887480166316	#212 Zinc Screw Eye	Home Depot	1	\$1
028400029582	Smartfdcheed		1	\$2
887480012446	Wire Brads		1	\$1
039003496442	1" Anti-Skid Pads		1	\$3
099443002221	3/4 FLT MLD PINE	Home Depot	44	\$23
5032594	ALUM TUBE 36"X5/16"	Kroegers	3	\$13
5032586	ALUM TUBE 36"X9/32"		4	\$21
099443002221	3/4 FLT MLD PINE	Home Depot	20.83	\$11
754826200488	1/2"X10' PVC40 PIPE		1	\$2
007181506328	32 BANDS	Walmart	3	\$2
007181506548	54 BANDS		\$1	\$3
005638908235	EMR BLANKET		1	\$5
076594018226	WOOD STICKS		2	\$2
001117950209	TC BLUE RND		1	\$2
N/A	2 yards of Mesh		Beverly's	2
97525A305	18-8 StainlessSteel Rivet	McMASTER-CARR	1	\$21
N/A	Tooling	Home Depot	1	\$5
N/A	Tooling	Home Depot	1	\$80
N/A	Tooling	Home Depot	1	\$55
N/A	Tooling	Home Depot	1	\$16
		Total Cost (w/tax)		\$323

Appendix I: Concept Design Hazard Identification Checklist

Team: Cal Poly Antenna Deployment

Advisor: Sarah Harding

Y	N	Description of Hazard
X		Will any part of the design create hazardous revolving, reciprocating, running, shearing, punching, pressing, squeezing, drawing, cutting, rolling, mixing or action, including pinch points and shear points?
	X	Can any part of the design undergo high accelerations/decelerations?
	X	Will the system have any large moving masses or large forces?
	X	Will the system produce a projectile?
	X	Would it be possible for the system to fall under gravity creating injury?
	X	Will a user be exposed to overhanging weights as part of the design?
X		Will the system have any sharp edges?
	X	Will any part of the electrical systems not be grounded?
	X	Will there be any large batteries or electrical voltage in the system above 40 V either AC or DC?
	X	Will there be any stored energy in the system such as batteries, flywheels, hanging weights or pressurized fluids?
	X	Will there be any explosive or flammable liquids, gases, or dust fuel as part of the system?
	X	Will the user of the design be required to exert any abnormal effort or physical posture during the use of the design?
	X	Will there be any materials known to be hazardous to humans involved in either the design or the manufacturing of the design?
	X	Can the system generate high levels of noise?
X		Will the device/system be exposed to extreme environmental conditions such as fog, humidity, cold, high temperatures, etc?
	X	Is it possible for the system to be used in an unsafe manner?
	X	Will there be any other potential hazards not listed above? If yes, please explain on next page.

Safety Checklist Actions List

Description of Hazard	Corrective Actions to Be Taken	Planned Completion Date	Actual Completion Date
Pressing and pinching of fingers between scissoring struts and/or moving sliders when expanding or stowing the dish and antenna	Requiring authorization to deploy or stow design, including a warning label on the device and within the report.	5/20/15	
Potential sharp edges on all machined or cast parts including sliders, struts, and vertices	Via a lather, grinder, or handheld tool we will de-burr, chamfer, grind down, or break sharp edges on all components that will be used in prototype construction.	5/20/2015	
Rivets form sharp edge or sharp point due to poor installation	Inspection of all rivets used in antenna assembly, remove and replace any installed rivets that are defective, check that rivets are flush to joint surfaces.	5/20/15	
Possible lubrication of sliders in vertices may cause slippage and injury	Wipe and dry off excess lubrication from outer surfaces, use appropriate solvent for cleaning, must wear gloves while cleaning	5/20/15	
Quick expansion of deploying drum may cause injury to handler	Safety lock will be installed on device while being handled by personnel, safety lock will only be removed once device is installed in CubeSat housing.	5/20/15	
Extreme temperatures - the device will be launched into space	The device will be tested via thermal cycling to NASA standards	5/20/2015	

Appendix J: Future Work and Recommendations

Net and Mesh

- Finish creating parabolic shape via tension ties
 - Look into the use of springs as tension ties
- Examine other materials to determine if there is one better suited to create the net and tension ties than Kevlar
- Attach a mesh placebo (tulle is very close to the gold plated molybdenum mesh generally used). Wait to attach the mesh until you have completed testing or ensure the mesh can survive the testing environments (thermal!)

Truss

- Examine all joints and sides for excessive wear or damage (buckling, shear out, etc)
 - Think about replacements for rivets (barrel nuts, Chicago screws, etc)
 - Change slider and vertex slot design to decrease friction and failure modes
- Finish or redo testing (see Table 12: Design Verification Plan of required design specifications)
- Create improved caps – in particular, the cap diameter should be close to 0.32” or 8.128 mm. The cap diameter should be as close as possible to the internal diameter of the vertices.
- Find a better way to attach the net to the truss than thumb screws

Deployment and Function

- Create telescoping mast or other deployment system to raise antenna out of the 1.5U housing
- Develop feed horn system
- Determine a method of releasing the truss to deploy out to its fully expanded state
 - Look into the use of Nichrome wire
- Attempt to create a fully automated deployment sequence
 - Use of gears, motor, electricity
- Design a locking mechanism (aside from the springs remaining in slight tension) to keep the antenna locked in the deployed position